Eng. Sci., 2025, **38**, 1918

Engineered Science
DOI: https://dx.doi.org/10.30919/es1918

Ferroelectricity in Two Dimensional Indium(III) Selenide: Coupled In-Plane and Out-of-Plane Polarization for Next-Generation Electronics

Muhammad Faizan,[1,2] Jinshun Bi,[1,*] Xuefei Liu,[1,*] Jinbo Pang,[4,*] Mingqiang Liu,[1] Sania Niaz,[3] Ghulam Abbas Khan,[2] Abuduwayiti Aierken,[1] Changsong Gao,[1] Degui Wang,[1] Gang Wang[1] and Yan Wu[1]

Abstract

Ferroelectric memory has emerged as a promising candidate for next-generation non-volatile memory, owing to its low power consumption, rapid switching speeds, and high endurance. However, the miniaturization of traditional ferroelectric materials is hindered by the emergence of the depolarization field that emerges at the nanoscale. This limitation has impeded the compatibility of ferroelectric memory technologies with the continuous scaling of integrated circuits (ICs). The recent discovery of two dimensional indium(III) selenide has introduced a paradigm shift, as it maintains stable ferroelectricity even at the monolayer scale, thereby offering a viable solution to overcoming these challenges. Devices based on two dimensional indium(III) selenide including ferroelectric field-effect transistors (FeFETs), ferroelectric channel transistors, synaptic junctions, and memristors, have demonstrated considerable promise for emerging memory and computing applications. However, a comprehensive understanding of the material's atomic structure, as well as the underlying mechanisms of its ferroelectric switching, remains incomplete. This article provides a comprehensive review of the atomic structure of two dimensional indium(III) selenide across its various phases, its ferroelectric switching dynamics, and the performance of recent device implementations. Furthermore, the key challenges hindering the scalability and reliability of these devices are outlined, along with strategic research directions to accelerate the development of two dimensional indium(III) selenide based ferroelectric memory and neuromorphic computing systems. By identifying critical knowledge gaps and proposing targeted research avenues, a foundation is established for the integration of two dimensional indium(III) selenide into practical, high-performance industrial applications, thereby facilitating the advancement of next-generation memory solutions and cutting-edge computing architectures.

Keywords: Ferroelectric memory; 2D materials; 2D ferroelectrics; Indium selenide; α-In_2Se_3 Synaptic devices; In-memory computing; Non-volatile memory.
Received: 16 October 2025; Revised: 26 November 2025; Accepted: 03 December 2025
Article Type: Review article.

1. Introduction

Ferroelectric materials are a distinctive category of functional materials that exhibit a stable and reversible spontaneous polarization, which can be modulated by an externally applied electric field. These materials are of paramount technological importance, offering a wide range of potential applications in advanced fields such as memristive devices, non-volatile memory systems, logic circuits, artificial intelligence, and in-memory computing, among others (Fig. 1). The demand for high-density memory in future artificial intelligence (AI) applications has significantly advanced research into memristors, particularly concerning their scaling in both lateral and vertical dimensions.[1,2] As electronic devices continue to miniaturize, the need for robust ferroelectric properties in ultrathin ferroelectric layers has become critical for the fabrication of ultrahigh-density devices and for sustaining Moore's Law.[3] Traditional ferroelectric materials lose ferroelectricity below a critical thickness due to surface effects and depolarizing electrostatic fields, limiting their use in nanodevices (Fig. 1a).[4-6] Atomically thin 2D materials offer a promising solution, enabling the development of next-generation nanoelectronics with low power consumption and nanoscale dimensions.[7,8] Two-dimensional (2D) materials, consisting of one or a few atomic layers, are ideal for minimal

[1]*Guizhou Normal University, Guiyang, Guizhou, 550025, China*
[2]*Key Laboratory of Optoelectronic Devices and System of Ministry of Education and Guangdong Province, College of Physics and Optoelectronic Engineering, Shenzhen University, Shenzhen, Guangdong, 518060, China*

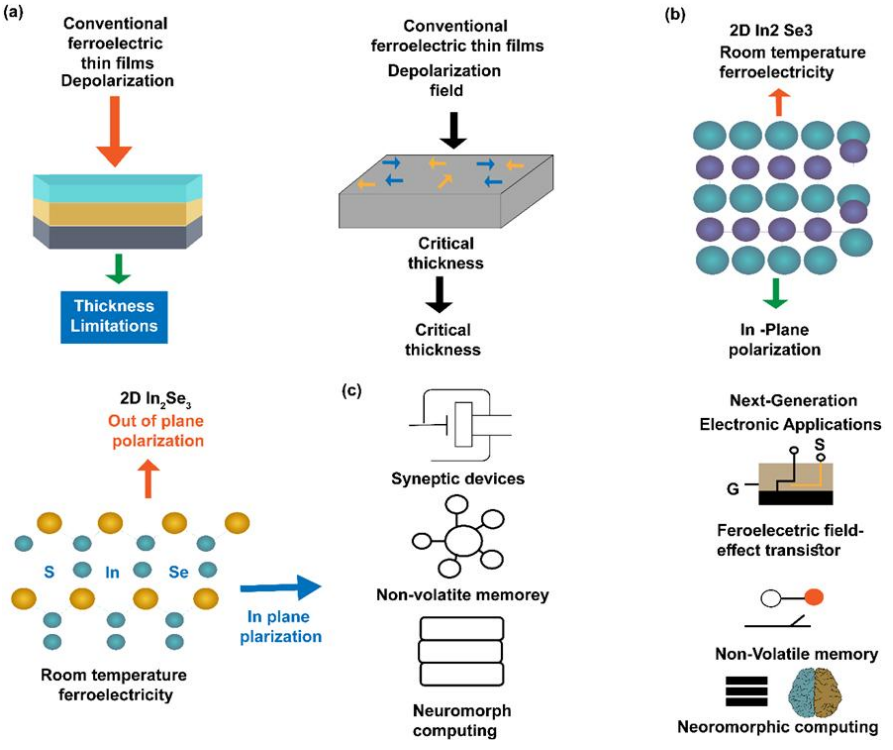

Fig. 1: Schematic representation of the limitations of conventional ferroelectrics in nanoscale devices and the emergence of 2D ferroelectrics as a promising alternative. (a) Polarization suppression in traditional ferroelectrics below critical thickness. (b) Crystal structure and robust polarization in monolayer α-In_2Se_3. (c) Versatile applications of 2D In_2Se_3-based ferroelectrics in nonvolatile memory, optoelectronics, and neuromorphic computing.

sustaining ferroelectric polarization due to their distinct characteristics, such as exceptional strain resistance, surface defects, and fewer surface states.[9] Since the groundbreaking isolation of graphene by Novoselov *et al*. in 2004, a variety of 2D materials, including hexagonal boron nitride, transition metal dichalcogenides (TMDs), carbon nitrides and MXenes, have been identified.[10,11] The reduced size of 2D materials, as opposed to their bulk equivalents, results in robust intralayer chemical bonds and weak interlayer forces, which decrease symmetry and facilitate the emergence of low-dimensional Ferroelectricity.[12] Both theoretical and experimental investigations have confirmed that ferroelectricity can persist in 2D materials, even when reduced to a single atomic layer.[13,14]

Two dimensional In_2Se_3 not only overcome the miniaturization limitations of traditional ferroelectrics but also offer distinct advantages over conventional 2D semiconductors. The polarization in ferroelectric materials induces high-density surface charges, generating an internal electric field that can be modulated. This interaction between In_2Se_3, ferroelectricity, and semiconductor properties could lead to the discovery of novel physical phenomena, as well as the development of innovative devices and applications, including synaptic transistors and negative capacitance devices (Fig. 1b).[15,16] Among 2D ferroelectrics, α-In_2Se_3 is particularly distinguished by its interdependent in-plane (IP) and out-of-plane (OOP) polarization, which enables manipulation of the horizontal ferroelectric field through an applied vertical bias, and vice versa.[14,17-21] Particularly, α-In_2Se_3 is also unique due to its unique coupling between out-of-plane (OOP) and in-plane (IP) polarization, making it a key focus of ongoing research (Fig. 1b).[22-24] In recent years, the exploration of emerging two-dimensional (2D) materials has revealed a diverse range of promising candidates for advanced electronic and optoelectronic applications. Among these materials, α-In_2Se_3 has gained significant attention due to its unique combination of semiconductor and ferroelectric properties. This material, unlike many other 2D semiconductors, exhibits room-temperature ferroelectricity, which makes it highly suitable for devices requiring both tunable electronic properties and non-volatile memory capabilities. As demonstrated in,[25] α-In_2Se_3 shows strong polarization switching and a narrow bandgap, features that are essential for non-volatile memory devices and other memory technologies. Furthermore, recent advances in integrating α-In_2Se_3 with other 2D materials in heterostructures have shown great promise for boosting device performance. These heterostructures leverage the ferroelectric properties of α-In_2Se_3 to modulate the electronic characteristics of adjacent

[3]*Institute of Physics, Bahauddin Zakariya University, Multan, 60800, Pakistan*
[4]*University of Jinan, Jinan, Shandong, 250022, China*
[*]*Email:* bijinshun@gznu.edu.cn (J. Bi),
201307129@gznu.edu.cn (X. Liu),
ifc_pangjb@ujn.edu.cn (J. Pang)

layers, enabling the design of reconfigurable and highly efficient devices.[26] In addition, the material's ability to maintain ferroelectricity even at reduced dimensions is a critical factor that sets it apart from other emerging 2D materials. The work of Wang *et al*. (2024) highlights the exceptional potential of α-In_2Se_3 in integrated circuits, where it is used to control charge transport in field-effect transistors (FETs), achieving both low energy consumption and high switching speed.[27] This makes α-In_2Se_3a prime candidate for the next generation of energy-efficient, high-performance electronic devices. The material's compatibility with existing fabrication techniques for 2D materials and its ability to enhance the performance of devices such as photodetectors and memory systems make it a compelling choice for inclusion in this review.[28] Moreover, α-In_2Se_3's versatility is further demonstrated by its integration with ferroelectrics in the development of multifunctional devices. Ferroelectrics, known for their electrically switchable polarization and non-volatile features, provide a means to enhance the performance of 2D materials in a variety of applications, including non-volatile memory, photodetectors, and neuromorphic computing. The combination of α-$In_2Se_3$with ferroelectrics offers additional degrees of freedom in device design, enabling precise modulation of electronic and optical properties through polarization-induced electrostatic doping.[29] This synergy between 2D materials and ferroelectrics opens up new possibilities for creating highly efficient, low-power devices, which are essential for the development of next-generation electronics.

Nanoscale-thin films of In_2Se_3 have been successfully fabricated, demonstrating exceptional ferroelectricity with a Curie temperature (T_c) of approximately 700 K, significantly surpassing room temperature.[13,23,24,30-33] Unlike conventional ferroelectric insulators, In_2Se_3 is an n-type semiconductor with a direct bandgap of around 1.4 eV, making it ideal for integration into field-effect transistors (FETs) and optical sensing devices.[34] Recent molecular dynamics simulations have forecasted a very high T_c of about 650 K for α-In_2Se_3, providing a broader operational temperature range compared to materials such as CIPS (T_c = 315 K) or $MoTe_2$ (T_c = 340 K).[35,36] These unique characteristics have facilitated the realization of innovative applications in reconfigurable p-n junctions, neuromorphic computing systems,[37-39] optoelectronic memories,[40-42] photovoltaics, FETs, switchable rectifiers and synaptic transistors.[15,34,37,43,44] Since 2018, 2D In_2Se_3 has found growing application in ferroelectric synaptic junctions, field-effect transistors (FETs), and neuromorphic memory systems (Fig. 1c). Its intrinsic ferroelectricity at the atomic scale positions it as a promising candidate for high-temperature 2D ferroelectrics, ultrathin nonvolatile memory, and neuromorphic computing platforms.[16,34,37,45-48]

In this review, a comprehensive analysis of 2D In_2Se_3 is provided, focusing on the atomic structure and phases of the material, the dynamic processes of phase transitions, and the mechanisms driving ferroelectric switching. The advances in data memory and computing electronic devices based on 2D In_2Se_3 are examined, and explored how material properties correlate with device performance. The review delves into the relationships between the material's structure, properties, and its performance in functional devices, such as ferroelectric field-effect transistors (FeFETs), memristors and synaptic devices. Additionally, the challenges and open questions in the field, including issues of environmental stability and encapsulation techniques, phase stability and reproduction during fabrication, toward monolithic integration with existing IC platform and, interface and contact engineering for reliable devices are highlighted. Finally, an outlook on the future of 2D In_2Se_3 is provided, offering potential research directions and strategies for overcoming current limitations to advance its application in next-generation data storage and computing technologies. The remaining paper is organized as follows: Section 2 discusses the structural characteristics along with the mechanisms of its ferroelectric switching and contact properties. Section 3 focuses on the performance of 2D In_2Se_3in different device architectures, examining the role of material properties in the functionality of FeFETs, synaptic devices, and memristors. Section 4 addresses the novel applications of 2D In_2Se_3 with key challenges to commercialization, including switching speed, scalability, and integration into existing semiconductor technologies. Finally, Section 5 concludes by highlighting future research directions and proposing strategies to overcome current limitations, aiming to facilitate the widespread adoption of 2D In_2Se_3-based technologies in next-generation ferroelectronic devices.

2. Crystal structure and phase engineering of In_2Se_3

Group III-VI semiconductors with layered crystal structures, such as indium selenide (In_2Se_3), have emerged as a key focus in 2D material research. In_2Se_3, consisting of quintuple layers (Se-In-Se-In-Se) held together by weak van der Waals forces, was theoretically predicted by density functional theory in 2017 to exhibit ferroelectric properties in its monolayer form. This material demonstrates both out-of-plane and in-plane spontaneous polarization at room temperature. The vertical polarization arises from the asymmetric In-Se bonds, resulting from the varying distances between the indium (In) and selenium (Se) layers. These structural characteristics facilitate polarization reversal via two mechanisms: a single-step lateral shift of central Se layer or a more intricate three-step process, transitioning from a nonpolar state.[14,49] These findings are crucial for understanding and predicting ferroelectricity in two-dimensional materials.

Indium(III) selenide (In_2Se_3) exhibits significant polymorphism, allowing it to exist in various crystalline phases through unit cell interlayer stacking modifications. In_2Se_3 primary polymorphs are α, β, and γ[50-55] Fig. 2 provides an overview of the various polytypes and polymorphs of In_2Se_3. Initially known as indium sesquiselenide, it was first synthesized by Brice *et al*. in 1957 through a solid-state reaction between elemental selenium and indium.[50] After nine

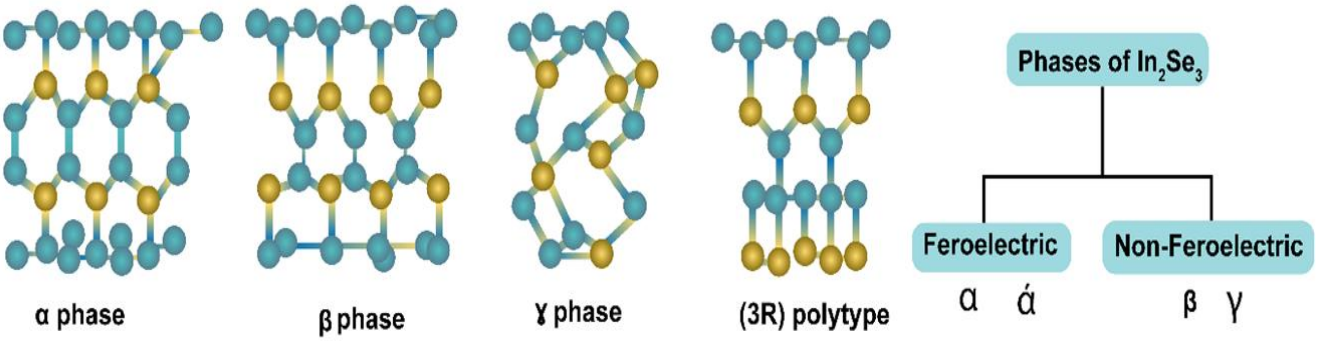

Fig. 2: Atomic model of different phases and polytypes of In_2Se_3.

years, Murakami, Tomiie and Osamura explored polymorphism of In_2Se_3, identifying the β-phase and α-phase crystal structures using Weissenberg photographs.[56] Both α and β phases exhibit rhombohedral crystal structures, with unit cell parameters of a = 4.05 A° and c = 28.77 A° (for α) and a = 4.05 A° and c = 29.41A° (for β). These polymorphs feature layered architectures, where each layer consists of Se−In−Se−In−Se atoms quintuple sheet, and the interlayer stacking sequences can vary. In addition to single unit cell interlayer stacking variations, the crystal structure may exhibit differing stacking arrangements across multiple unit cells, leading to the formation of distinct polytypes. These polytypes are considered subclasses of the α and β polymorphs. Two polytypes of the α-phase In_2Se_3—2H and 3R—and three of the β-phase—1T, 2H, and 3R—have been identified.[57] The numeral denotes the number of quintuple layers per unit cell, while the letter indicates the stacking sequence. For example, α(3R)- In_2Se_3 consists of three quintuple layers with an AaCbA*CcBaC*BbAcB stacking configuration, where indium atoms occupy tetrahedral voids within selenium framework.[56] In_2Se_3 γ phase was first identified by Julien and Kambas in 1982.[58] It is obtained via thermal treatment involving heating to 1000 °C, followed by annealing for 10 days and controlled cooling to 500 °C. Raman spectroscopy confirmed the phase transition, evidenced by a prominent blue shift in the main vibrational mode from 108 to 151 cm^{-1}. Subsequent studies revealed a concurrent transition in electrical behavior, shifting from metallic to insulating. The extensive polymorphism and polytypism of In_2Se_3 lead to the development of crystals with varying band gaps and ferroic properties. However, the coexistence and interconversion of multiple phases present significant challenges in achieving phase-pure In_2Se_3, limiting its consistency and reliability for practical applications.

Among the polymorphs of In_2Se_3 , the α phase is of particular interest due to its intrinsic ferroelectricity, characterized by electrically switchable spontaneous polarization—an essential feature for ferroelectric semiconductor field-effect transistors.[34,37] Material design in this context focuses on achieving high on/off ratios, wide memory windows and low switching voltages. In contrast, the β phase, with a narrower bandgap (~0.7 eV) and higher carrier concentration, is better suited for photodetector applications.[59,60] The γ phase, owing to its insulating character, supports melt-free low-entropy phase-change memory designs based on In_2Se_3.[61] Recent research has successfully isolated a one-dimensional nanostriped β′ phase of In_2Se_3 and showcased its potential for in-plane ferroelastic switching as it transitions into the zigzag-striped β″ phase, opening up possibilities for domain-wall-based nanoelectronics.[62-64] Despite the material's promising ferroelectric properties, critical uncertainties persist regarding the atomic configurations of its various phases and the underlying mechanisms of ferroelectric switching. These unresolved factors hinder the optimization of key device parameters—such as miniaturization, switching speed, data retention, reliability, and endurance—posing significant barriers to large-scale industrial implementation.

Several synthesis methods are employed to fabricate α-In_2Se_3, each offering distinct advantages depending on the specific requirements of the application. Chemical Vapor Deposition (CVD) is one of the most widely used techniques for producing high-quality, large-area films of α-In_2Se_3. It allows for precise control over the film's thickness, crystallinity, and uniformity, which is critical for device integration. CVD's high degree of control makes it ideal for applications requiring uniform, high-performance material, although the method demands precise control of process parameters, including temperature and precursor flow rates, making it more complex and costly. Mechanical Exfoliation is a simpler and cost-effective method that enables the isolation of monolayer or few-layer α- In_2Se_3 from bulk crystals. This technique is especially useful for fundamental research and small-scale device fabrication due to its ability to produce high-quality films, but it is limited by scalability and the relatively small size of the material produced. Liquid-Phase Exfoliation offers a more scalable solution by dispersing bulk α- In_2Se_3 in a solvent and applying ultrasonic treatment to exfoliate nanosheets. This method can produce large quantities of material but typically results in less uniformity in thickness and quality compared to CVD or mechanical exfoliation. Molecular Beam Epitaxy (MBE) is a high-precision method that allows for the growth of epitaxial films of α- In_2Se_3 with atomic-level control over stoichiometry and thickness. MBE

is ideal for applications that require high-quality, well-ordered films, such as in integrated electronic devices, but it is more complex and expensive due to the need for ultra-high vacuum conditions and precise flux control. Selenization of indium thin films is another widely used method that involves exposing indium films to selenium vapor under controlled heating conditions. This approach is cost-effective and scalable, making it suitable for large-area applications. However, the films produced by selenization may exhibit more defects and grain boundaries, which can affect the material's performance in high-end applications.

In conclusion, each of these synthesis methods presents unique trade-offs in terms of material quality, scalability, cost, and performance. CVD and MBE are the preferred methods for producing high-quality, uniform films of α-In_2Se_3, making them suitable for high-performance device applications. However, these techniques require more complex and expensive equipment, limiting their scalability and accessibility for large-scale production. In contrast, Mechanical and Liquid-Phase Exfoliation are simpler and more cost-effective, with Liquid-Phase Exfoliation offering greater scalability, making it suitable for applications that require larger quantities of material. However, both exfoliation methods typically produce material with less uniformity and higher defect densities compared to CVD or MBE. The Selenization method, while cost-effective and scalable for large-area production, results in material with more defects and grain boundaries, which may reduce its performance in applications requiring high-quality material. The choice of synthesis method thus depends on the specific requirements of the application, including the desired material quality, the scale of production, and the associated costs.

3. Origin of ferroelctricity in 2D In_2Se_3

Historically, ferroelectricity in two-dimensional (2D) materials was deemed an uncommon phenomenon. However, pioneering work, particularly the 2017 theoretical prediction by Wenguang Zhu and collaborators, proposed the existence of intrinsic 2D ferroelectricity in In_2Se_3. The unique polarization properties of α-In_2Se_3 arise from its crystal symmetry, which is broken along both the in-plane and out-of-plane directions. The material adopts a layered van der Waals (vdW) structure, where each quintuple layer consists of alternating layers of indium (In) and selenium (Se), with a central Se layer laterally shifted relative to the In layers. This structural feature breaks the inversion symmetry, allowing the material to develop spontaneous polarization. The weak interlayer interactions via vdW forces permit individual layers to act as independent units, making the material highly tunable in both its in-plane and out-of-plane polarization components.

In-plane Polarization (PIP) Mechanism: In-plane polarization in α-In_2Se_3 arises from the inherent asymmetry within the individual layers of the material (Fig. 3). This symmetry breaking leads to charge displacement within the plane, creating a net dipole moment. The key factors contributing to the in-plane polarization are:

- Layered structure and atomic bonding within layers: The shift in the atomic positions within the layers, specifically the stronger bonding between indium and selenium atoms along certain directions, leads to spontaneous dipole moments along the in-plane direction.
- Symmetry breaking: The asymmetric arrangement of atoms

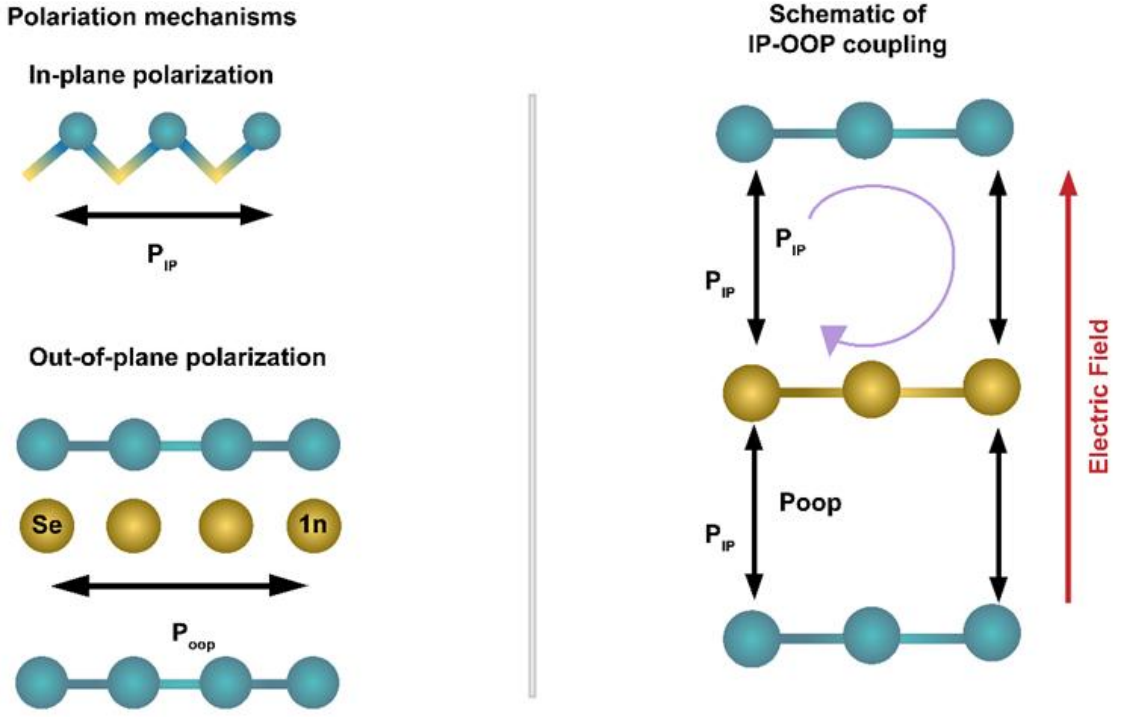

Fig. 3: Polarization mechanisms and schematic of IP–OOP coupling under electric field.

in the unit cell further contributes to charge redistribution, inducing an in-plane polarization. This is particularly observable in thinner films or monolayers of α-In_2Se_3, where the polarization becomes more pronounced due to the reduced symmetry.

• External electric field effects: Applying an external out-of-plane electric field can induce a shift in the selenium atoms, rotating the in-plane dipoles, and thus allowing the control of the in-plane polarization direction.

Out of Plane (OOP) Ferroelectricity in α − In2Se3: Out-of-plane polarization, on the other hand, arises from the displacement of the selenium layer relative to the indium layers along the vertical axis (Fig. 3). This creates a net dipole moment in the direction perpendicular to the plane of the layers. Key factors contributing to out-of-plane polarization include:

• Interlayer van der Waals interactions: The relatively weak bonding between layers in α-In_2Se_3 allows the layers to shift relative to each other, breaking the symmetry along the vertical direction and leading to an OOP polarization.

• Atomic displacement and piezoelectric effects: The atomic displacement between layers and the material's piezoelectric properties result in a polarization component along the OOP direction. When an external electric field is applied in the OOP direction, the polarization can be switched, making the material highly sensitive to external stimuli.

• Energy barriers: Reversal of OOP polarization requires overcoming a certain energy barrier, making the material suitable for non-volatile applications, such as memory devices.

Intercorrelated Nature of IP and OOP Polarization: A fascinating feature of α-In_2Se_3 is the intercorrelation between in-plane and out-of-plane polarization components. The polarization mechanisms in both directions are coupled, meaning that switching the polarization in one direction can influence the other (Fig. 3). This interdependence stems from the atomic displacements within the crystal structure that affect both the in-plane and out-of-plane dipoles simultaneously. For instance, applying an out-of-plane electric field induces a lateral shift in the selenium atoms, which in turn affects the in-plane polarization direction. This coupled behavior has been experimentally observed using techniques such as Piezoresponse Force Microscopy (PFM), which has demonstrated the ability to control both IP and OOP polarizations in α-In_2Se_3 simultaneously, and Second-Harmonic Generation (SHG) (SHG) measurements have confirmed that the reversal of OOP polarization results in a corresponding change in the IP polarization, providing further evidence of the intercorrelated nature of these two polarization components. This interlocking of IP and OOP polarizations has crucial implications for device engineering, where the polarization in one direction can be used to tune or switch the polarization in the other direction, enhancing the versatility of α-In_2Se_3 in functional devices. Several advanced experimental techniques have been employed to study the polarization mechanisms in α-In_2Se_3. Piezoresponse Force Microscopy (PFM) has been widely used to directly observe and manipulate the polarization switching behavior in both IP and OOP directions. It allows for nanoscale resolution in studying the ferroelectric properties of α-In_2Se_3. Second-Harmonic Generation (SHG) has provided insights into the symmetry properties and polarization states of α-In_2Se_3, further confirming the intercorrelation between IP and OOP polarization components. These techniques have enabled a deeper understanding of the spontaneous polarization mechanisms and provided a pathway for tuning and controlling the polarization properties in α-In_2Se_3-based devices.

The dual polarization characteristics of α-In_2Se_3 make it an excellent candidate for a variety of advanced applications. For example, the ability to control both IP and OOP polarizations enables tuning of Schottky barriers in FTJs, which are crucial for non-volatile memory devices. The coupling of polarization components allows for more efficient switching and better retention properties. Furthermore, the coupled polarization states in α-In_2Se_3 mimic the behavior of synapses in biological systems, making it ideal for use in neuromorphic devices. These devices rely on the ability to store and process information in a way that is similar to the human brain, and the intercorrelated polarization in α-In_2Se_3 offers a promising approach for realizing such systems. The material's polarization properties also make it suitable for optoelectronic applications, such as polarization-sensitive photodetectors and modulators.

Unlike materials such as $MoTe_2$, which only exhibit ferroelectricity in monolayer forms and typically require higher temperatures for polarization switching, In_2Se_3 shows robust ferroelectric properties even at room temperature. Other 2D materials like transition metal dichalcogenides (TMDs) (*e.g.*, MoS_2, WS_2, and WSe_2) do not naturally exhibit ferroelectricity and instead rely on external factors such as strain or electrostatic gating to induce it, often leading to less stable polarization switching. Materials like hafnium oxide (HfO_2) can show ferroelectricity but tend to have more complex, defect-dependent behaviors. Bismuth selenide (Bi_2Se_3) may exhibit some induced polarization, but its ferroelectric properties are not as strong or well-defined as those of In_2Se_3. The intrinsic and stable polarization switching in In_2Se_3 provides it with significant advantages for non-volatile memory and logic devices, marking it as superior to many other 2D materials where ferroelectricity is less stable or induced under specific conditions. Thus, In_2Se_3 offers a reliable, room-temperature ferroelectric response that sets it apart from other 2D materials, making it a leading candidate for next-generation ferroelectric applications.

Theoretical models of polarization coupling in α-In_2Se_3 can be effectively described using the Landau-Ginzburg-Devonshire (LGD) theory, which is widely utilized to model ferroelectric phase transitions and polarization switching behaviors in materials. The LGD model for α-In_2Se_3 includes

cross-coupling terms that account for the interdependence between in-plane (IP) and out-of-plane (OOP) polarization components. These cross-coupling terms characterize how polarization in one direction influences the other, resulting in an efficient nonlinear response to external electric fields. The free energy of the system is expanded in terms of order parameters for both IP and OOP polarization, with the coupling coefficients representing the strength of interaction between the two directions. This formalism helps explain the simultaneous switching of polarization in both directions, facilitating more efficient memory switching and enhancing retention properties in ferroelectric devices. Additionally, the LGD theory predicts energy barriers for switching each polarization direction. Specifically, the OOP polarization requires overcoming a higher energy barrier for reversal, which is advantageous for non-volatile memory applications. In contrast, the IP polarization typically has a lower switching barrier, enabling faster responses to external stimuli. Experimental validation of polarization coupling in α-In_2Se_3 has been provided through advanced techniques such as Piezoresponse Force Microscopy (PFM) and Second-Harmonic Generation (SHG). PFM has been used to observe and manipulate the switching behavior of both IP and OOP polarizations, revealing that switching one polarization component induces corresponding changes in the other. These findings confirm the coupling between the two polarization components, supporting the theoretical models. Moreover, SHG measurements have shown that the reversal of OOP polarization leads to a corresponding shift in the IP polarization, further confirming the intercorrelated nature of the two polarization directions. These experimental techniques offer critical insights, demonstrating the interlocked behavior of IP and OOP polarization in α-In_2Se_3, which is a key feature for its versatility in applications.

The polarization coupling in α-In_2Se_3 opens up significant possibilities for a variety of device applications, especially in fields requiring non-volatile memory and neuromorphic computing. The ability to simultaneously control both polarization directions enables more efficient switching and improves retention, making α-In_2Se_3 an ideal material for memory devices such as FeFETs and memristors. Additionally, the intercorrelated polarization in α-In_2Se_3 mimics the behavior of synapses in biological systems, making it an excellent candidate for neuromorphic devices that store and process information similarly to the human brain. Furthermore, the polarization-sensitive properties of α-In_2Se_3 make it suitable for use in optoelectronic devices, including photodetectors, modulators, and photovoltaic devices, where polarization plays a crucial role in performance. In conclusion, the microscopic mechanisms and theoretical models of polarization coupling in α-In_2Se_3 reveal its unique ferroelectric behavior. The ability to control both in-plane and out-of-plane polarization components simultaneously opens up new opportunities for designing advanced ferroelectric devices. By leveraging these coupled polarization states, α-In_2Se_3 holds tremendous potential for applications in non-volatile memory, neuromorphic computing, and optoelectronics. As research advances, understanding the interdependence of polarization components will be critical for the development of next-generation electronic devices, driving innovation in a wide range of technologies.

4. Ferroelectric switching and domain dynamics in 2D $\alpha-In_2Se_3$

The prediction of two-dimensional ferroelectricity in α-In_2Se_3 was initially made using density functional theory (DFT) calculations and later experimentally validated. Functional device structures, such as ferroelectric channel transistors and synaptic semiconductor junctions, have been successfully demonstrated using quasi-2D In_2Se_3 films with thicknesses on the order of tens of nanometers.[20,23,24,32,34,45,65] Beyond the ferroelectric α-phase, In_2Se_3 also stabilizes in the β′-phase, characterized by in-plane polarization (PIP), and the centrosymmetric paraelectric β-phase.[22,63,66,67] This polymorphism, combined with tunable ferroelectric properties, makes In_2Se_3 a promising candidate for nanoelectronic and neuromorphic applications (Fig. 4(a) shows the domain imaging of PIP).[68] Initial theoretical models predicted PIP due to lateral displacements of Se atoms, consistent with the asymmetric cross-sectional structure.[14] However, subsequent analyses argue that the crystal's C_{3v} symmetry, featuring a threefold rotational axis perpendicular to the plane, may preclude switchable PIP according to Neumann's principle.[69-71] This is further corroborated by the top view of α-In_2Se_3, which, akin to h-BN, remains unchanged under 3-fold rotational symmetry, thereby preventing any in-plane spontaneous polarization. However, experimental investigations have reported switching-like behaviors when in-plane electric fields (εIP) are applied to α-In_2Se_3 thin films.[2,37]

The coercive field required to switch out-of-plane polarization in monolayer α-In_2Se_3 remains a subject of active debate Fig. 4(b). While DFT calculations estimate a low switching barrier of ~66 meV per unit cell, experimental measurements consistently report much higher switching fields, typically exceeding 1 V/nm—several times of magnitude above those observed in $PbTiO_3$-based perovskites (~10 kV/cm), despite their higher energy barriers (~200 meV/uc).[14,32,69] This disparity questions the validity of the "dipole locking mechanism," which attributes the large switching field to constrained motion of the central Se atom along both in-plane and out-of-plane directions. However, this mechanism is often misinterpreted as implying coupling between IP and OOP dipoles Fig. 4(c, d). The original formulation clarifies that while in-plane asymmetry is present, it does not yield a net in-plane dipole due to the material's threefold rotational symmetry. Nonetheless, this asymmetry permits strong in-plane second-order nonlinear optical responses. Analogous inconsistencies between theoretical switching barriers and experimental coercive fields are also

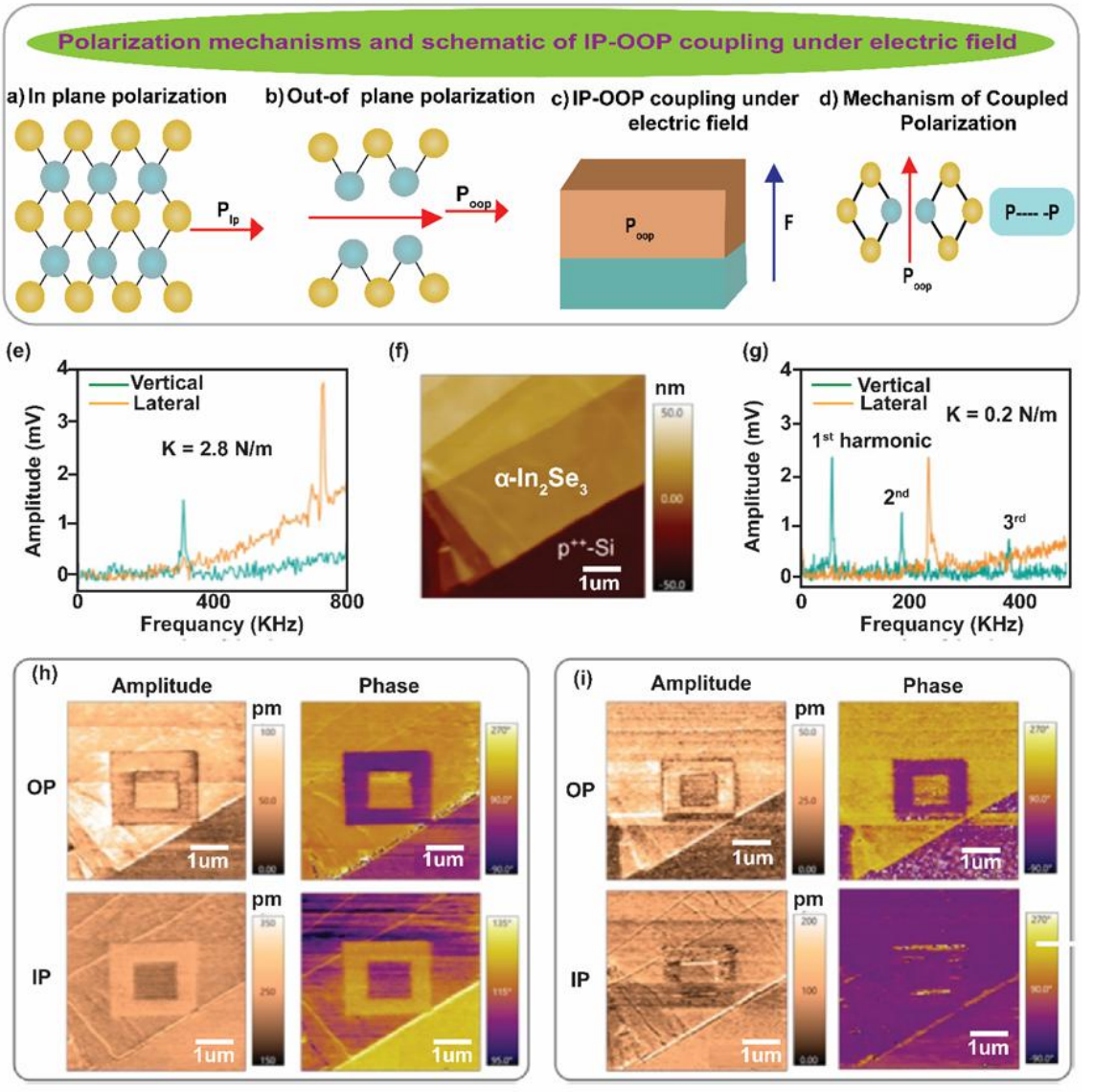

Fig. 4: (a-d) Domain imaging and switching hysteresis loops of In_2Se_3. OOP and IP PFM characterization of α-In_2Se_3 utlizing AFM probes with varying force constants. Vertical and lateral tuning spectra acquired with probes of differing stiffness: (e) k = 2.8 N/m and (g) k = 0.2 N/m. (f) AFM topography of measured α-In_2Se_3 flake. IP- and OOP-PFM phase and amplitude images recorded using probes: (h) k ≈ 2.8 N/m and (i) k ≈ 0.2 N/m Reproduced form.[65] Copyright 2024, American Chemical Society.

evident in other van der Waals systems exhibiting sliding ferroelectricity. For example, in Bernal-stacked h-BN, DFT predicts an ultralow barrier of ~8 meV/uc,[72] yet the observed switching field approaches 0.1 V/nm,[73,74] underscoring the limitations of current theoretical models in accurately capturing dynamic ferroelectric switching in 2D materials.

A comparative PFM analysis was performed on α-In_2Se_3 thin flakes exfoliated onto a doped silicon substrate using two AFM probes with differing force constants (Fig. 4f). The stiffer probe (k ≈ 2.8 N/m) commonly employed in prior studies, was compared with a softer probe (k ≈ 0.2 N/m) offering enhanced torsional sensitivity.[75] Distinct resonance peaks corresponding to lateral torsion modes and vertical deflection were observed for both probes as shown in Fig. 4(e, g). The α-In_2Se_3 sample, containing mixed 2H and 3R stacking, confirmed by Raman and SHG measurements, helped rule out the existence of in-plane polarization (PIP) in both stacking types.[57,76] IP- and OOP- PFM measurements were performed utilizing both probes by applying AC voltage at corresponding 1st harmonic frequencies. A box-in-box domain pattern was inscribed using a DC-biased tip as a reference. In OOP-PFM, both probes exhibited strong amplitude responses and clear 180° phase contrast, confirming robust out-of-plane polarization. Although the stiff probe yielded an IP-PFM phase image with a domain pattern resembling that of OP-PFM, the phase contrast was significantly less than 180°, indicating a likely non-ferroelectric origin. This suggests observed IP piezoresponse is a crosstalk effect from OOP signal, which was reduced but still visible with the soft probe (Fig. 4(h, i)).[77,78]

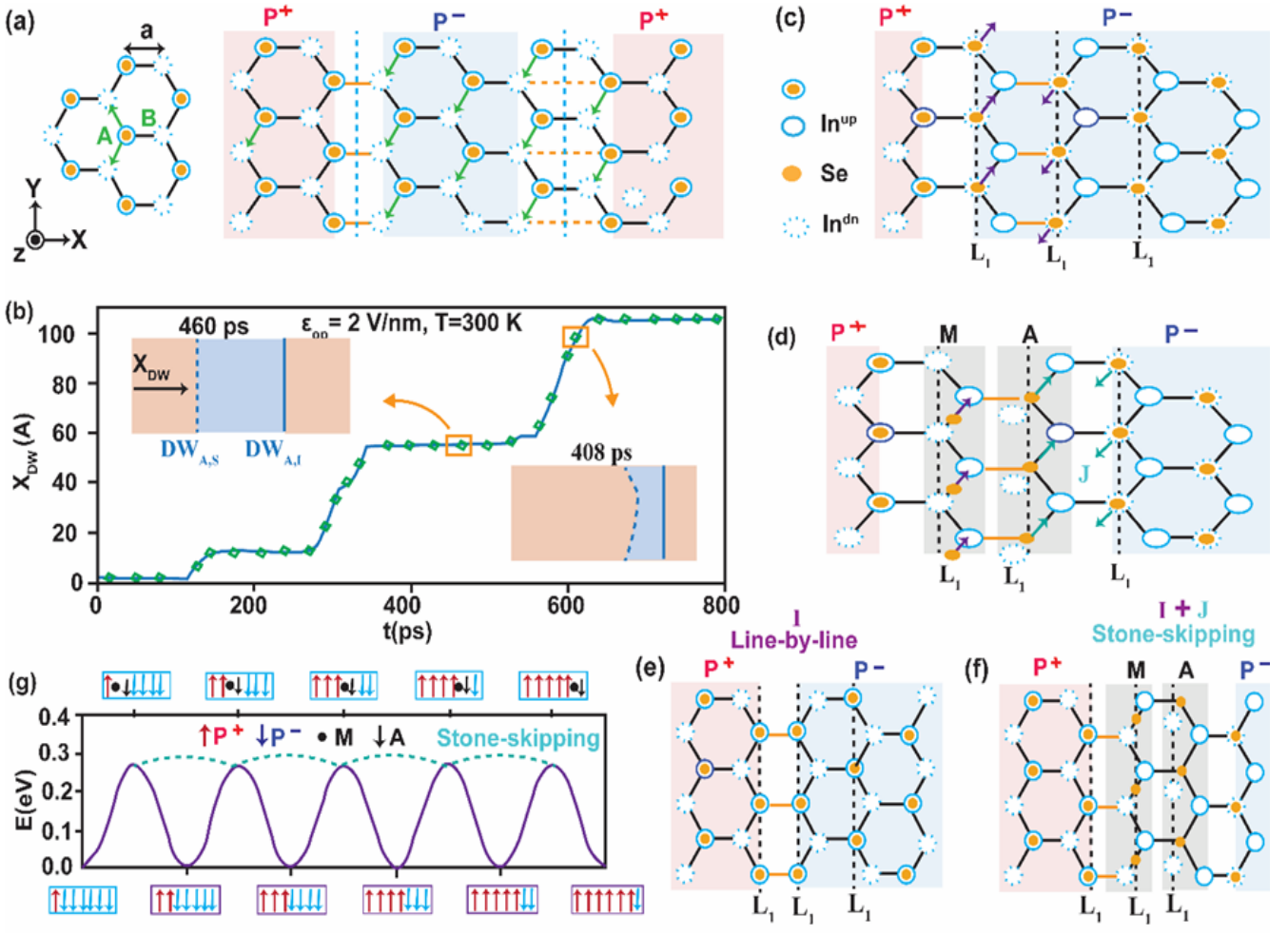

Fig. 5: Avalanche dynamics of one-dimensional domain walls (DWs) in 2D α-In_2Se_3 under an OOP electric field (εOOP).(a) Schematic of 180° domain wall formation separating P^- and P^+ domains, created by IP displacements of middle-layer Se atoms along directions A or B by a lattice constant a, accompanied by OOP shifts that reverse polarization. Type-A domain walls include a narrow wall (DWA,s) with short Se–Se bonds and a wide wall (DWA,1) with larger Se–Se separations. displacement vectors of Se atoms are shown by Green arrows. (b) Averaged position time evolution ($x_(DW)$) of DWA,s under εOOP from molecular dynamics (MD) simulations using a 4000-atom super-cell. DWA,s exhibits abrupt, intermittent motion characteristic of avalanche dynamics, while DWA,1 remains pinned. Error bars reflect geometric roughness. Insets display the increasing curvature of DWA,s at 608 ps and 460 ps, indicating dynamic roughening. (c–f) Two atomic-scale mechanisms for DWA,s motion identified via MD. Under εOOP, DWA,s (c) transitions into a metastable interface (MA) in (d), via coupled transitions at layers L1 and L2. Coordinated atomic rearrangements (paths I and J) result in rapid lateral motion of MA (f), whereas incomplete progression along path J reverts the system to a stepwise, Miller–Weinreich-like motion (e). (g) Schematic energy profiles comparing the conventional line-by-line (solid) and the "stone-skipping" (dashed) mechanisms. The intermittent bursts observed in (b) correspond to rapid MA propagation, while quiescent intervals reflect reactivation delays of DWA,s Reproduced form.[65] Copyright 2024, Applied Chemical Society.

Despite significant advances in understanding two-dimensional (2D) ferroelectric materials, several key questions about α- In_2Se_3 remain unresolved and require further experimental and theoretical exploration. These include: (i) existence of switchable persistent in-plane polarization (PIP) in monolayer α- In_2Se_3; (ii) the mechanisms underlying the unusually high OOP switching field observed in 2D α-In_2Se_3, especially in comparison to van der Waals (vdW) bilayers exhibiting stacking-induced ferroelectricity; and (iii) the detailed dynamics of polarization switching within 2D domains and along one-dimensional (1D) domain walls.

Domain-Wall-Assisted (DWA) Ferroelectric Switching. Reference[65] demonstrated that the presence of pre-existing one-dimensional domain walls can significantly lower the coercive field required for polarization switching. Structurally, the two In atom layers in α-In_2Se_3 form a hexagonal lattice analogous to monolayer h-BN when viewed along the OOP direction, with a lattice constant a; central Se atoms occupy a single lattice site. Four distinct 180° domain wall configurations can emerge through in-plane displacements of the middle-layer Se atoms by a, accompanied by out-of-plane shifts that reverse polarization.[65] These domain walls, classified into two pairs (A and B), consist of a wide variant

($DW_{A,l}$) characterized by long Se–Se separations and a narrow variant ($DW_{A,s}$) with shorter Se–Se bonds as shown in Fig. 5(a). Molecular dynamics simulations indicate that only the narrow domain wall ($DW_{A,s}$) is responsive to an applied out-of-plane electric field (ε_OOP), whereas the wide domain wall ($DW_{A,l}$) remains pinned due to a high energy barrier (~0.7 eV). The motion of $DW_{A,s}$, driven by an OOP electric field (ε_{OP}), exhibits avalanche-like dynamics and dynamic roughening, as shown in Fig. 5(b). Initially flat, the domain wall becomes curved during propagation, with a global roughness amplitude of approximately 1.8 Å.

Through the analysis of MD trajectories with femtosecond time resolution, we observe a mechanism akin to 'stone skipping' that accounts for the two intrinsic characteristics of DWA motion, which arise in the absence of defects (disorder pinning). As shown in Fig. 5(c), under the influence of ε_{OP}, a row of Se atoms (L_1) closest to the boundary moves towards the adjacent In^{up} atoms (designated as P^- @$L_1 \rightarrow$ M@L_1). Simultaneously, a line of In^{dn} atoms (L_2) shifts towards the Se atoms of L_1 (denoted as P^-@$L_2 \rightarrow$A@L2). This behavior contrasts with the layer-by-layer switching mechanism initially proposed by Weinreich and Miller for thelateral motion of 2D domain walls.[79] Notably, the motion of the 1D $DW_{A,S}$ involves two atomic lines and bears resemblance to the proposed 'nuclei stacking' mechanism thought to occur in high-field-induced mobile rough walls, despite being rarely observed.[80] The motion of $DW_{A,S}$ is driven by atomic shifts, with a transient interface M@L1 and A@ L2 and serving as moving front. Particularly, subsequent processes of P^-@L3 → A@L3 and A@$L_2 \rightarrow$ M@L_2, attained by atomic movement pattern J (Fig. 5(d)), efficiently displace the metastable state (MA) interface literally by a distance of a (Fig. 5(f)) while failure to execute movement J leads to a line-by-line switching mechanism with net outcome P^-@$L_1 \rightarrow$ P^+@L_1 (Fig. 5(e)). This “stone skipping”-like mechanism allows the MA interface to overcome a small kinetic barrier, while a larger barrier is needed for $DW_{A,S}$ movement (Fig. 5(g)). This explains the bursts of domain wall motion interspersed with periods of inactivity, with differential movement speeds across the interface contributing to its curvature during motion.

α-In_2Se_3 has shown exceptional stability, retention, and fatigue resistance in nanoscale ferroelectric domains, making it an ideal candidate for non-volatile memory applications. α-In_2Se_3 maintains its polarization states over extended periods, with demonstrating excellent retention of ferroelectric properties, making it suitable for long-term data storage. Additionally, the material exhibits robust fatigue resistance, with ferroelectric field-effect transistors (FeFETs) based on α-In_2Se_3 capable of withstanding over 10^5 switching cycles without significant degradation. Furthermore, modifications to the material, such as incorporating SnPz, have been explored to further enhance its fatigue resistance, with first-principles studies suggesting improved durability and performance. These characteristics position α- In_2Se_3 as a promising material for non-volatile memory technologies, and ongoing research is focused on optimizing these properties to ensure the development of reliable and durable ferroelectric devices.

5. Device applications leveraging coupled polarization

The unique ferroelectric properties of 2D In_2Se_3 offer significant potential for advancing next-generation ferroelectric field-effect transistors (FeFETs), synaptic and neuromorphic devices, and photonic and optoelectronic devices by exploiting the coupled in-plane (IP) and out-of-plane (OOP) polarization mechanisms. These coupled polarization effects enable the design of memory devices with tailored characteristics, making In_2Se_3 an ideal material for applications requiring both high-speed operation and long-term data retention. As shown in Fig.6(a, b), in the OOP memory configuration, the device architecture positions the gate above the In_2Se_3 material, optimizing vertical charge transport and enabling rapid switching speeds. This setup is particularly suited for high-performance applications, such as dynamic memory modules or fast-access caches, where quick data retrieval and processing are paramount. On the other hand, the IP memory configuration places the source and drain terminals within the same plane as the In_2Se_3 substrate, leveraging in-plane polarization to enhance data retention times (Fig.6(a, b)). This design is ideal for non-volatile memory applications, where stability and long-term data retention are crucial. In Fig. 6(c), the performance comparison further illustrates the distinctions, with OOP memory demonstrating high switching speeds but more moderate retention times, making it ideal for applications that demand fast access but not necessarily long-term data storage. In contrast, IP memory strikes a balance, offering a moderate switching speed alongside extended retention times, making it suitable for applications that require both speed and stable data storage. Flash memory, while offering excellent retention, is slower in terms of switching speed and thus better suited for applications where long-term storage is prioritized over fast access. Meanwhile, DRAM provides the fastest switching speed but lacks data retention once power is removed, making it suited for volatile memory applications where speed is essential but data persistence is not needed. The ability to control and optimize both in-plane and out-of-plane polarization in 2D In_2Se_3 offers a promising path forward for creating multifunctional memory devices. By tailoring these polarization effects, it's possible to design memory solutions that excel in both speed and data retention, expanding the range of applications in modern electronics, from high-speed computing to energy-efficient, non-volatile storage. The integration of coupled polarization states thus positions 2D In_2Se_3 as a versatile material for the development of next-generation memory technologies. This section reviews the latest work on 2D In_2Se_3-based devices and discusses the ongoing issues in device development.

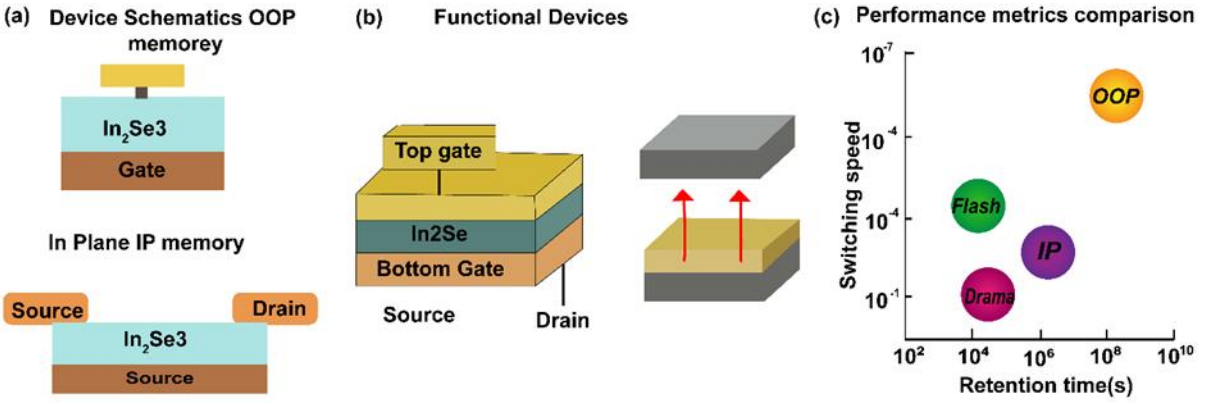

Fig. 6: Device schematic and performance metrics comparison (a) device schematic for OOP and IP memory (b) schematic of functional devices (c) performance metrics comparison of different memories.

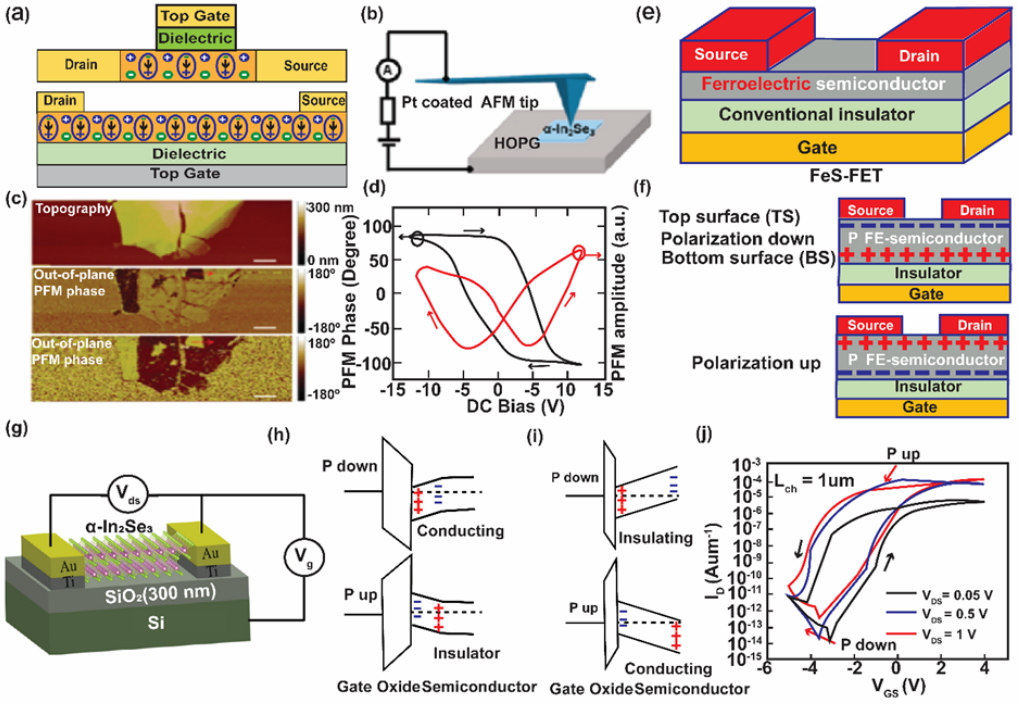

Fig. 7: (a) Schematic representations of typical bottom-gated (lower) and top-gated (upper) FeSFET device arrangements using 2D ferroelectric semiconductor channel layers. (b) Schematic diagram of the PFM test setup with the Pt/In_2Se_3/HOPG structure Reproduced from.[90] Copyright 2023, American Chemical Society. (c) OOP PFM phase (middle), Morphological (top) and IP phase (bottom) with opposing ferroelectric polarization images of In_2Se_3 nanoflakes Reproduced from.[37] (d) Hysteretic response of amplitude and OOP PFM phase under DC tip bias Reproduced from.[37] Copyright 2020, John Wiley & Sons. (e) Schematic of the FeSFET with a ferroelectric semiconductor and conventional gate insulator. (f) Distribution of polarization-bound charges in FeSFETs for downward polarization states under negative gate bias and upward polarization states under positive gate bias. (g) Schematic representation of a ferroelectric semiconductor field-effect transistor. (h) Band diagram of FeSFETs under opposite polarization states with a high effective oxide thickness (EOT). (i-j) Band diagrams of FeSFETs under opposite polarization states with low EOT and counterclockwise hysteretic transfer curves Reproduced from.[7,84] Copyright 2019, Springer Nature.

5.1 Ferroelectric field effect transistors

Ferroelectric semiconductor field-effect transistors (FeSFETs): Development of ferroelectric semiconductor field-effect transistors (FeSFETs), as seen in Fig. 7(a), was a revolutionary device design that capitalized on the discovery of 2D semiconductors, including In_2Se_3,[14] $MoTe_2$,[81] and SnS.[7,82] High-density integration and innovative device architectures are made possible by the substitution of 2D ferroelectric semiconductors for the traditional insulator layer in FeSFETs.[83] Mobile charges effectively screen depolarization field in 2D ferroelectric semiconductor channel, where polarization reversal takes place, in contrast to standard FeFETs.[84] This effectively addresses issues such as charge entrapment and leakage currents in conventional devices[83-86] due to the synergistic combination of ferroelectric and semiconducting properties in 2D materials, as well as their dangling-bond-free surfaces.[43] Following the transfer of CVD-grown α-In_2Se_3 flakes onto a highly oriented pyrolytic

graphite (HOPG) substrate, ferroelectric hysteresis curves were recorded, as depicted in Fig. 7(b). As illustrated in Fig. 7(c),[37] both IP and OOP polarization were detected, confirming the improved stability of α-In_2Se_3 ferroelectricity through OOP/IP polarization interlocking, as opposed to traditional long-range Coulomb interactions[87] and exhibiting the 180° phase shift characteristic of ferroelectric flipping (Fig. 7d). The α-In_2Se_3 semiconductor is a perfect fit for FeSFETs because of its advantageous characteristics, which include a moderate bandgap (~1.39 eV), high T_c (>200°C), and compatibility with large-area synthesis.[22,88,89] Chen *et al*. used α-In_2Se_3 to demonstrate 2D FeSFETs and investigated their performance, as illustrated in Fig. 7(e, f).[84] The interaction between mobile charge carriers and polarization of ferroelectric material, which varies according to the Fermi level (E_x) and the conduction/valence band edges, determines the channel conductance in FeSFETs. As demonstrated by the pronounced clockwise or counterclockwise hysteresis behavior, this interaction influences polarization switching by inducing an electric field distribution across the α-In_2Se_3 layers.[84] The FeSFET structure, which combines memory and processing capabilities for non-volatile memory applications, is shown in Fig. 7(g).

The fabrication process involves mechanically exfoliated α-In_2Se_3 placed on a metal electrode with a 300 nm SiO_2 gate insulator and heavily n-doped silicon serving as the bottom gate. The device features a channel length of 2 μm and a width of 3 μm. The hysteresis loop of the device (Fig. 7(h)) is influenced by the vertical gate electric field with current switching determined by the effective oxide thickness (EOT). In low-EOT FeSFETs with 15 nm HfO_2, the electric field fully polarizes α-In_2Se_3, resulting in electron accumulation at the top surface and producing counterclockwise hysteresis curves (Fig. 7(i)) and a high on/off ratio (>10^8), along with a maximized on-current (862 μA μm^{-1}) (Fig. 7(j)). These FeSFETs, utilizing 2D ferroelectric semiconductors as channel materials, demonstrate significant potential for advancements in memory technology, particularly for non-volatile memory applications.[121]

Ferroelectric gate based field-effect transistor: FeFETs are widely regarded for their fast switching speed,[91-95] nonvolatile properties[96-101] and nondestructive readout process,[102-105] making them significant in memory and computing applications. In 2019, Wan *et al*. introduced a 2D FeFET utilizing α-In_2Se_3 with thicknesses ranging from 2.6 to 70 nm.[45] The device structure, shown in Fig. 8(a) and 8 (b), employs α-In_2Se_3 as the top-gate dielectric while graphene is used as the conducting channel. To improve interface quality and enhance graphene conductivity, a hexagonal boron nitride (h-BN) interlayer is employed. The ferroelectric polarization of α-In_2Se_3 is reversibly switched via the top-gate voltage (V_{TG}), inducing charge carriers in the graphene channel. This results in modulation of the Fermi level and a corresponding change in device resistance. The transfer characteristics,

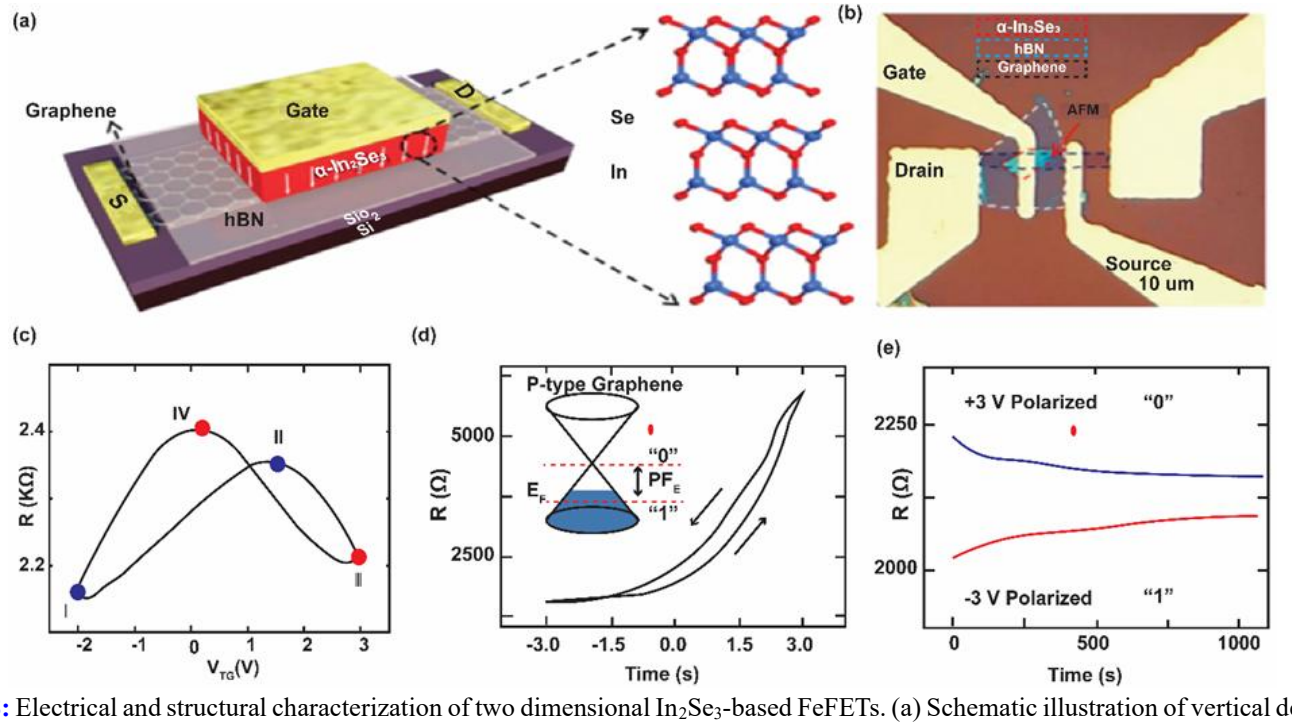

Fig. 8: Electrical and structural characterization of two dimensional In_2Se_3-based FeFETs. (a) Schematic illustration of vertical device architecture comprising α-In_2Se_3, graphene and h-BN. (b) Fabricated device optical micrograph (scale size: 10 μm). (c) Transfer characteristics of the pristine FeFET, exhibiting a butterfly-shaped resistance response as a function of top-gate voltage. (d) p-doped graphene channel FeFET Transfer curve, showing a monotonic resistance change during ferroelectric polarization switching. EF denotes initial Fermi level of p-type graphene; red dashed lines indicate final Fermi levels under opposite polarization states. (e) P-doped FeFET Retention performance, demonstrating stable resistance states over time Reproduced from.[45] © 2019 John Wiley & Sons.

shown in Fig. 8(c), exhibit a hysteresis loop characteristic of ferroelectric behavior. Points I and III represent stable polarization states with aligned electric dipoles, suitable for binary logic encoding, while points II and IV correspond to resistance maxima during polarization reversal.

However, the butterfly-shaped transfer curve complicates the differentiation between resistance states (RP" and RP#). To address this, the channel was replaced with heavily doped p-type graphene, yielding a monotonic resistance variation and significantly enhancing the resistance contrast (ΔR/R) from 1% to 58.5%, as illustrated in Fig. 8(d). Retention testing (Fig. 8(e)) confirms that the resistance states remain distinct for over 1000 seconds post polarization with ±3 V, indicating nonvolatile behavior. Endurance testing further demonstrates reliable performance over 10^5 write/erase cycles. Nevertheless, compared to conventional memory technologies, *i.e.*, phase-change and resistive memories,[106,107] this FeFET exhibits a relatively low on/off ratio (under one order of magnitude) and slower switching speed (~50 ms).[45]

Ferroelectric channel-based field-effect transistor: Ferroelectric layers in traditional ferroelectric field-effect transistors (FeFETs) control the conductivity of a nearby semiconductor channel, as shown in Fig. 9a, top. In a modified architecture created by Si *et al*., known as the ferroelectric semiconductor FET (FeSFET), the ferroelectric semiconductor In_2Se_3 (bandgap: 1.3–2.0 eV, thickness-dependent) serves as both the gate and the channel material at the same time.[30,34,108] This design is shown in Fig. 9a, bottom, and false-color SEM and 3D schematic picture of the device are shown in Fig. 9(b). Through the intrinsic semiconducting and ferroelectric features of In_2Se_3, modulation is made possible in this arrangement, where charge transport is controlled by Fermi level's position in relation to the valence bands and conduction. The operation of FeSFETs is inherently more intricate than that of conventional FeFETs due to interplay between the semiconducting and ferroelectric characteristics of In_2Se_3. Charge accumulation at both the bottom and top surfaces of channel modulates drain current, while ferroelectric switching is influenced not only by the gate voltage but also by carrier dynamics governed by Coulomb screening. This reciprocal interaction allows mobile charges to modulate the polarization state of In_2Se_3. The distribution of the electric field within the channel is further influenced by both the thickness and the dielectric properties of the insulating layer. In thick oxides or low-κ dielectrics devices, polarization remains confined near the channel/insulator interface. For instance, a 90 nm SiO_2 layer results in a clockwise hysteresis loop (Fig. 9c, d). Conversely, reducing the oxide thickness or employing a high-κ material such as 15 nm HfO_2 enables field penetration through the In_2Se_3 channel, activating the top surface and producing a counterclockwise hysteresis (Fig. 9e, f). Performance metrics show that the

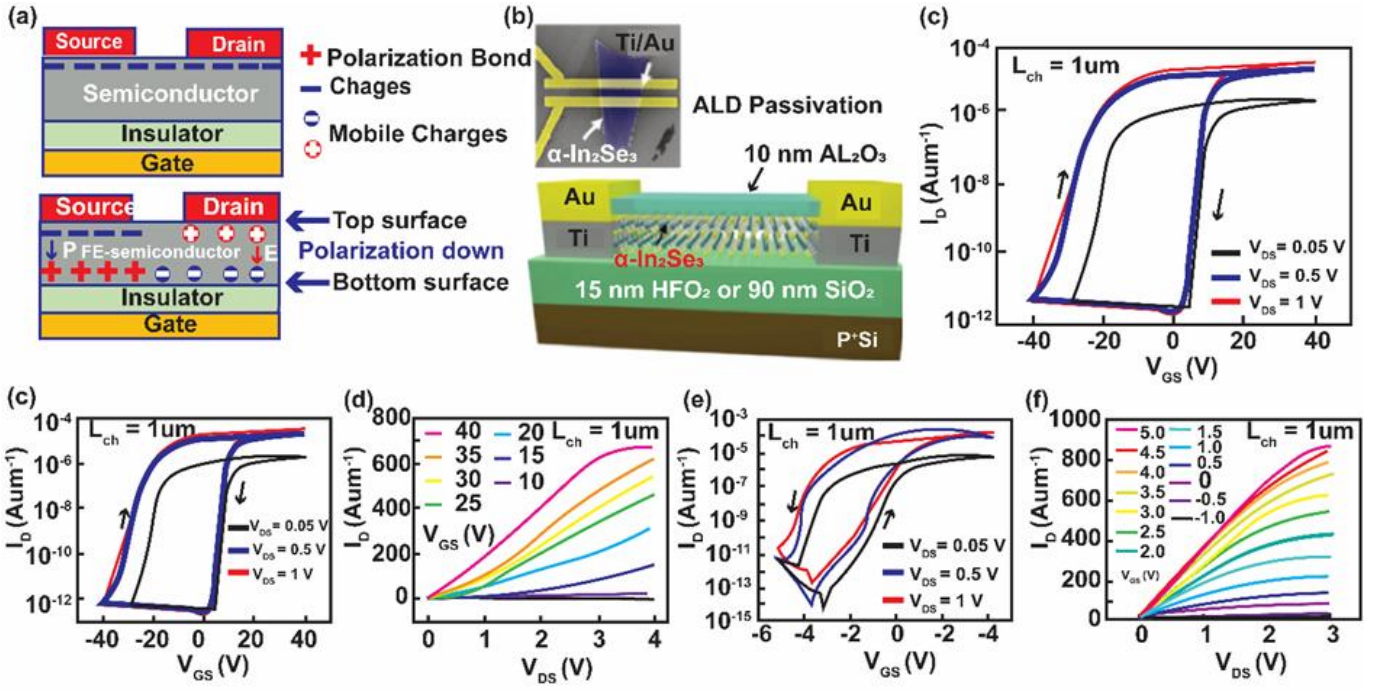

Fig. 9: Electrical and structural characterization of two dimensional ferroelectric FeSFETs. (a) Schematics of FeSFET (lower) and FeFET (upper), with red and blue arrows indicating built-in electric field and spontaneous polarization direction, respectively. (b) 3D schematic and False-color image of two dimensional α-In_2Se_3 FeSFET. (c, d) I_D–V_{DS} and I_D–V_{GS} characteristics of FeSFET using 90 nm gate insulator of SiO_2. The channel thickness and length of α-In_2Se_3 are 52.2 nm and 1 μm, respectively. (e, f) I_D–V_{GS} and I_D–V_{DS} characteristics of the FeSFET using 15 nm thick HfO_2 as the gate insulator. The channel length and thickness of α-In_2Se_3 are 1 μm and 92.1 nm, respectively Reproduced from.[34] Copyright 2019, Springer Nature.

device with 90 nm SiO_2 achieves highest drain current of 671 μA $μm^{-1}$ at V_G = 40 V, while the device with 15 nm HfO_2 reaches 862 μA $μm^{-1}$ at only 5 V, with an on/off current ratio exceeding 10^8—underscoring its suitability for low-power non-volatile memory applications.[34]

5.2 Synaptic and neromorphic devices

Ferroelectric channel transistors integrating ultrafast memory and neuromorphic computing: Ferroelectric devices, despite having only two polarization states, can record analog signals by controlling the volume of polarization domains, which enables the realization of neuromorphic computing to bypass von Neumann bottleneck.[109] Wang *et al*. (2021) demonstrated a ferroelectric channel field-effect transistor (FeCT) based on α-In_2Se_3, integrating cognitive computing with nonvolatile memory functionality.[16] As illustrated in Fig. 10(a), the device incorporates a 30 nm Al_2O_3 global dielectric deposited via atomic layer deposition (ALD), a 40 nm thick α-In_2Se_3 channel, and an h-BN top-gate dielectric, with a highly p-doped silicon substrate serving as global back gate. The global gate controls the memory function, and its working mechanism is similar to the FeSFET described in section 3.3.[34] The top gate, although also operating similarly to the global gate, exerts a weaker polarization due to its small area, causing it to depolarize to its initial state over time. With repeated pulsing, however, the polarization of the ferroelectric channel strengthens, resulting in nonvolatile polarization.[16] The FeCT device demonstrates both volatile and nonvolatile behaviors, controlled by the top gate, which mimics the long-term and short-term plasticity observed in biological systems, a key feature for neuromorphic computing.[110-113] Fig. 10(b) presents the transfer characteristics of the FeCT, showing a clockwise hysteresis loop that increases as the voltage sweep range expands. It is necessary to keep the gate voltage between -8 and +8 V in order to reach the highest memory window of 6 V. Over 500 program/erase cycles are sustained by the device, which also indicates rewritable nonvolatile current contrast greater than three times of magnitude in Fig. 10(c).

Presynaptic input and postsynaptic current (PSC) are represented by the corresponding channel current and top gate voltage, respectively, in order to emulate neural computing. Synaptic short-term plasticity demonstrates that a brief spike causes a temporary PSC response that rapidly returns to its starting condition. Applying positive and negative voltage pulses, respectively, results in long-term depression and long-term potentiation.[30] Its potential for low-power neuromorphic computing applications is highlighted by calculated power consumption for inhibition and excitation, which are 40 fJ and 234 and per event, respectively.[16] It is noteworthy that this FeCT's OFF current is extremely temperature-sensitive.

The research study on In_2Se_3 -based FeCTs has significantly advanced the integration of memory and computing functions, with notable improvements in write speed (reduced to 40 ns) compared to traditional FeFET

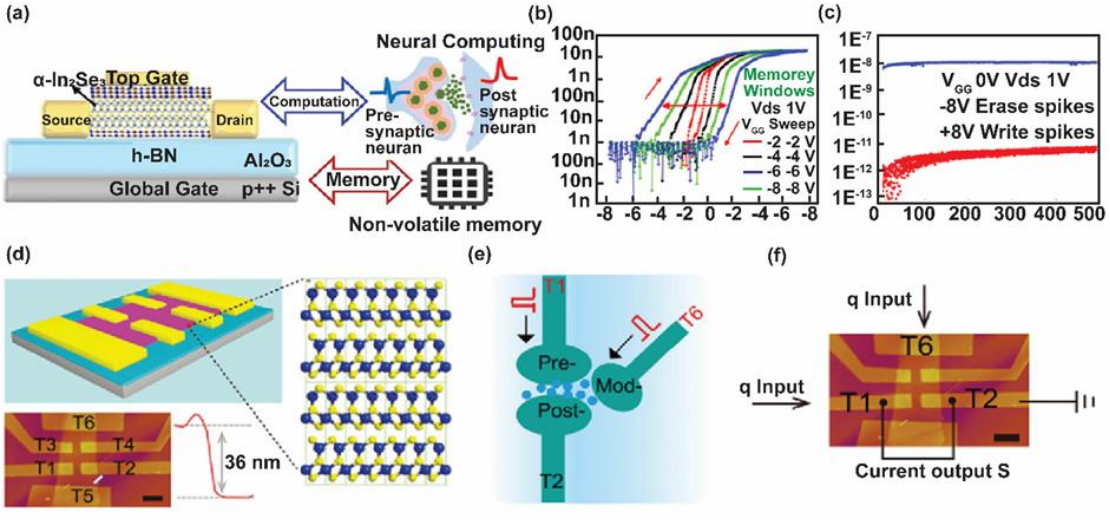

Fig. 10: Structural and functional characterization of 2D FeCTs based on α-In_2Se_3.(a) Schematic of the dual-gated FeCT, where the top gate enables neuromorphic computing and the global gate facilitates nonvolatile memory operation. (b) Transfer characteristics under varying global gate voltages, showing a highest memory window of 6 V within a ±8 V sweep range. (c) Retention performance with an on/off ratio $>10^3$ sustained over 500 s.(d) Endurance test results after 500 program/erase cycles.(e) Programming speed analysis, achieving 40 ns switching with on/off ratio of 10. (f) Transient channel current respond to spike inputs, indicating short-term synaptic plasticity. (g) Emulation of long-term potentiation and depression via progressive excitatory and inhibitory responses at ultra-low voltages. Reproduced with permission from Reproduced from,[16] Copyright 2021 Springer Nature.(h) AFM topography, atomic structure and Schematic of α-In_2Se_3-based ferroelectric memristor (scale size: 2 μm). (i) Schematic of heterosynaptic plasticity involving presynaptic (T1, T2), postsynaptic (T6), and modulatory neurons. (j) Representation of logic variables output s, q and p in the memristive system (scale size: 2 μm). Reproduced with permission from Reproduced from,[111] Copyright 2021 John Wiley & Sons.

memories. The on/off ratio varies with voltage pulse width, increasing from 10 to 103 as pulse width extends from 40 ns to 1 s. Additionally, the FeCT exhibits low energy consumption for computing, at 234 fJ for excitation and 40 fJ for inhibition per spike.[16] In_2Se_3 is also explored for heterosynaptic devices for neuromorphic in-memory computing. A heterosynaptic memristor with an on/off ratio larger than 10^3 was demonstrated by Xue *et al*. (2021), resulting in heterosynaptic plasticity, as illustrated in Fig. 10 (d-f).[111] With a high switching ratio that maintains stability for up to two days, this memristor is nonvolatile in contrast to normal volatile devices. The device's third terminal enables nonvolatile control of the channel current, simulating associative heterosynaptic learning with ultra-low read energy consumption in the picojoule range as shown in Fig. 10 (e). Moreover, device supports Boolean logic operations with picoampere operating currents. This research underscores potential of In_2Se_3 -based ferroelectric devices for neuromorphic and in-memory computing applications, positioning them as promising candidates for overcoming the von Neumann bottleneck.[111]

Gate-tunable Memristor: Memristive devices, recognized as the fourth fundamental circuit component,[30,114,115] have garnered considerable interest due to their potential applications in non-volatile memory, logic computation, and neuromorphic systems. Their performance hinges on controllable resistance switching pathways, which are essential for achieving high ON/OFF ratios. Ferroelectric memristors utilize polarization reversal to encode distinct resistance states, offering advantages such as large ON/OFF ratios, long data retention, and structural simplicity—making them well-suited for digital storage and synaptic emulation.[116,117] These characteristics also align with the demands of high-density memory integration in AI hardware. Nevertheless, challenges remain in realizing multiterminal programmable architectures with consistent performance and low variability. The emergence of 2D ferroelectric semiconductors like α-In_2Se_3 presents a promising direction. With intrinsic ferroelectricity and mobile charge carriers coexisting in the same channel, α-In_2Se_3 enables compact ferroelectric memristor designs that integrate both gate and channel functions. As depicted in Fig. 11(a), a monolayer α-In_2Se_3 consists of a five-layer atomic structure (Se–In–Se–In–Se), maintaining robust room-temperature ferroelectricity due to its non-centrosymmetric configuration.[14,32] Fig. 11(b) shows a two-terminal α-In_2Se_3 memristor, which switches from a low-resistance state (LRS) when the drain voltage is swept from negative to zero, to high-resistance state (HRS) as the voltage increases to a positive maximum. The switching from LRS to HRS demonstrates a high switching ratio of 10^3 when the voltage sweep exceeds 4-5 V. The introduction of a gate to this two-terminal ferroelectric memristor is essential

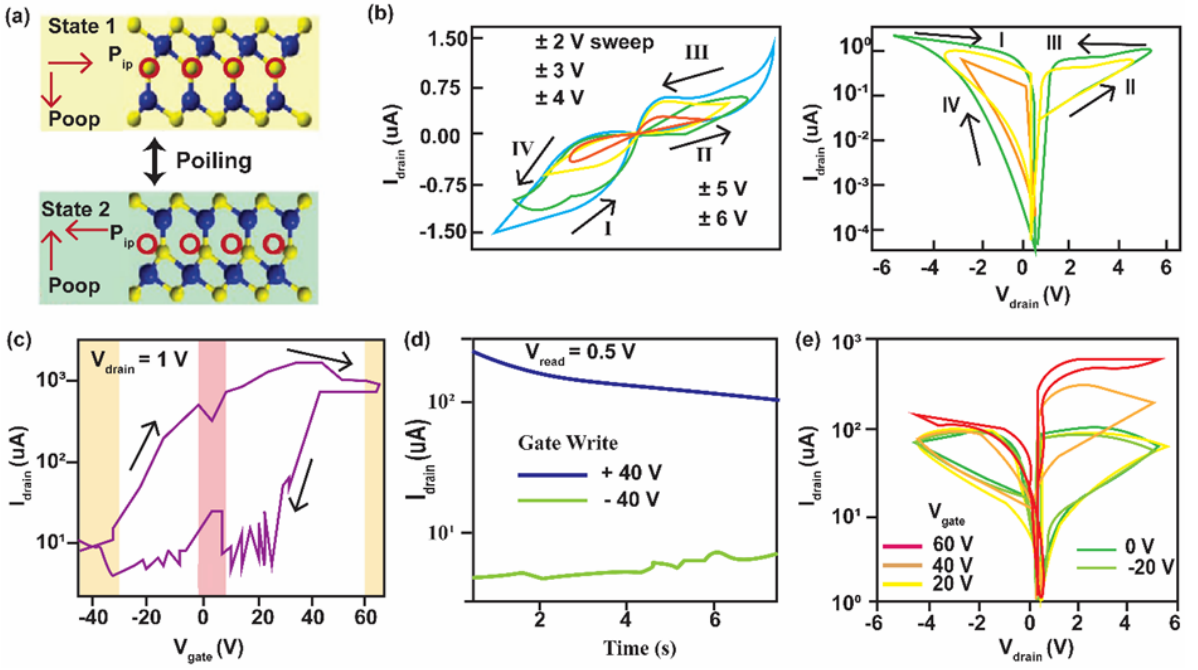

Fig. 11: (a) Schematic illustration of the interlocked IP and OOP ferroelectric polarization switching in α-In_2Se_3 (State 1 → State 2). Indium and Selenium atoms are represented in blue, and yellow, respectively. (b) Pinched hysteresis loops of drain current as function of V_{Drain}, measured with maximum sweep voltages ranging from 2 V to 6 V. Arrows indicate the voltage sweep directions. (c) Gate-tunable α-In_2Se_3 memristor transfer characteristics in response to the vertical electric field. (d) Channel conductance modulation during the reversal of ferroelectric polarization, controlled by the gate bias. The read bias is applied across the drain-source terminal. (e) Output characteristics at various gate voltages. Positive gate voltages notably inhibit resistance switching, while negative gate voltages promote its restoration Reproduced from.[2] Copyright 2019, John Wiley and Sons.

for advancing the device. As shown in Fig. 11(c), the hysteresis transfer characteristics reveal effective regulation of channel conductance through gate-controlled polarization switching. A vertical OOP gate bias above ±35 V switches polarization of α-In_2Se_3, adjusting the channel resistance to LRS or HRS. At gate voltages beyond ±40 V, polarization charge screening reduces the difference between reverse and forward sweeps at 0 V. The connected upward-leftward polarization of α-In_2Se_3 can be reversed by external gate bias, as shown by gate-write/drain-read functionality in Fig. 11(d). As illustrated in Fig. 11(e), these data offer the first proof that resistance switching is optimized by gate-induced polarization switching. The semiconducting nature of α-In_2Se_3 enables current switching ratio of memtransistor to be adjusted, offering excellent tunability in channel conductance and polarization flipping. These properties make α- In_2Se_3 memtransistors promising candidates for future functional electronic applications.

Non-volatile memory: Ferroelectric memories, known for their stable polarization states,[118] hold great potential for non-volatile data storage due to their ability to be electrically written. However, bulk ferroelectric materials frequently experience issues such as poor interface quality and thermodynamic instability, which result from unsaturated dangling bonds. In contrast, two-dimensional (2D) layered ferroelectric devices exhibit enhanced retention, endurance, and greater potential for commercialization. Recently, Lee *et al*. reported a fully van der Waals (vdWs) integrated metal–ferroelectric–insulator–semiconductor (MFIS) field-effect transistor (FET) memory cell fabricated on a 285 nm SiO_2/Si substrate (Fig. 12a).[119] This device employs mechanically exfoliated $CuInP_2S_6$ (CIPS, ~70 nm) as the ferroelectric layer, hexagonal boron nitride (h-BN, ~8 nm) as insulating layer, and indium selenide (InSe, ~10 nm) as channel. The top-gated vdWs FeFET demonstrates a big hysteresis window (Fig. 12b), with an on/off current ratio of 10^4 and a subthreshold slope of 147 mV/dec. Notably, the transfer characteristics reveal a clockwise hysteresis loop, typical of n-type semiconductors, setting it apart from conventional 2D vdW heterostructure FeFETs.[84,120-122] The distinct conduction mechanism in the InSe channel results from the coexistence of polarization-bound charges and mobile carriers, leading to a charge distribution that differs from that in traditional semiconductors. Fig. 12 (c) depicts the band diagrams of the CIPS/h-BN/InSe FeFET structure under forward and reverse gate biases reveal that at negative gate voltages, polarization in both InSe and CIPS layers induces accumulation of mobile electrons at the interface, forming a low-resistance state (LRS). However, due to the high effective oxide thickness of the CIPS/h-BN stack, the electric field is insufficient for complete polarization switching throughout the entire InSe layer, resulting in partial polarization reversal limited to several atomic layers. The strong interfacial dipoles at the CIPS/InSe boundary maintain stable channel resistance states even beyond coercive voltage of CIPS.

The transient response in Fig. 12(d) shows a steady

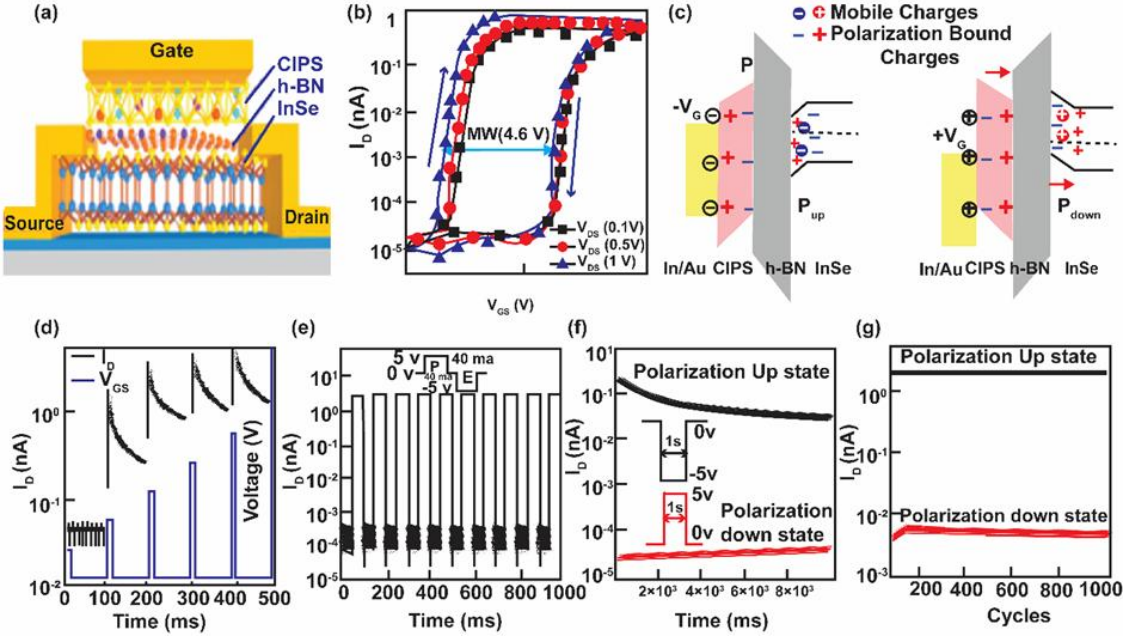

Fig. 12: (a) Schematic of the 2D InSe van der Waals heterostructure (vdWH) FeFET, with $CuInP_2S_6$ (CIPS) as the ferroelectric gate and hexagonal boron nitride (h-BN) as insulating layer. (b) Transfer characteristics of the FeFET under various drain voltages (V_{DS}) during bidirectional gate voltage sweeps. (c) CIPS/h-BN/InSe FeFET Band diagrams under forward and reverse gate biases, illustrating distinct charge accumulation mechanisms. (d) Drain current response as a function of varying gate biases. (e) Dynamic current response under periodic gate voltage modulation, showing program/erase operations. (f) Retention performance (g) endurance over multiple program/erase cycles Reproduced from.[119] Copyright 2022 American Chemical Society.

increase in drain current as gate voltage sweeps from −1 to −5 V, confirming that ferroelectric polarization reversal induces the low-resistance state (LRS). Program/erase (P/E) cycles depicted in Fig. 12(e) demonstrate stable P/E current ratio exceeding 10^3 without degradation at V_{DS} = 1 V. Retention and endurance tests (Fig. 12(f)) reveal consistent channel conductance with minimal current decay over time. Using ±5 V pulses at 50 ms intervals for endurance evaluation, the device maintains nearly unchanged current after 10^3 cycles, sustaining an on/off ratio above 10^3 depicted in Fig. 12(g). Compared to bulk 3D ferroelectrics, the vdWs CIPS/h-BN/InSe heterostructures exhibit enhanced channel modulation, attributed to their reduced interlayer spacing. This leads to a stronger dipole electric field, which scales inversely with the cube of the surface-to-depth distance (R^{-3}).[30,123-125] The device's remarkable durability and stability stem from the synergistic interaction between CIPS and InSe layers, corroborated by piezoresponse force microscopy (PFM), transmission electron microscopy (TEM) and electrical characterization results. The IP ferroelectricity of α-In_2Se_3 has demonstrated considerable promise for non-volatile memory applications. FeSFETs based on α-In_2Se_3 have been fabricated, exhibiting a wide memory window, an on/off current ratio of approximately 30, and robust cycling stability over nearly 500 cycles. These findings highlight the promising potential of α-$In_2Se_3$and similar ferroelectric semiconductors as viable materials for next-generation non-volatile memory devices.

Artificial synapse: FeFET-based brain-like computing hardware has emerged as a leading candidate for future artificial neural networks.[1 2 6] However, neuromorphic synaptic devices made from bulk materials encounter challenges, such as defects and impurities from dangling bonds, which worsen as device dimensions shrink, limiting their stability and performance. In contrast, 2D ferroelectric-based devices, which do not have unpaired surface bonds in the ferroelectric layers, provide better resistance to performance degradation. Lee *et al*. introduced an all-ferroelectric Fe-FET that integrates 2D ferroelectrics in both the gate insulator and channel layers, improving the device's overall stability.[127] As shown in Fig. 13(a), the synaptic device, designed to replicate the behavior of biological synapses, consists of mechanically exfoliated flakes transferred onto a SiO_2/Si substrate. The device includes α-In_2Se_3 (52 nm), h-BN (6 nm), and CIPS (84 nm) layers. Both the FeSFET (α-In_2Se_3/h-BN) and vdWH FeFET (α-In_2Se_3/h-BN/CIPS) show n-type conduction with clockwise hysteresis, but the vdWH FeFET has a significantly larger memory window (Fig. 13(b)). This improvement is attributed to the ferroelectric polarization of CIPS, which enhances channel conduction in α-In_2Se_3. Fig. 13(c) presents the energy band diagrams of the α-In_2Se_3/h-BN/CIPS heterostructure under polarization-up and polarization-down states, elucidating the device operation. Unlike CIPS, which hosts only polarization-bound charges, ferroelectric semiconductors such as α-In_2Se_3 feature both mobile carriers and polarization-bound charges, reflecting their combined semiconducting and ferroelectric nature. The high effective oxide thickness (EOT) of the gate dielectric

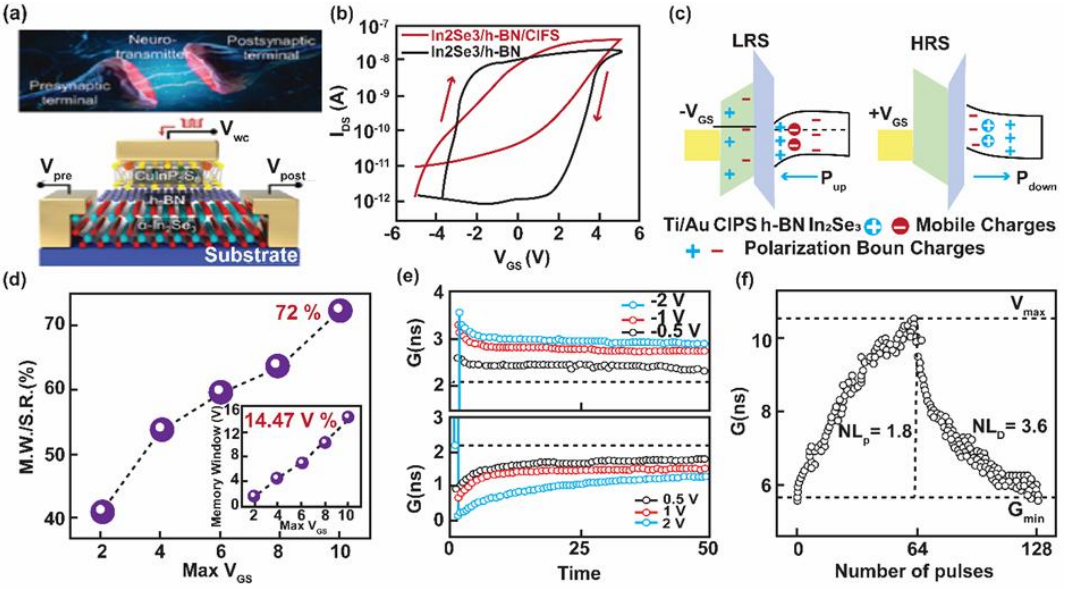

Fig. 13: (a) Schematic diagram of a biological synapse alongside the three-terminal vdW heterostructure α-In_2Se_3h-BN/CIPS FeFET synapse device. (b) Transfer characteristics comparing α-In_2Se_3h-BN/CIPS (black) and α-In_2Se_3/h-BN (red) FeFETs at VDS = 1 V, with the gate voltage varied from −5 to +5 V. (c) Energy band diagrams of the α-In_2Se_3/h-BN/CIPS FeFET under polarization-up (left) and polarization-down (right) conditions. (d) Memory window to sweep range (M.W./S.R.) ratio as a function of maximum gate voltage (VGS), with the inset showing a linear increase in the memory window. (e) Excitatory (EPSC, top) and inhibitory (IPSC, bottom) postsynaptic conductance responses triggered by voltage pulses applied to the weight control terminal (WCT). (f) Conductance modulation during long-term potentiation/depression (LTP/LTD) cycles, with corresponding nonlinearity (NL) values of 1.8 and 3.6 Reproduced from.[129] Copyright 2022, John Wiley & Sons.

restricts full polarization reversal within the α-In_2Se_3channel, resulting in partial switching during gate voltage sweeps. Under negative gate bias, polarization-bound charges in both α-$In_2Se_3$and CIPS align in the polarization-up state, inducing channel accumulation and a low-resistance state. Conversely, positive gate bias switches the system to the polarization-down state, causing channel depletion and a high-resistance state, which collectively produce the observed clockwise hysteresis.

The interlayer coupling between CIPS and α- In_2Se_3 facilitates the alignment of their dipoles under an applied electric field, stabilizing polarization states and expanding the memory window. The ratio of the memory window to the sweep range increases linearly, reaching up to 72% at a memory window of 14.47 V with a gate voltage of 10 V Fig. 13(d). Electrical stimulation at the weight control terminal (WCT) induces partial ferroelectric switching, modulating channel conductivity through potentiation or depression.[128] To assess excitatory and inhibitory postsynaptic current (EPSC and IPSC) behaviors, VWC pulses with amplitudes ranging from ±0.5 to ±2 V and a fixed interval of 100 ms were applied to the WCT, while conductance was measured at a constant post-synaptic voltage (V_{post}) of 1 V as shown in Fig. 13(e). Conductance progressively increases with excitatory pulses and decreases with inhibitory pulses, with notable retention as conductance remains elevated even 50 seconds post-stimulation. Long-term depression and potentiation (LTD/LTP) were evaluated by applying 64 consecutive excitatory and inhibitory pulses. As shown in Fig. 13(f), channel conductance increased from 10.0 to 22.6 nS (nonlinearity factor: 1.8) following potentiation and decreased from 22.6 to 9.31 nS (nonlinearity factor: 3.6) after depression. These observations indicate gradual dipole reversal in both CIPS and α-In_2Se_3 under the electric field, resulting in continuous conductance modulation. The reversible ferroelectric polarization in α-In_2Se_3 enables the realization of artificial neural networks with configurable, multilevel conductance states and near-ideal linearity and low variability in conductance response. Collectively, these results demonstrate strong potential of 2D vdW heterostructure ferroelectrics in FeFETs for next-generation artificial synaptic devices.

In-memory computing: Since data flow between processors and memory has increased due to the growth of data-intensive applications in the artificial intelligence (AI) and Internet of Things (IoT), Von Neumann architectures—also known as the "memory wall"—have experienced severe bandwidth constraints.[130] Through the integration of memory and processing units, in-memory computing offers an effective way to reduce latency and energy consumption, hence mitigating the bottlenecks of Von Neumann systems.[131-133] While traditional in-memory computing utilizes floating-gate charge-trapping mechanisms, 2D ferroelectric-based architectures leverage ferroelectric order parameters to control channel conductivity. These ferroelectric devices offer fast response times and high reliability under external electric stimuli.

Xie *et al*. have reported a metal-oxide-ferroelectric semiconductor field-effect transistor (MOfeS-FET) tailored for in-memory computing applications, incorporating a van der Waals (vdWs) ferroelectric semiconductor InSe channel and an HfO_2 gate dielectric (Fig. 14a).[134] High-resolution scanning transmission electron microscopy (STEM) imaging (Fig. 14(b)) confirms the formation of a sharp, uniform interface devoid of interfacial diffusion or structural degradation. The atomically thin InSe exhibits intrinsic out-of-plane ferroelectric polarization, enabling the coexistence of memory storage and logic functionalities within a single device.[84,119,135,136] Electrical characterization under bidirectional gate voltage sweeps reveals n-type semiconducting functionality with on/off current ratio of 10^6 and a clockwise hysteresis loop in the transfer characteristics (Fig. 14c). A memory window of 3.9 V is observed at a gate voltage of 4 V, indicative of bistable OOP polarization states in the InSe channel (Fig.14d). The device demonstrates robust endurance, maintaining program/erase cycling stability over 100 cycles with reliable switching between high-resistance and low-resistance states (Fig. 14e). Retention measurements confirm sustained low leakage currents in both programmed states (Fig. 14f).

Band structure analyses of the metal– HfO_2 –InSe heterostructure under opposing polarization states (Fig. 14(g, h)) illustrate the modulation of channel conduction by ferroelectric polarization. Application of a positive gate bias induces an upward shift of the energy bands, leading to electron depletion and the high-resistance state, whereas a negative bias results in band lowering, electron accumulation, and the low-resistance state. This mechanism underlies the reversible resistance switching governed by the gate voltage. Moreover, the MOfeS-FET exhibits functional integration of memory and logic operations. Logic gates such as NAND and NOR are implemented by programming the device to distinct resistance states through application of positive or negative gate voltage pulses, representing logic “0” and “1,” respectively. The operation of programmable inverter circuit with 10 GΩ load resistor under ±8 V gate pulses confirm reliable logic inversion (Fig. 14i). NAND and NOR functions are realized using the device’s intrinsic memory and logic capabilities, minimizing transistor count and enhancing device integration density (Fig. 14(j, k)). The corresponding truth table (Fig. 14(l)) validates the accuracy of logical operations, highlighting the potential of this MOfeS-FET platform for future compact and energy-efficient non-volatile memory and in-memory computing applications.

Table 1 provides the performance metrics for device based on 2D In_2Se_3, such as FeFETs, FeSFETs, Synaptic Devices and Memristors. These metrics include key values such as switching speeds, endurance and retention times.

In order to provide a concise comparison of the performance characteristics of 2D α-In_2Se_3-based devices, key metrics relevant to ferroelectric memory and neuromorphic

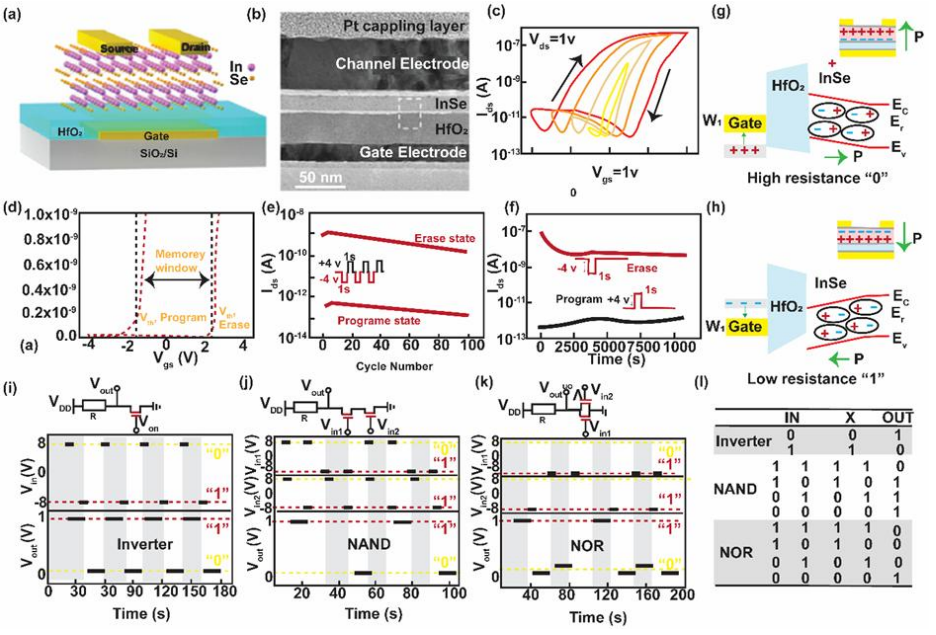

Fig. 14: (a) Schematic diagram and (b) cross-sectional STEM image of the 2D InSe MOfeS-FET device. (c) Transfer characteristics measured under bidirectional gate voltage sweeps, showing increasing clockwise hysteresis with higher V_{GS}, indicative of enhanced out-of-plane ferroelectric polarization. (d) Transfer curves corresponding to program and erase states; the memory window is defined by threshold voltage difference between these states. (e) Endurance performance over 100 cycles of alternating program (4 V, 1 s) and erase (−4 V, 1 s) pulses. (f) Retention characteristics with current read at V_{GS} = V_{DS} = 1 V. (g, h) Band diagrams of the metal/$Hf O_2$/InSe heterostructure under (LRS and HRS ferroelectric polarization orientations, respectively. (i–k) Schematics of programmable logic circuits demonstrating inverter (i), NAND (j), and NOR (k) operations. (l) Truth table of NOR, inverter and NAND gates, with V_{GS} = 3 V and output voltages measured at V_{DD} = 1. Inverter each resistor and logic circuits has a resistance of 10 GΩ Reproduced from.[134] Copyright 2023, American Chemical Society

Table 1: Performance metrics for 2D In_2Se_3-based device applications.

Metric	FeFETs	FeSFET)	Synaptic Devices	Memristors
Switching Speed (Rise Time)	50–100 ns	50–100 ns	10–40 ms	1 ms
Endurance (Switching Cycles)	$>10^5$ cycles	$>10^5$ cycles	$>10^4$ cycles	$>10^4$ cycles
Retention Time	$>10^6$ seconds	$>10^6$ seconds	$>10^6$ seconds	$>10^6$ seconds

Table 2: Performance summary of 2D α-In_2Se_3-based ferroelectric memory and neuromorphic computing systems.

Device	Performance Metric	Value/Range	Application
FeFETs (Ferroelectric Field-Effect Transistors)	Switching Speed (Rise Time)	50–100 ns	Non-volatile memory devices, logic circuits
	Endurance (Switching Cycles)	$>10^5$ cycles	Long-term data storage
	Retention Time	$>10^6$ seconds	Non-volatile memory
	On/Off Ratio	$>10^8$	High-contrast switching for memory operation
FeS-FETs (Ferroelectric Channel Transistors)	Switching Speed (Rise Time)	50–100 ns	High-speed computing, low-power devices
	Endurance	$>10^5$ cycles	Non-volatile memory
	Retention Time	$>10^6$ seconds	Long-term stable data storage
	Memory Window	>6 V	Analog memory, synaptic devices
Synaptic Devices	Switching Speed (Rise Time)	10–40 ms	Neuromorphic computing, AI hardware
	Endurance (Programming Cycles)	$>10^4$ cycles	Learning and memory functions in neuromorphic systems
	Energy Consumption per Event	40 fJ (inhibition), 234 fJ (excitation)	Low-power computing in neuromorphic systems

Device	Performance Metric	Value/Range	Application
Memristors	Switching Ratio (On/Off)	$>10^3$	Non-volatile memory, logic circuits
	Endurance	$>10^4$ cycles	Stable and durable data storage
	Retention Time	$>10^6$ seconds	Long-term stable data retention
	Switching Speed	1 ms	High-speed memory and logic devices
Optoelectronic Devices	Switching Speed	50 ns to 100 ns	Optical communication, photodetectors
	Responsivity (Photocurrent)	0.1–1 A/W	Light-sensitive memory, photovoltaics
	Energy Consumption	100–200 μW	Energy-efficient optoelectronics

computing systems are summarized in Table 2. This table includes switching speed, endurance, retention time, and other important parameters for various device types, such as FeFETs, FeS-FETs, synaptic devices, memristors, and optoelectronic devices. These performance metrics are critical for evaluating the potential of α-In_2Se_3 in applications such as non-volatile memory, high-speed computing, and energy-efficient neuromorphic systems.

5.3 Photonic and Optpelectronic Devices

α-In_2Se_3 has gained significant attention as a promising material for optoelectronic applications due to its unique combination of properties, including a direct bandgap (~1.3 eV), strong photoluminescence, and high absorption coefficient. These properties make it an excellent candidate for a wide range of optoelectronic devices, such as photodetectors, photovoltaics, and light-emitting devices (LEDs). According to,[137] α-In_2Se_3 exhibits efficient charge carrier generation upon light absorption, making it suitable for high-performance photodetectors and solar cells. Its ability to absorb light in the visible and near-infrared regions, combined with its direct bandgap, results in high photocurrent efficiency, positioning it as a key material for optoelectronic sensors and infrared optoelectronics, such as night vision and medical diagnostics. The material's strong photoluminescence also enables its use in light-emitting diodes (LEDs) and lasers, with tunable emission wavelengths depending on the material thickness, offering potential for both visible and infrared optoelectronics. In addition, Fang *et al*. (2021) further highlight that the material's nonlinear optical response is beneficial for the development of optical modulators and switches, which are essential for high-speed data transmission and telecommunication systems.[138] Furthermore, the integration of α-In_2Se_3 with other 2D materials enhances its properties, making it an ideal candidate for hybrid optoelectronic devices. These devices leverage the advantages of multiple materials, offering superior performance in areas like photovoltaics, optical communication, and low-power computing. α-In_2Se_3 also demonstrates impressive stability, maintaining its performance over extended periods, which is crucial for long-term data retention in non-volatile memory applications, further expanding its potential in neuromorphic computing systems.[138] Overall, α-In_2Se_3's combination of high absorption efficiency, nonlinear optical properties, and compatibility with other 2D materials makes it a versatile material for advancing next-generation optoelectronic devices, neuromorphic systems, and energy-efficient computing technologies.

Polarization Induced Bulk Photovoltaic Effect in $\alpha - In_2Se_3$: The photovoltaic effect (BPVE) is the ability of non-centrosymmetric materials to produce spontaneous photocurrents when continuously illuminated. By operating p-n or Schottky junctions independently, BPVE enables homogeneous materials to produce a spontaneous current under uniform light, in contrast to typical photovoltaic effect, which based on built-in electric fields from these junctions to separate photoexcited carriers. This characteristic allows for zero-bias operation and has the potential to surpass the Shockley-Queisser limit in photoelectric conversion efficiency, as it is not limited by the bandgap of optical absorption semiconductors.[139,140] Additionally, BPVE shows great promise for polarization detection due to its typical sensitivity to the polarization of incident light.[141-144] BPVE-based devices are gaining attention for their simple fabrication and high quantum efficiency, making them ideal for energy collection and photoelectric detection.[145-147]

Strong light absorption and photoelectric response are guaranteed by multilayer α-In_2Se_3, which has a direct bandgap of about 1.4 eV and is therefore a good material for BPVE applications.[148] I-V characteristics of α-In_2Se_3-based devices were studied under homogeneous laser irradiation at various polarization states in order to investigate relationship between the photocurrent and polarization direction in BPVE. In the absence of light, a straight I-V curve intersecting origin was seen, as seen in Fig. 15(a). In accordance with normal BPVE behavior, linear I-V curves with significant spontaneous photocurrents at zero bias were seen in a variety of polarization states upon illumination with a 637 nm laser at 5.1 W/cm^2 power density. The qualitative analysis was unaffected by slight variations in I(V) data for light and downward polarization (P_{down}), which were ascribed to the device's susceptibility to outside influences. Interestingly, a zero-bias photocurrent in fresh state suggested spontaneous downward polarization in α-In_2Se_3, which is in line with the asymmetry of the PFM loop and SHG observations. Additionally, a negative spontaneous photocurrent was detected when α-In_2Se_3 was polarized downward by applying +2 V, but a positive photocurrent was regulated by a −2 V poling voltage. This decrease in photocurrent during upward polarization is attributed to charge transfer between α-In_2Se_3

layers and graphene, which lowers the electric dipoles in α-In_2Se_3.[14] The I-V characteristics during polarization switching revealed different short-circuit photocurrent (I_{sc}) values for oppositely polarized configurations (−66.7 and 23.5 pA). Increasing the light power density and photoresponse area or annealing the electrode-ferroelectric layer contact could be two ways to improve the photocurrent. Because of their low optical conductivity, the open-circuit voltage (V_{oc}) in various polarization states was −23 mV and 31 mV, respectively. This is lower than that of conventional ferroelectrics.[149,150] Photocurrents produced by the Schottky photovoltaic effect at the graphene/α-In_2Se_3 interface cancel each other out due to the symmetric graphene contacts. Therefore, BPVE is a primary mechanism in the devices, and it is principally responsible for spontaneous photocurrents. Furthermore, spontaneous photocurrent direction can be reversed with polarization direction, this feature also seen in other ferroelectric materials, and the BPVE in α-In_2Se_3 can be regulated by applying external electric field.[147,151-154]

To investigate the physical mechanism behind ferroelectric-modulated BPVE, energy band diagrams of the multi-layer graphene (MLG)/α-In_2Se_3/MLG heterostructure are shown in Fig. 15(b). When a voltage is applied to the top MLG, polarization is induced in α-In_2Se_3, causing the Se atoms to shift off-center and generate an out-of-plane polarization that opposes the built-in electric field (E_{bi}). As a result, the vacuum levels on either side of α-In_2Se_3 shift, causing the energy bands to tilt. This out-of-plane polarization alters the chemical potential of graphene, inducing equal amounts of charge with opposite polarities in the top and bottom MLG electrodes. As a result, a significant Isc is generated when the device is illuminated, as E_{bi} separates the photo-generated electron-hole pairs, which then drift toward the interface and are collected by the graphene electrodes. The direction of I_{sc} can be controlled by adjusting the polarization direction. The device was scanned under a focussed 520 nm laser beam to create a spatial distribution map of I_{sc}, which further validated the presence of BPVE in α-IIn_2Se_3 as shown in Fig. 15(c). A negative polarity indicates downward polarization within α-In2Se3, and the current mapping in Fig. 15(d) only shows non-zero I_{sc} within overlapping region of bottom and top MLG electrodes. Uniform BPVE incidence is implied by uniform I_{sc} generation in the overlapping region. Outside this region, I_{sc} was negligible, excluding contributions from the Schottky photovoltaic effect. These results are consistent with observations in another 2D ferroelectric material, $CuInP_2S_6$[147,154] α-In_2Se_3 offers stable IP and OOP polarization, enhanced polarization stability, and the ability to maintain a single-domain state in ultra-thin films, which distinguishes it from $CuInP_2S_6$.[24] These features, along with

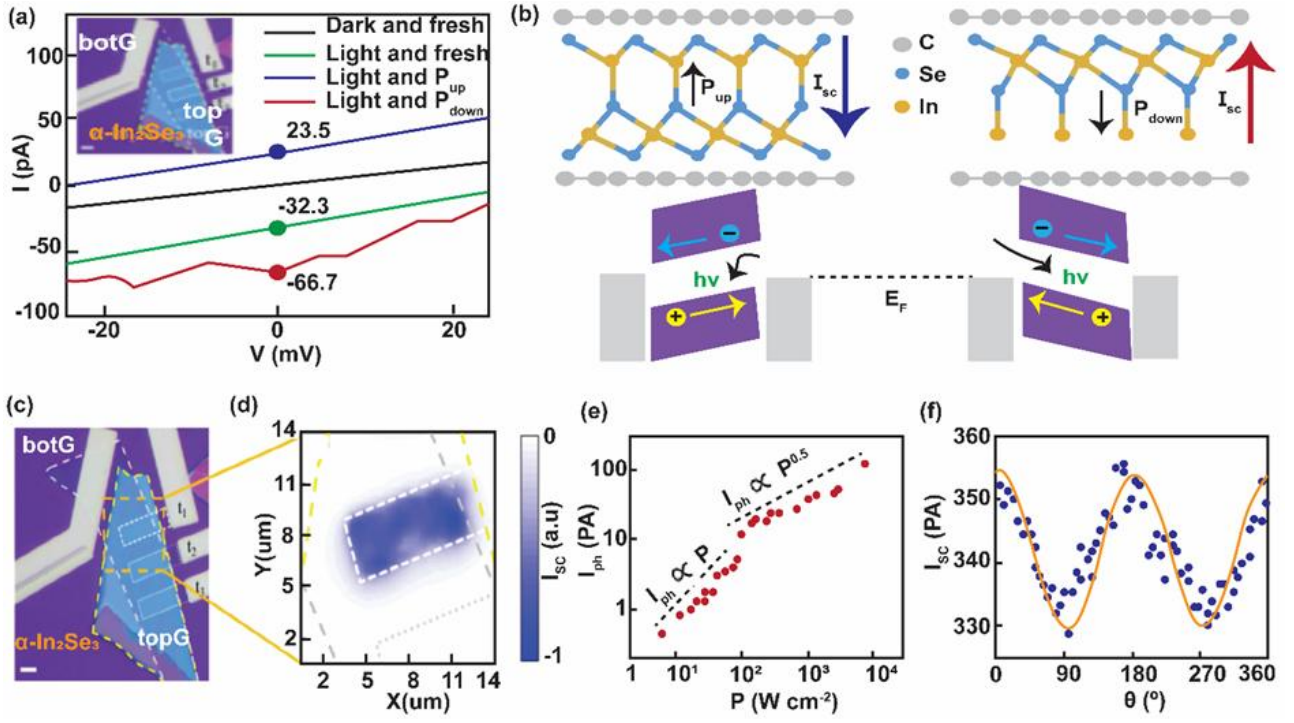

Fig. 15: Direction of switchable photocurrent in α-In_2Se_3 thin layers driven by BPVE. (a) I-V characteristics of MLG/α-In_2Se_3/MLG device under dark (black) and illuminated (colored) conditions. The blue red and green curves correspond to the upward, downward and fresh polarization states, respectively. Inset: Optical image of device (scale size = 4 μm). (b) Band diagram of device in upward and downward polarization states, with arrows indicating polarization and short-circuit photocurrent (I_{sc}) directions. (c) Optical image of device (scale size = 4 μm). (d) Normalized I_{sc} mapping in overlapping area near top and bottom graphene contacts. (e) Spontaneous photocurrent dependence on laser power density (520 nm). Inset: Laser spot position on the device (scale size = 4 μm). (f) Polarization dependence of I_{sc}, with experimental data fitted by a cosine function Reproduced from.[159]

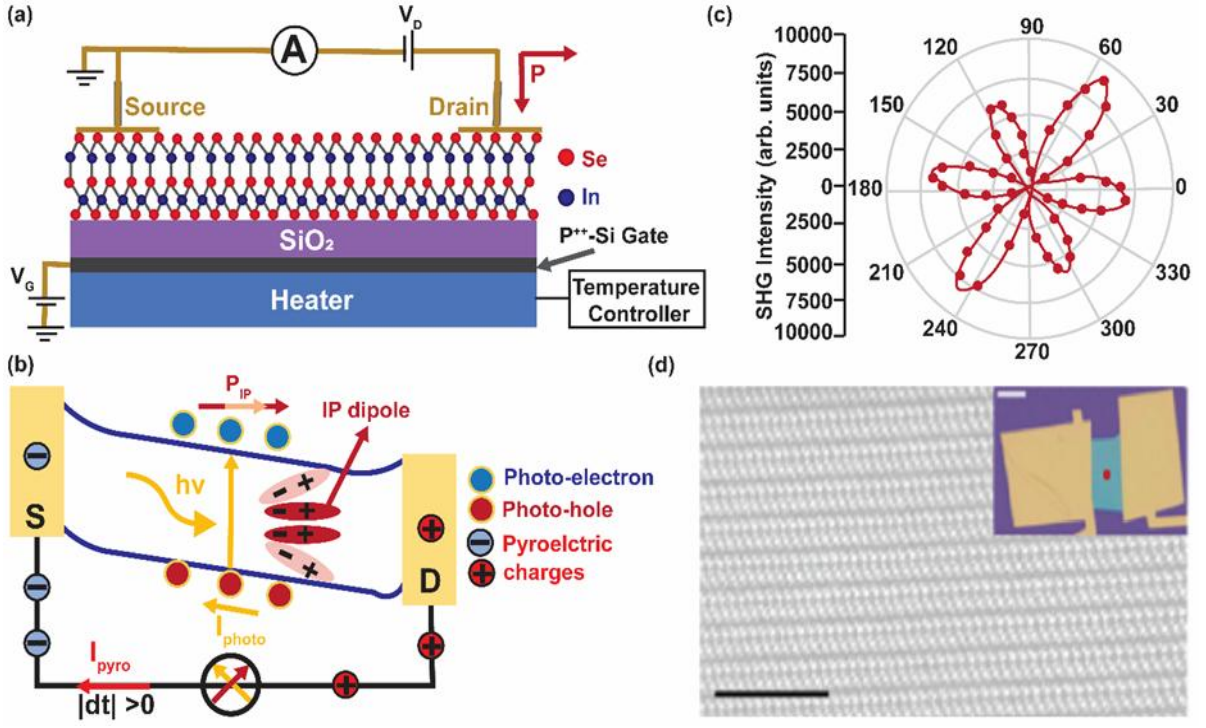

Fig. 16: α-In_2Se_3 -based device characterization. (a) Pyroelectric-photovoltaic measurement setup and Schematic of the α-In_2Se_3 based FET device. (b) Band structure diagram showing the coexistence of photovoltaic effects and pyroelectric (c) Polar plot of excitation laser polarization (s-s polarization) versus SHG intensity. (d) Cross-sectional HRTEM image of α-In_2Se_3 with R3m space group symmetry (scale size = 5 nm). Inset: Optical image of device, with red point marking measurement area from (c) (scale size = 10 μm) Reproduced from.[17]

α- In_2Se_3 's higher Curie temperature,[155] lower coercive field,[31] and broader light response spectrum due to its smaller bandgap, make it an ideal material for high-temperature and low-power photodetection applications.

The photocurrent's dependence on laser power density (P) was investigated to explore its origin. The spontaneous photocurrent (I_{ph}) was calculated by averaging the photocurrent from I-t curves under chopped laser irradiation using a focused 520 nm laser with a 1 μm diameter. The power dependence, plotted on a log-log scale in Fig. 15(e), showed a transition from linear to square-root dependence at approximately 103 Wcm^{-2}. This transition indicates that the shift current mechanism is responsible for the photocurrent generated by BPVE.[156] The shift current mechanism (I_{ph} / |E| / $P^{0.5}$) explains the nonlinear behavior observed at higher power densities, while the linear increase at lower power densities suggests a second-order optoelectronic response to the light's electric field (I_{ph} / $|E|^2$ / P).[157] It was confirmed that BPVE is absent in devices with horizontal α-In_2Se_3 structures, as they did not exhibit this power density dependence.[44,158] This MLG/α-In_2Se_3/MLG device enables polarization-resolved photodetection at zero bias, utilizing BPVE and anisotropic nature of α-In_2Se_3. Prior to polarization testing, the device was vacuum-annealed to enhance interface contact. A 520 nm laser with a power density of 273.6 W/cm^2 was used to measure the I_{sc} dependence on the linear polarization direction of the input laser beam, as illustrated in Fig. 15(f).[159]

Coupled pyroelectric-photovoltaic effect in 2D-ferroelctric α−In_2Se_3: Solar energy harvesting and sophisticated broadband sensors both heavily rely on the pyroelectric and photovoltaic phenomena. In two-dimensional (2D) materials, recent advancements have demonstrated potential of BPVE, which can exceed the Shockley-Queisser limit. Superior pyroelectric response is provided by 2D ferroelectrics, including α−In_2Se_3, due to their room-temperature ferroelectricity, high thermal conductivity, and atomic thickness. Direct pyroelectric-photovoltaic measurements of 2D α- In_2Se_3 were integrated in,[17] yielding ~135.9 m^2/C figure of merit and ~30.7 mC/m^2K significant pyroelectric coefficient. These findings show a linked pyroelectric-photovoltaic action, in which short-circuit current tracks pyroelectric current and temperature follows the temperature derivative. Temperature-induced variations in spontaneous polarization give rise to the pyroelectric effect, whereby the net dipole moment produces capacitive current proportional to the temperature derivative over time (dT/dt). For waste heat-energy harvesting and self-powered infrared thermal sensing, this effect is essential.[160,161] Because ferroelectric films must be made smaller for the nanoelectronics industry, 2D materials' low heat capacity and ultra-low thickness produce a reduced thermal time constant that improves pyroelectric responsivity.[162] A back-gated field-effect transistor (FET) based on α-In_2Se_3 was subjected to direct pyroelectric tests in[17] in both light and dark environments. The figure of merit (~135.9 m^2/C) and extracted pyroelectric coefficient (~30.7 mC/m^2K) demonstrate remarkable thermal-sensing

performance, outperforming traditional materials.[163]

The intrinsic semiconducting nature and IP polarization of α-In_2Se_3 present BPVE under light illumination, allowing for self-powered energy-harvesting devices without requiring the creation of complex heterostructures to form p-n junctions. The coupled pyroelectric-photovoltaic phenomenon was particularly noteworthy, where the pyroelectric current is governed by the temperature derivative, and the short-circuit current responds to temperature modulation. To achieve non-volatile switching of the short-circuit current polarity, the IP polarization in α-In_2Se_3 was regulated by the back-gate electrode. The results highlight the strong sensitivity of both pyroelectric and photovoltaic effects to temperature, allowing a single device to simultaneously track changes in both temperature and its derivatives. This method makes it possible to create monolithic, integrated photovoltaic-pyroelectric elements for optoelectronic in-memory and thermal-sensing applications. The experimental configuration is depicted in Fig. 16(a), where a programmable heating stage was utilized to support the back-gated FET. Illumination of the device was achieved using a broadband white LED source with a wavelength range of 420–720 nm, providing an intensity of approximately 332 μW/cm^2. The pyroelectric and photoelectric currents were measured using a semiconductor parameter analyzer (Keysight B1500A). Fig. 16(b) presents a schematic illustration of the energy band structure and the current generation mechanism in the pyroelectric-photovoltaic α-In_2Se_3 device under both light exposure and temperature variations. Fluctuations in temperature in the absence of light result in variations in the net dipole moment, which in turn generates capacitive currents that balance the differences in bound charges. When illuminated, photogenerated electron-hole pairs are separated by the intrinsic in-plane (IP) ferroelectric field, leading to the production of a short-circuit current in the In_2Se_3 semiconductor. As the temperature increases, a reduction in ferroelectric polarization causes a decrease in photocurrent. Hence, the short-circuit current follows the modulation of temperature, while the pyroelectric current corresponds to the temperature derivative. The six-fold inversion symmetry breaking of the IP polarization in α-In_2Se_3 is verified by the angular-dependent second-harmonic generation (SHG) polar plot of normal incident light prior to device poling (Fig. 16c, with the optical microscope image shown in Fig. 16d). The cross-sectional high-resolution transmission electron microscopy (HRTEM) image (Fig. 16d) confirms the R3m space group of the 3R α-In_2Se_3 phase, while the six-fold angular symmetry of the SHG plot is also consistent with this result.[23,32,76]

Switchable Photodetectors: A switchable photodetector functions by employing a mechanism that enables it to alternate between different detection modes, typically photovoltaic (PV) and photoconductive (PC) modes. This capability is made possible by a material system that can dynamically adjust its electrical properties, often controlled by an external input such as a gate voltage, which alters the polarization or charge distribution within the device. In PV mode, the device generates photocurrent in response to incident light without requiring an external bias, while in PC mode, an applied bias is necessary to generate photocurrent. The transition between these modes is usually non-volatile, meaning the device retains its configuration even after the external input is removed. This switchable feature allows the device to perform advanced functions, such as logic operations, by using the modes as inputs. These photodetectors offer excellent light sensitivity, wide spectral range, and fast response times, making them versatile for various optoelectronic applications, including energy-efficient photodetection and integrated logic circuits.

In,[164] a FeS-PD based on 2D α-In_2Se_3/WSe2 van der Waals heterojunctions is developed, taking advantage of the ferroelectric-tunable conductance of 2D α-In_2Se_3 (Fig. 17(a)). An optical micrograph of the ferroelectric switchable photodetector (FeS-PD) is shown in Fig. 17(b), where the junction area of the device measures 30 μm². The α-In_2Se_3/WSe2 vdW heterostructures are fabricated using mechanical exfoliation and a PDMS-assisted dry transfer process. WSe2 is placed on the surface of α-In_2Se_3, and two Au electrodes are deposited on both α- In_2Se_3 and WSe2, serving as the source (S) and drain (D) electrodes. Raman spectra taken from various regions of the fabricated device, shown in Fig. 17(c), confirm the high quality of the heterostructure. Atomic force microscopy (AFM) (Fig. 17(d)) is used to measure the thickness of the flakes, revealing thicknesses of ≈37 nm for α-In_2Se_3 and ≈10 nm for WSe2, as indicated by height profiles in the inset image (additional details on the device fabrication are provided in the experimental section). Kelvin Probe Force Microscopy (KPFM) is employed to measure the surface potential difference (SPD) between the two materials and assess the relative positioning of their Fermi levels. The results show that the surface potential of α-In_2Se_3 is approximately 30 mV higher than that of WSe2 (Fig. 17e). Fig. 17(f) illustrates the band alignment of the heterostructure, with electron affinities of 3.6 eV for In_2Se_3 and 4.0 eV for WSe2. The bandgaps of In2Se3 and WSe2 are approximately 1.45 eV and 1.50 eV, respectively. This configuration results in a type-II band alignment between In_2Se_3 and WSe2.

In the designed FeS-PD, the photodetection mode can be switched between the photovoltaic (PV) and photoconductive (PC) modes by applying a gate voltage pulse (Vp). Typically, PV photodetectors provide open circuit voltage (Voc) and short circuit current (Isc) outputs without requiring an external bias, while PC photodetectors require an external bias to generate a photocurrent (Y). In contrast to conventional photodetector designs, which struggle to achieve freely switchable modes due to the fixed potential in the device, this switchable operation mode offers two distinct Voc states (1 for PV and 0 for PC), which is crucial for utilizing the bias as an input.

While α-In_2Se_3 shows considerable promise for

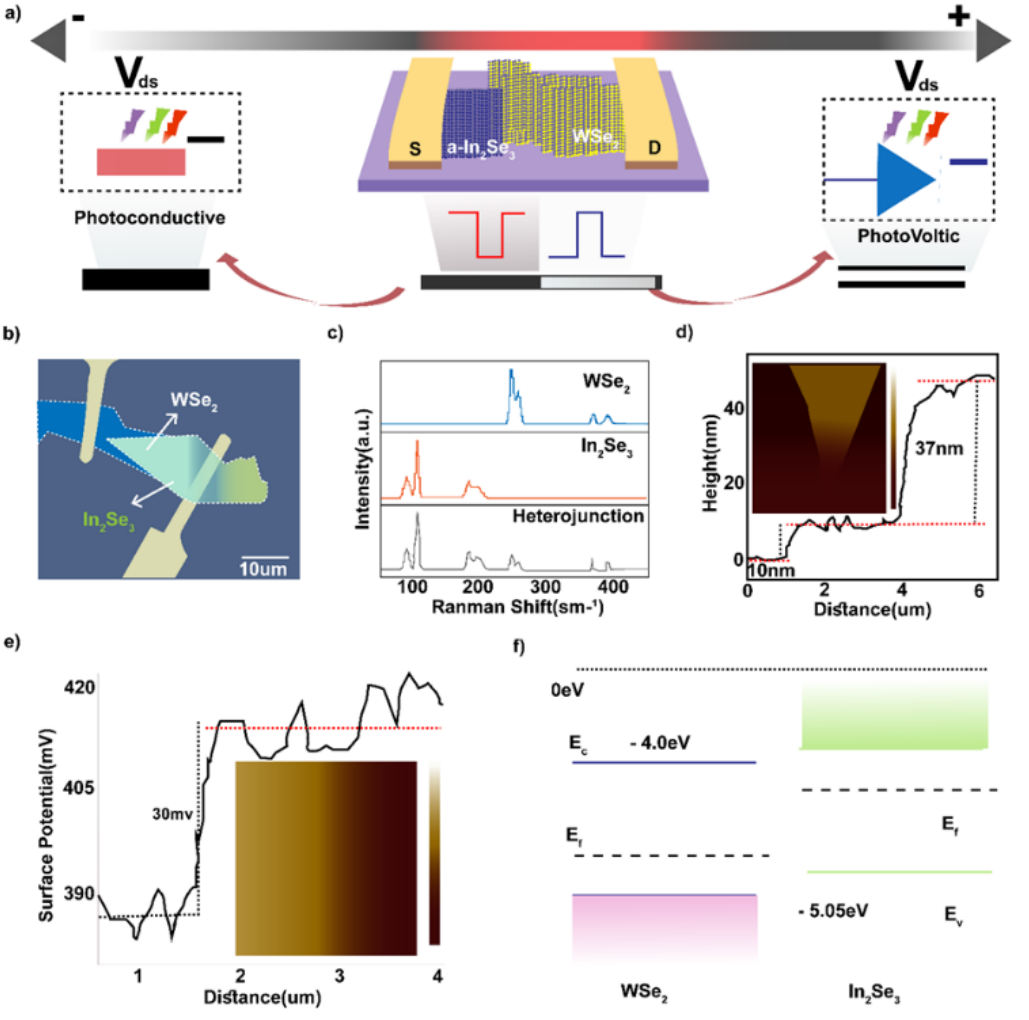

Fig. 17: a) The conceptual illustration of a single device realizing complex optoelectronic logic functions b) Image for optical micrograph of stacked In_2Se_3/WSe_2 heterostructure. b) Raman spectra of WSe_2, In_2Se_3, and In_2Se_3/WSe_2 heterostructure. c) AFM characterization of In_2Se_3/WSe_2 heterostructure. d) KPFM image acquired under dark conditions. e) Energy level alignment of p-type WSe_2 and n-type In_2Se_3 before contact Reproduced from.[164] Copyright 2025, Wily Online Library.

Table 3: Key advances in 2D In_2Se_3 research and development.

Finding	Method	Technique	Year
Demonstration of a coupled pyroelectric-photovoltaic effect in 2D α-In_2Se_3, with a gigantic pyroelectric coefficient and stable short-circuit current switching.[17]	Mechanical exfoliation	Pyroelectric-photovoltaic effect measurements, figure of merit analysis	2025
Observation of the bulk photovoltaic effect (BPVE) in 2D α-In_2Se_3 multilayer flakes.[166]	Mechanical exfoliation	Spontaneous photocurrent measurement, vacuum annealing	2025
Dismisses previous claims of in-plane ferroelectricity in α-In_2Se_3 and reveals vertical polarization switching.[65]	Atomic modeling	PFM, symmetry analysis, molecular dynamics simulations	2024
Exploration of nonvolatile switching between junction configurations and enhanced photogenerated carrier separation in α-In_2Se_3−MoS_2 heterostructures.[21]	Van der Waals epitaxy	Photoluminescence measurements, edge state actuation mechanism	2023
Demonstration of a planar ferroelectric-semiconductor heterojunction (FeS-HJ) FET using α-In_2Se_3 and In_2O_3, with strong sensitivity to visible-to-near-infrared illumination.[42]	Van der Waals epitaxy	KPFM, electrical probing	2022
Exploring the reversible antiferroelctric (AFE) and OOP ferroelectric phase transition in 2D In_2Se_3.[66]	Van der Waals epitaxy	TEM	2022
Exploring the underlying mechanisms of ferroelectric resistance switching in α-In_2Se_3 memristors.[167]	Mechanical exfoliation	Electrical measurements, AFM, and PFM	2021

Finding	Method	Technique	Year
Discovery of a new pseudo-centrosymmetric phase and Mexican-hat PES of 2D In_2Se_3.[168]	Atomic modeling	DFT	2021
Investigating the microscopic operational mechanisms of the α-In_2Se_3 ferroelectric memristor.[169]	Mechanical exfoliation	PFM and KPFM	2021
Showcasing a nonvolatile ferroelectric domain wall engineered by optical means.[48]	Mechanical exfoliation	PFM and electrical characterizations	2020
Exploring planar and vertical ferroelectric memristors utilizing α-In_2Se_3.[2]	Mechanical exfoliation	PFM and electrical measurements	2019
Scalable energy-efficient synaptic crossbar.[46]	Chemical vapor transport	PFM and electrical measurements	2019
Development of FeSFET using 2D α-In_2Se_3 as channel material.[34]	Mechanical exfoliation	I–V characteristics and PFM	2019
Exhibition of nonvolatile memory effect in the 2D In_2Se_3 FeFET.[45]	Chemical vapor deposition	Electric measurements	2019
Detection of IP ferroelectricity in β′-In_2Se_3.[22]	Mechanical exfoliation	LEEM, PFM, STM, and DFT	2018
Demonstration of switchable room-temperature ferroelectric diode based on 2D α-In_2Se_3.[31]	Mechanical exfoliation	PFM and I–V characteristic	2018
Unveiling the dipole locking mechanism between in-plane and out-of-plane polarization.[32]	Mechanical exfoliation, van der Waals epitaxy	PFM and SHG	2018
Simultaneous presence of in-plane and out-of-plane piezoelectricity in α-In_2Se_3 from monolayer to bulk.[33]	Mechanical exfoliation	piezoelectric current measurements, SHG, and PFM	2018
Detection of in-plane and out-of-plane ferroelectricity in 2D α-In_2Se_3 at room temperature.[24]	Chemical vapor deposition	PFM, electrical measurements and DFT	2018
Demonstration of out-of-plane piezoelectricity and ferroelectricity in layered 2D In_2Se_3 nanoflakes.[23]	van der Waals epitaxy	I–V measurements, PFM and AFM	2017
Forecasting the existence of intrinsic 2D ferroelectrics in In_2Se_3.[14]	Atomic modeling	DFT	2017
Gate-controlled high-gain phototransistors with photocurrent based on 2D In_2Se_3[170]	Mechanical exfoliation	AFM and optoelectronic measurements	2015
Tailored synthesis of high-quality 2D In_2Se_3[171]	Physical vapor deposition	photocurrent measurements, TEM and Raman/PL spectra	2015
Revelation of the dynamic stability of 2D In_2Se_3[59]	Atomic modeling	DFT	2015
Strong response to visible light[172]	Mechanical exfoliation	Photocurrent measurements	2014
Atomically thin In_2Se_3 flakes Controlled growth[173]	van der Waals epitaxy	AFM, I–V characteristic, Electron microscopy	2013

optoelectronic applications due to its direct bandgap, high absorption coefficient, and strong photoluminescence, it does have certain drawbacks compared to other 2D materials. One significant limitation is its relatively low electron mobility, which can hinder its performance in high-speed optoelectronic devices, such as photodetectors and solar cells, where materials like graphene or transition metal dichalcogenides (TMDs) often outperform it in terms of charge carrier mobility.[138] Additionally, α-In_2Se_3's stability under ambient conditions is a concern, as it is more prone to degradation compared to more robust 2D materials like MoS_2, which exhibit better environmental stability and resistance to oxidation. Furthermore, while α-In_2Se_3 offers a tunablebandgap, it still has limitations in terms of scalable production and integration into large-area devices, which remains a challenge when compared to other 2D materials that have well-established fabrication methods.[165] Despite these drawbacks, ongoing research into improving its material properties, such as doping and heterostructure engineering, holds potential for overcoming these limitations and enhancing its applicability in optoelectronic systems. Table 3 summarizes significant findings and advancements in 2D α In_2Se_3research, highlighting the synthesis methods, experimental techniques, and key discoveries made over the years. It includes developments in ferroelectricity, piezoelectricity, photovoltaic effects, and memristor functionality, along with innovations in fabrication techniques such as mechanical exfoliation and van der Waals epitaxy. These advances pave the way for future applications in non-volatile memory, phototransistors, and neuromorphic computing.

6. Challenges and strategies for integration

To bridge the gap between the applications of ferroelectric 2D In_2Se_3 and the challenges associated with its integration into next-generation electronic devices, it is essential to consider the practical aspects of deploying this material in real-world systems. While the previous section highlighted the promising

potential of In_2Se_3in various applications, its successful commercialization and widespread use depend on overcoming several key challenges. These challenges span from maintaining phase stability during fabrication to ensuring environmental resilience and achieving compatibility with existing IC platforms. Addressing these hurdles requires innovative strategies that combine material science, fabrication techniques, and device engineering to unlock the full potential of ferroelectric 2D In_2Se_3. Below, we explore these challenges in detail and propose strategies to overcome them for reliable, large-scale integration.

(1) Phase Stability and Reproducibility During Fabrication: The phase stability of In_2Se_3 during fabrication is a critical challenge due to the material's susceptibility to environmental conditions, such as temperature and pressure variations. In particular, maintaining the ferroelectric properties of the material at the nanoscale in a reproducible manner requires precise control over the synthesis process. Strategies to address this challenge include optimizing the growth conditions for high-quality monolayers or few-layer In_2Se_3 using methods like chemical vapor deposition (CVD) or molecular beam epitaxy (MBE). The incorporation of buffer layers or controlled post-synthesis annealing processes may help to stabilize the ferroelectric phase while minimizing defects that could hinder performance. Additionally, advanced in-situ characterization techniques, such as synchrotron X-ray diffraction or Raman spectroscopy, can be employed to monitor phase transitions in real-time during fabrication, ensuring consistent phase stability and reproducibility across multiple batches.

(2) Interface and Contact Engineering for Reliable Devices: The interface between In_2Se_3 and other materials in electronic devices poses a significant challenge due to the high sensitivity of the material's ferroelectric properties to surface defects and contact resistance. For reliable device performance, minimizing interfacial charge traps and ensuring stable contact are essential. Strategies to overcome this challenge include designing and fabricating optimized electrode materials that form strong, low-resistance contacts with In_2Se_3 without compromising its polarization behavior. In particular, materials with high work function compatibility, such as platinum or gold, can be explored, while the introduction of passivation layers at the interfaces can help reduce surface charge traps. Moreover, the use of van der Waals heterostructures and optimized electrode geometries can help preserve the ferroelectric properties and minimize contact-induced degradation.

(3) Environmental Stability and Encapsulation Techniques: Environmental stability is a key concern when integrating In_2Se_3-based devices, as 2D materials are highly susceptible to degradation from factors such as humidity, oxygen, and UV exposure. To maintain the ferroelectric properties of In_2Se_3 over time, effective encapsulation techniques are required to protect the material from the surrounding environment. Strategies include encapsulating In_2Se_3 with inert 2D materials such as hexagonal boron nitride (h-BN) or graphene to provide a protective barrier while maintaining the material's electrical properties. Additionally, the development of flexible and transparent encapsulation layers that can shield In_2Se_3 from moisture and other environmental factors without compromising device performance is an important avenue for enhancing long-term stability. Tailoring the thickness and composition of the encapsulating materials can be crucial for ensuring both the mechanical integrity and the ferroelectric functionality of the device.

(4) Toward Monolithic Integration with Existing IC Platforms: For the successful integration of ferroelectric 2D In_2Se_3into existing integrated circuit (IC) platforms, several challenges must be addressed, including compatibility with standard CMOS processes, scalability, and device architecture. One of the primary goals is to achieve seamless monolithic integration, where In_2Se_3can function alongside traditional silicon-based components. This requires careful design of heterostructures that allow for efficient charge transport and low-loss switching while minimizing the impact on the performance of existing devices. Strategies for achieving this include developing low-temperature processing techniques for In_2Se_3 deposition, which would be compatible with conventional CMOS fabrication processes, and using In_2Se_3 as a non-volatile memory or logic element in combination with standard Si-based transistors. Furthermore, research into the scalable production of high-quality In_2Se_3 monolayers is critical for realizing large-scale integration without compromising performance or increasing costs. A clear summary of the key challenges and proposed strategies provided in Table 4 for the integration of 2D α-In_2Se_3 into practical electronic devices. This table summarizes the critical areas that require attention and the corresponding material/device engineering strategies to address these challenges.

7. Outlook and future directions

The exploration of 2D α-In_2Se_3 as a ferroelectric material has opened up exciting opportunities for next-generation electronics. However, to fully realize its potential, several key open questions and opportunities remain in the development and integration of this material into practical applications.

1) Phase Engineering, Domain-Wall Conduction, Dynamic Polarization Control: One of the most pressing challenges lies in understanding and controlling the different crystalline phases of α-In_2Se_3, such as the α, β, and γ polymorphs, which exhibit distinct polarization behaviors. More research is required to explore the phase transitions and their impact on ferroelectric switching. Additionally, domain-wall conduction—especially in ultrathin 2D materials—remains an underexplored area, which could provide insights into speeding up switching times and enhancing device performance. Dynamic polarization control, including the interplay between in-plane and out-of-plane polarization, is also an area of critical importance. Unlocking the mechanisms

Table 4: Summary of challenges and proposed material/device engineering strategies.

Challenges	Proposed Material/Device Engineering Strategies
Phase Stability and Reproducibility	• Optimize growth conditions (*e.g.*, temperature, pressure) for high-quality monolayers/few-layers. • Use controlled annealing and buffer layers to stabilize desired ferroelectric phase. • Employ advanced in-situ characterization methods (*e.g.*, synchrotron X-ray diffraction, Raman spectroscopy) to monitor phase transitions in real-time. • Design high-work-function electrode materials (*e.g.*, platinum, gold) to ensure low-resistance contacts. • Implement passivation layers to minimize surface charge traps and enhance device stability. • Explore van der Waals heterostructures to preserve ferroelectric properties while improving contact quality.
Environmental Stability and Encapsulation	• Use 2D materials like h-BN or graphene for encapsulation to protect In_2Se_3 from moisture and oxygen while maintaining electrical properties. • Develop flexible, transparent encapsulation layers to ensure device performance in various environmental conditions. • Investigate hybrid encapsulation solutions to optimize long-term stability and resilience.
Toward Monolithic Integration with IC Platforms	• Develop low-temperature processing techniques to integrate α-In_2Se_3 with conventional CMOS processes. • Research scalable fabrication techniques for large-area In_2Se_3 monolayers to meet industrial demands. • Design hybrid devices combining 2D ferroelectrics with other materials (*e.g.*, graphene, TMDs) for improved scalability, switching speed, and endurance.
Switching Speed and Performance Optimization	• Investigate mechanisms to accelerate domain wall motion and reduce switching time (*e.g.*, carrier relaxation, strain engineering). • Optimize in-plane and out-of-plane polarization coupling to enhance switching dynamics. • Explore doping and strain engineering to enhance the material's ferroelectric response and decrease energy dissipation.
Scalability and Reliability in Device Fabrication	• Focus on improving reproducibility during synthesis for large-scale production. • Investigate the use of 2D ferroelectric semiconductors in next-generation FeFETs and memristors for integration into logic and memory devices. • Optimize the design and reliability of devices for high-density, low-power applications, with minimal degradation over time.

that govern polarization switching in real-time could pave the way for more precise and faster memory and logic devices.

2) Opportunities in Logic-Memory Fusion, Adaptive Electronics, and AI Hardware: The unique properties of 2D α-In_2Se_3 present compelling opportunities for logic-memory fusion, where non-volatile memory can be seamlessly integrated with logic functions. This hybrid architecture could lead to significant advancements in energy-efficient and high-speed computing, eliminating the need for separate memory and processing units. Furthermore, α-In_2Se_3's ability to undergo polarization switching with low energy dissipation offers opportunities for adaptive electronics, where devices can reconfigure their functionality based on the application. The adaptability of these materials also makes them highly attractive for neuromorphic computing and AI hardware, where learning and memory processes are modeled after biological systems.

3) Roadmap for Industrial Implementation of 2D In_2Se_3 Ferroelectric Devices: For α-In_2Se_3-based devices to be industrially viable, several steps are required. A key part of this roadmap involves scaling up synthesis techniques to produce high-quality, large-area 2D α-In_2Se_3 sheets in a reproducible and cost-effective manner. Ensuring compatibility with existing semiconductor fabrication processes, such as CMOS technology, is also crucial for smooth integration into the industry. Furthermore, addressing challenges related to device reliability, such as minimizing charge trapping, leakage currents, and interface quality, will be necessary for the commercialization of 2D α-In_2Se_3-based ferroelectric devices. Collaborative efforts across academia, industry, and research institutions will be essential to overcome these barriers and expedite the path to large-scale implementation.

8. Conclusion

In conclusion, 2D α-In_2Se_3 has emerged as a transformative material with significant potential for next-generation electronic devices, particularly in the fields of non-volatile memory, neuromorphic computing, and advanced logic circuits. Its unique ferroelectric properties, including the coupled in-plane and out-of-plane polarization mechanisms, offer new opportunities for device performance enhancement and innovation. The material's ability to maintain stable ferroelectricity at the monolayer scale, combined with its high Curie temperature and robust switching dynamics, sets it apart from traditional ferroelectric materials, making it ideal for integration into ultrathin, high-performance devices. However, despite its promise, key challenges remain in harnessing the full potential of 2D α-In_2Se_3. These include improving the

understanding of its complex phase behavior, optimizing switching dynamics for faster operation, and addressing issues related to scalability, stability, and integration with existing semiconductor technologies. Further research is needed to unravel the detailed mechanisms governing its ferroelectric switching, to fine-tune device architectures, and to ensure reliable performance under real-world conditions. Moving forward, the successful integration of 2D α-In_2Se_3 into practical, large-scale applications will require addressing these challenges through a combination of advanced material design, novel fabrication techniques, and innovative device engineering. With continued advancements, 2D α-In_2Se_3 is poised to play a central role in the development of energy-efficient, high-performance memory systems, neuromorphic computing platforms, and hybrid logic-memory devices, pushing the boundaries of what is achievable in modern electronics.

Looking ahead, several key avenues of research will be essential to unlock the full potential of α-In_2Se_3. First and foremost, in-depth investigations into the material's phase stability and switching dynamics are necessary to understand and optimize its ferroelectric behavior, particularly at the monolayer scale. This includes gaining a clearer understanding of the mechanisms driving polarization switching, such as the interplay between in-plane and out-of-plane polarization components, and how these affect device performance under varying operational conditions. By refining our knowledge of these fundamental processes, we can enhance the material's reliability and performance in practical applications. Furthermore, scaling up the production of α-In_2Se_3-based devices is crucial for their commercial viability. Robust fabrication techniques that can reliably produce large-area, high-quality α-In_2Se_3 films with uniform properties across devices will be necessary for their integration into real-world applications. This will involve overcoming challenges in material synthesis, including controlling defects, ensuring consistent phase purity, and optimizing the growth of α-In_2Se_3 at different thicknesses and across various substrates. Another critical challenge for the widespread adoption of α-In_2Se_3 is its integration with existing semiconductor technologies. To enable its use in large-scale commercial devices, research efforts must focus on improving material interfaces and addressing issues related to encapsulation and device reliability. Moreover, α-In_2Se_3 must be compatible with CMOS technology, as it needs to integrate seamlessly into current electronic platforms. Addressing these compatibility challenges will be key to bridging the gap between fundamental research and practical applications, particularly in fields like non-volatile memory and advanced computing. In addition, the exploration of α-In_2Se_3 in neuromorphic computing systems represents an exciting direction for future research. The coupled polarization properties of α-In_2Se_3 could be leveraged to develop novel synaptic devices, memristors, and in-memory computing architectures that mimic the functioning of biological synapses. Such devices would offer significant advantages in terms of energy efficiency, speed, and the ability to perform complex computational tasks in real-time, making them ideal candidates for artificial intelligence (AI) applications. Furthermore, α-In_2Se_3 could play a pivotal role in overcoming the limitations of traditional von Neumann architectures by enabling the co-location of memory and processing units, thus addressing the bottleneck in data transfer and latency that currently hampers many computing systems. As these research efforts progress, α-In_2Se_3 holds the potential to be a transformative material for a wide range of high-performance, energy-efficient electronic devices. With continued optimization of its properties and the development of novel fabrication and integration techniques, α-In_2Se_3 could lead the way for the next generation of non-volatile memory, reconfigurable logic devices, and advanced computational systems. The continued advancement of this material not only promises to impact fundamental science but also has the potential to catalyze the development of new electronic architectures, driving innovations across industries from data storage to AI, and beyond.

Acknowledgments

This work was supported in part by Construction of Key Technology Innovation Talent Team for Micro-Nano Information Devices and Integrated Circuits in Guizhou Province BQW [2024]014; Functional Materials and Devices Technology Innovation Team of Guizhou Province University, Qian Jiaoji [2023]058; Guizhou Provincial Scientists Workstation of Photovoltaic Materials and Devices KXJZ [2024]031.

Conflict of Interest

The authors declare that they have no known conflict of interest interests or personal relationships that could have appeared to influence the work reported in this paper.

Supporting Information

Not applicable.

CRediT Statement

Muhammad Faizan: Responsible for data curation, Formal analysis, Investigation, Resources, Software, and Writing – Original draft. **Jinshun Bi:** Responsible for overall funding acquisition, Investigation, Methodology, Supervision, and Writing – Review & editing. **Xuefei Liu**, **Jinbo Pang**, **Mingqiang Liu** and **Sania Niaz:** Responsible for conceptualization, Formal analysis, Funding acquisition, Investigation, Writing Original - draft and Visualization. **Ghulam Abbas Khan** and **Abuduwayiti Aierken:** Responsible for investigation, Project administration, and Visualization. **Changsong Gao**, **Degui Wang**, **Gang Wang** and **Yan Wu:** Responsible for formal analysis, Conceptualization and Validation.

References

[1] Z. Li, Y. Chen, J. Yuan, W. Xu, X. Yang, H. Wang, C. Cai, T. Taniguchi, K. Watanabe, Y. Guo, Z. Liu, W. Ren, Ferroelectric switching behavior in two-dimensional semiconductor α-In_2Se_3 for nonvolatile memory, *ACS Applied Electronic Materials*, 2024, **6**, 2507-2513, doi: 10.1021/acsaelm.4c00136.

[2] F. Xue, X. He, J. R. D. Retamal, A. Han, J. Zhang, Z. Liu, J.-K. Huang, W. Hu, V. Tung, J.-H. He, L.-J. Li, X. Zhang, Gate-tunable and multidirection-switchable memristive phenomena in a van der waals ferroelectric, *Advanced Materials*, 2019, **31**, 1901300, doi: 10.1002/adma.201901300.

[3] M. A. Zidan, J. P. Strachan, W. D. Lu, The future of electronics based on memristive systems, *Nature Electronics*, 2018, **1**, 22-29, doi: 10.1038/s41928-017-0006-8.

[4] B. Liu, F. Lyu, B. Tang, X. Li, J. Liao, Q. Chen, Contact properties of two-dimensional ferroelectric α-In_2Se_3, *ACS Applied Electronic Materials*, 2021, **3**, 4604-4610, doi: 10.1021/acsaelm.1c00724.

[5] Z. Zhao, V. Buscaglia, M. Viviani, M. T. Buscaglia, L. Mitoseriu, A. Testino, M. Nygren, M. Johnsson, P. Nanni, Grain-size effects on the ferroelectric behavior of dense nanocrystalline $BaTiO_3$ ceramics, *Physical Review B*, 2004, **70**, 024107, doi: 10.1103/physrevb.70.024107.

[6] Spaldin, N.A., Fundamental size limits in ferroelectricity, *Science*, 2004, **304**, 1606-1607, doi: 10.1126/science.1099822

[7] W. Wang, Y. Meng, W. Wang, Y. Zhang, B. Li, Y. Yan, B. Gao, J. C. Ho, 2D ferroelectric materials: Emerging paradigms for next-generation ferroelectronics, *Materials Today Electronics*, 2023, **6**, 100080, doi: 10.1016/j.mtelec.2023.100080.

[8] M. Chhowalla, D. Jena, H. Zhang, Two-dimensional semiconductors for transistors, *Nature Reviews Materials*, 2016, **1**, 16052, doi: 10.1038/natrevmats.2016.52.

[9] Y. Liu, Y. Huang, X. Duan, Van der waals integration before and beyond two-dimensional materials, *Nature*, 2019, **567**, 323-333, doi: 10.1038/s41586-019-1013-x.

[10] N. Rohaizad, C. C. Mayorga-Martinez, M. Fojtů, N. M. Latiff, M. Pumera, Two-dimensional materials in biomedical, biosensing and sensing applications, *Chemical Society Reviews*, 2021, **50**, 619-657, doi: 10.1039/d0cs00150c.

[11] K. S. Novoselov, A. K. Geim, S. V. Morozov, D. Jiang, Y. Zhang, S. V. Dubonos, I. V. Grigorieva, A. A. Firsov, Electric field effect in atomically thin carbon films, *Science*, 2004, **306**, 666-669, doi: 10.1126/science.1102896.

[12] M. Zhao, J. Chen, S.-S. Wang, M. An, S. Dong, Multiferroic properties of oxygen-functionalized magnetic i-MXene, *Physical Review Materials*, 2021, **5**, 094408, doi: 10.1103/physrevmaterials.5.094408.

[13] F. Xue, W. Hu, K.-C. Lee, L.-S. Lu, J. Zhang, H.-L. Tang, A. Han, W.-T. Hsu, S. Tu, W.-H. Chang, C.-H. Lien, J.-H. He, Z. Zhang, L.-J. Li, X. Zhang, Room-temperature ferroelectricity in hexagonally layered α-In_2Se_3 nanoflakes down to the monolayer limit, *Advanced Functional Materials*, 2018, **28**, 1803738, doi: 10.1002/adfm.201803738.

[14] W. Ding, J. Zhu, Z. Wang, Y. Gao, D. Xiao, Y. Gu, Z. Zhang, W. Zhu, Prediction of intrinsic two-dimensional ferroelectrics in In_2Se_3 and other III2-VI_3 van der Waals materials, *Nature Communications*, 2017, **8**, 14956, doi: 10.1038/ncomms14956.

[15] B. Tang, S. Hussain, R. Xu, Z. Cheng, J. Liao, Q. Chen, Novel type of synaptic transistors based on a ferroelectric semiconductor channel, *ACS Applied Materials & Interfaces*, 2020, **12**, 24920-24928, doi: 10.1021/acsami.9b23595.

[16] S. Wang, L. Liu, L. Gan, H. Chen, X. Hou, Y. Ding, S. Ma, D. W. Zhang, P. Zhou, Two-dimensional ferroelectric channel transistors integrating ultra-fast memory and neural computing, *Nature Communications*, 2021, **12**, 53, doi: 10.1038/s41467-020-20257-2.

[17] M. Uzhansky, A. Rakshit, Y. Kalcheim, E. Koren, Coupled pyroelectric-photovoltaic effect in 2D ferroelectric α-In_2Se_3, *NPJ 2D Materials and Applications*, 2025, **9**, 6, doi: 10.1038/s41699-024-00523-3.

[18] D. Dutta, S. Mukherjee, M. Uzhansky, E. Koren, Cross-field optoelectronic modulation *via* inter-coupled ferroelectricity in 2D In_2Se_3, *NPJ 2D Materials and Applications*, 2021, **5**, 81, doi: 10.1038/s41699-021-00261-w.

[19] Y. Li, M. Gong, H. Zeng, Atomically thin α-In_2Se_3: an emergent two-dimensional room temperature ferroelectric semiconductor, *Journal of Semiconductors*, 2019, **40**, 061002, doi: 10.1088/1674-4926/40/6/061002.

[20] S. Wan, Q. Peng, Z. Wu, Y. Zhou, Nonvolatile ferroelectric memory with lateral β/α/β In_2Se_3 heterojunctions, *ACS Applied Materials & Interfaces*, 2022, **14**, 25693-25700, doi: 10.1021/acsami.2c04032.

[21] D. Dutta, S. Mukherjee, M. Uzhansky, P. K. Mohapatra, A. Ismach, E. Koren, Edge-based two-dimensional α-In_2Se_3–MoS_2 ferroelectric field effect device, *ACS Applied Materials & Interfaces*, 2023, **15**, 18505-18515, doi: 10.1021/acsami.3c00590.

[22] C. Zheng, L. Yu, L. Zhu, J. L. Collins, D. Kim, Y. Lou, C. Xu, M. Li, Z. Wei, Y. Zhang, M. T. Edmonds, S. Li, J. Seidel, Y. Zhu, J. Z. Liu, W.-X. Tang, M. S. Fuhrer, Room temperature in-plane ferroelectricity in van der waals In_2Se_3, *Science Advances*, 2018, **4**, eaar7720, doi: 10.1126/sciadv.aar7720.

[23] Y. Zhou, D. Wu, Y. Zhu, Y. Cho, Q. He, X. Yang, K. Herrera, Z. Chu, Y. Han, M. C. Downer, H. Peng, K. Lai, Out-of-plane piezoelectricity and ferroelectricity in layered α-In_2Se_3 nanoflakes, *Nano Letters*, 2017, **17**, 5508-5513, doi: 10.1021/acs.nanolett.7b02198.

[24] C. Cui, W.-J. Hu, X. Yan, C. Addiego, W. Gao, Y. Wang, Z. Wang, L. Li, Y. Cheng, P. Li, X. Zhang, H. N. Alshareef, T. Wu, W. Zhu, X. Pan, L.-J. Li, Intercorrelated in-plane and out-of-plane ferroelectricity in ultrathin two-dimensional layered semiconductor In_2Se_3, *Nano Letters*, 2018, **18**, 1253-1258, doi: 10.1021/acs.nanolett.7b04852.

[25] R. Thayil, C. Amaravathi, C. V. Ramana, V. Kathirvelu, S. R. Parne, Magnetic nanoparticle-incorporated molybdenum disulfide nanocomposites for enhanced antimicrobial applications, *Journal of Operations Management*, 2025, doi: 10.1007/s11837-025-07352-9.

[26] R. Thayil, S. R. Parne, Morphology-tuned molybdenum dichalcogenide nanostructures for enhanced microwave absorption studies, *Journal of Electronic Materials*, 2025, **54**,

9315-9325, doi: 10.1007/s11664-025-12190-1.
[27] C. Wang, L. You, D. Cobden, J. Wang, Towards two-dimensional van der waals ferroelectrics, *Nature Materials*, 2023, **22**, 542-552, doi: 10.1038/s41563-022-01422-y.
[28] R. Thayil, S. R. Parne, C. V. Ramana, 2D MoS_2 for next-generation electronics and optoelectronics: from material properties to manufacturing challenges and future prospects, *Small*, 2025, **21**, 2412467, doi: 10.1002/smll.202412467.
[29] Q. Liu, S. Cui, R. Bian, E. Pan, G. Cao, W. Li, F. Liu, The integration of two-dimensional materials and ferroelectrics for device applications, *ACS Nano*, 2024, **18**, 1778-1819, doi: 10.1021/acsnano.3c05711.
[30] Y.-T. Huang, N.-K. Chen, Z.-Z. Li, X.-P. Wang, H.-B. Sun, S. Zhang, X.-B. Li, Two-dimensional In_2Se_3: a rising advanced material for ferroelectric data storage, *InfoMat*, 2022, **4**, e12341, doi: 10.1002/inf2.12341.
[31] S. Wan, Y. Li, W. Li, X. Mao, W. Zhu, H. Zeng, Room-temperature ferroelectricity and a switchable diode effect in two-dimensional α-In_2Se_3 thin layers, *Nanoscale*, 2018, **10**, 14885-14892, doi: 10.1039/c8nr04422h.
[32] J. Xiao, H. Zhu, Y. Wang, W. Feng, Y. Hu, A. Dasgupta, Y. Han, Y. Wang, D. A. Muller, L. W. Martin, P. Hu, X. Zhang, Intrinsic two-dimensional ferroelectricity with dipole locking, *Physical Review Letters*, 2018, **120**, 227601, doi: 10.1103/physrevlett.120.227601.
[33] F. Xue, J. Zhang, W. Hu, W.-T. Hsu, A. Han, S.-F. Leung, J.-K. Huang, Y. Wan, S. Liu, J. Zhang, J.-H. He, W.-H. Chang, Z. L. Wang, X. Zhang, L.-J. Li, Multidirection piezoelectricity in mono- and multilayered hexagonal α-In_2Se_3, *ACS Nano*, 2018, **12**, 4976-4983, doi: 10.1021/acsnano.8b02152.
[34] M. Si, A. K. Saha, S. Gao, G. Qiu, J. Qin, Y. Duan, J. Jian, C. Niu, H. Wang, W. Wu, S. K. Gupta, P. D. Ye, A ferroelectric semiconductor field-effect transistor, *Nature Electronics*, 2019, **2**, 580-586, doi: 10.1038/s41928-019-0338-7.
[35] M. Soleimani, M. Pourfath, Ferroelectricity and phase transitions in In_2Se_3 van der waals material, *Nanoscale*, 2020, **12**, 22688-22697, doi: 10.1039/d0nr04096g.
[36] X.-Q. Yan, X. Zhao, H. Xu, L. Zhang, D. Liu, Y. Zhang, C. Huo, F. Liu, J. Xie, X. Dong, Z.-B. Liu, J.-G. Tian, Temperature-tunable optical properties and carrier relaxation of $CuInP_2S_6$ crystals under ferroelectric-paraelectric phase transition, *Journal of Materials Chemistry C*, 2022, **10**, 696-706, doi: 10.1039/d1tc04984d.
[37] L. Wang, X. Wang, Y. Zhang, R. Li, T. Ma, K. Leng, Z. Chen, I. Abdelwahab, K. P. Loh, Exploring ferroelectric switching in α-In_2Se_3 for neuromorphic computing, *Advanced Functional Materials*, 2020, **30**, 2004609, doi: 10.1002/adfm.202004609.
[38] Y. Zhang, L. Wang, H. Chen, T. Ma, X. Lu, K. P. Loh, Analog and digital mode α-In_2Se_3 memristive devices for neuromorphic and memory applications, *Advanced Electronic Materials*, 2021, **7**, 2100609, doi: 10.1002/aelm.202100609.
[39] S. Mukherjee, D. Dutta, A. Ghosh, E. Koren, Graphene-In_2Se_3 van der waals heterojunction neuristor for optical in-memory bimodal operation, *ACS Nano*, 2023, **17**, 22287-22298, doi: 10.1021/acsnano.3c03820.
[40] S. Yuan, X. Luo, H. L. Chan, C. Xiao, Y. Dai, M. Xie, J. Hao, Room-temperature ferroelectricity in $MoTe_2$ down to the atomic monolayer limit, *Nature Communications*, 2019, **10**, 1775, doi: 10.1038/s41467-019-09669-x.
[41] S. Mukherjee, D. Dutta, P. K. Mohapatra, L. Dezanashvili, A. Ismach, E. Koren, Scalable integration of coplanar heterojunction monolithic devices on two-dimensional In_2Se_3, *ACS Nano*, 2020, **14**, 17543-17553, doi: 10.1021/acsnano.0c08146.
[42] S. Mukherjee, D. Dutta, M. Uzhansky, E. Koren, Monolithic In_2Se_3–In_2O_3 heterojunction for multibit non-volatile memory and logic operations using optoelectronic inputs, *NPJ 2D Materials and Applications*, 2022, **6**, 37, doi: 10.1038/s41699-022-00309-5.
[43] K. Xu, W. Jiang, X. Gao, Z. Zhao, T. Low, W. Zhu, Optical control of ferroelectric switching and multifunctional devices based on van der Waals ferroelectric semiconductors, *Nanoscale*, 2020, **12**, 23488-23496, doi: 10.1039/d0nr06872a.
[44] B. Tang, L. Hou, M. Sun, F. Lv, J. Liao, W. Ji, Q. Chen, UV-SWIR broad range photodetectors made from few-layer α-In_2Se_3 nanosheets, *Nanoscale*, 2019, **11**, 12817-12828, doi: 10.1039/c9nr03077h.
[45] S. Wan, Y. Li, W. Li, X. Mao, C. Wang, C. Chen, J. Dong, A. Nie, J. Xiang, Z. Liu, W. Zhu, H. Zeng, Nonvolatile ferroelectric memory effect in ultrathin α-In_2Se_3, *Advanced Functional Materials*, 2019, **29**, 1808606, doi: 10.1002/adfm.201808606.
[46] M. Si, Y. Luo, W. Chung, H. Bae, D. Zheng, J. Li, J. Qin, G. Qiu, S. Yu, P. D. Ye, A novel scalable energy-efficient synaptic device: crossbar ferroelectric semiconductor junction, *IEEE International Electron Devices Meeting*, San Francisco, USA, December 7-11, 2019, 6.6.1-6.6.4, doi: 10.1109/IEDM19573.2019.8993622.
[47] S. M. Poh, S. J. R. Tan, H. Wang, P. Song, I. H. Abidi, X. Zhao, J. Dan, J. Chen, Z. Luo, S. J. Pennycook, A. H. Castro Neto, K. P. Loh, Molecular-beam epitaxy of two-dimensional In_2Se_3 and its giant electroresistance switching in ferroresistive memory junction, *Nano Letters*, 2018, **18**, 6340-6346, doi: 10.1021/acs.nanolett.8b02688.
[48] F. Xue, X. He, W. Liu, D. Periyanagounder, C. Zhang, M. Chen, C.-H. Lin, L. Luo, E. Yengel, V. Tung, T. D. Anthopoulos, L.-J. Li, J.-H. He, X. Zhang, Optoelectronic ferroelectric domain-wall memories made from a single van der waals ferroelectric, *Advanced Functional Materials*, 2020, **30**, 2004206, doi: 10.1002/adfm.202004206.
[49] Jiang, S., Y. Wang, and G. Zheng, Two-Dimensional Ferroelectric Materials: From Prediction to Applications, *Nanomaterials*, 2025, **15**, 109, doi: 10.3390/nano15020109
[50] Tan, C.K.Y., W. Fu, and K.P. Loh, Polymorphism and ferroelectricity in indium (III) selenide, *Chemical Reviews*, 2023, **123**, 8701-8717.
[51] J. van Landuyt, G. van Tendeloo, S. Amelinckx, Phase transitions in In_2Se_3 as studied by electron microscopy and electron diffraction, *Physica Status Solidi (a)*, 1975, **30**, 299-314, doi: 10.1002/pssa.2210300131.
[52] S. Popović, A. Tonejc, B. Gržeta-Plenković, B. Čelustka, R.

Trojko, Revised and new crystal data for indium selenides, *Journal of Applied Crystallography*, 1979, **12**, 416-420, doi: 10.1107/s0021889879012863.
[53] Kambas, K., *et al*., Raman Spectra of α-and γ-In2Se3, *Physica status solidi (b)*, 1984, 124, K105-K108, dio: 10.1002/pssb.2221240241.
[54] Manolikas, C., New results on the phase transformations of In2Se3, *Journal of Solid State Chemistry*, 1988, **74**, 319-328, doi: 10.1016/0022-4596(88)90361-1.
[55] J. Ye, S. Soeda, Y. Nakamura, O. Nittono, Crystal structures and phase transformation in In_2Se_3 compound semiconductor, *Japanese Journal of Applied Physics*, 1998, **37**, 4264, doi: 10.1143/jjap.37.4264.
[56] K. Osamura, Y. Murakami, Y. Tomiie, Crystal structures of α-and β-indium selenide, In_2Se_3, *Journal of the Physical Society of Japan*, 1966, **21**, 1848, doi: 10.1143/jpsj.21.1848.
[57] L. Liu, J. Dong, J. Huang, A. Nie, K. Zhai, J. Xiang, B. Wang, F. Wen, C. Mu, Z. Zhao, Y. Gong, Y. Tian, Z. Liu, Atomically resolving polymorphs and crystal structures of In_2Se_3, *Chemistry of Materials*, 2019, **31**, 10143-10149, doi: 10.1021/acs.chemmater.9b03499.
[58] Kambas, K. and C. Julien, Preparation and some optical and electrical measurements of a new phase α′-In2Se3, *Materials Research Bulletin*, 1982, **17**, 1573-1579, doi: 10.1016/0025-5408(82)90214-8.
[59] Debbichi, L., O. Eriksson, and S. Lebègue, Two-dimensional indium selenides compounds: an ab initio study, *The Journal of Physical Chemistry Letters*, 2015, **6**, 3098-3103.
[60] W. Feng, F. Gao, Y. Hu, M. Dai, H. Liu, L. Wang, P. Hu, Phase-engineering-driven enhanced electronic and optoelectronic performance of multilayer In_2Se_3 nanosheets, *Applied Materials & Interfaces*, 2018, **10**, 27584-27588, doi: 10.1021/acsami.8b10194.
[61] M. S. Choi, B.-K. Cheong, C. H. Ra, S. Lee, J.-H. Bae, S. Lee, G.-D. Lee, C.-W. Yang, J. Hone, W. J. Yoo, Electrically driven reversible phase changes in layered In_2Se_3 crystalline film, *Advanced Materials*, 2017, **29**, 1703568, doi: 10.1002/adma.201703568.
[62] C. Xu, Y. Chen, X. Cai, A. Meingast, X. Guo, F. Wang, Z. Lin, T. W. Lo, C. Maunders, S. Lazar, N. Wang, D. Lei, Y. Chai, T. Zhai, X. Luo, Y. Zhu, Two-dimensional antiferroelectricity in nanostripe-ordered In_2Se_3, *Physical Review Letters*, 2020, **125**, 047601, doi: 10.1103/physrevlett.125.047601.
[63] F. Zhang, Z. Wang, J. Dong, A. Nie, J. Xiang, W. Zhu, Z. Liu, C. Tao, Atomic-scale observation of reversible thermally driven phase transformation in 2D In_2Se_3, *ACS Nano*, 2019, **13**, 8004-8011, doi: 10.1021/acsnano.9b02764.
[64] Z. Chen, W. Fu, L. Wang, W. Yu, H. Li, C. K. Y. Tan, I. Abdelwahab, Y. Shao, C. Su, M. Sun, B. Huang, K. P. Loh, Atomic imaging of electrically switchable striped domains in *β*'-In_2Se_3, *Advanced Science*, 2021, **8**, 2100713, doi: 10.1002/advs.202100713.
[65] L. Bai, C. Ke, Z. Luo, T. Zhu, L. You, S. Liu, Intrinsic ferroelectric switching in two-dimensional α-In_2Se_3, *ACS Nano*, 2024, **18**, acsnano.4c06619, doi: 10.1021/acsnano.4c06619.
[66] X. Zheng, W. Han, K. Yang, L. W. Wong, C. S. Tsang, K. H. Lai, F. Zheng, T. Yang, S. P. Lau, T. H. Ly, M. Yang, J. Zhao, Phase and polarization modulation in two-dimensional In_2Se_3 *via in situ* transmission electron microscopy, *Science Advances*, 2022, **8**, eabo0773, doi: 10.1126/sciadv.abo0773.
[67] Z. Chen, M. Sun, H. Li, B. Huang, K. P. Loh, Oscillatory order–disorder transition during layer-by-layer growth of indium selenide, *Nano Letters*, 2023, **23**, 1077-1084, doi: 10.1021/acs.nanolett.2c04785.
[68] W. Han, X. Zheng, K. Yang, C. S. Tsang, F. Zheng, L. W. Wong, K. H. Lai, T. Yang, Q. Wei, M. Li, W. F. Io, F. Guo, Y. Cai, N. Wang, J. Hao, S. P. Lau, C.-S. Lee, T. H. Ly, M. Yang, J. Zhao, Phase-controllable large-area two-dimensional In_2Se_3 and ferroelectric heterophase junction, *Nature Nanotechnology*, 2023, **18**, 55-63, doi: 10.1038/s41565-022-01257-3.
[69] C. Xiao, F. Wang, S. A. Yang, Y. Lu, Y. Feng, S. Zhang, Elemental ferroelectricity and antiferroelectricity in group-V monolayer, *Advanced Functional Materials*, 2018, **28**, 1707383, doi: 10.1002/adfm.201707383.
[70] J. Bi, M. Faizan, X. Liu, Y. Ma, X. Wang, V. Stempitsky, Ferroelectric devices for artificial intelligence chips, *Chip*, 2025, **4**, 100129, doi: 10.1016/j.chip.2025.100129.
[71] M. Liu, X. Liu, W. Xiao, G. Wang, D. Wang, C. Gao, Y. Wu, Z. Wang, A. Aierken, J. Bi, Controlled growth of Large-Area 2D palladium diselenide with tunable electronic properties for optoelectronics and artificial synapses devices, *Journal of Colloid and Interface Science*, 2025, **694**, 137683, doi: 10.1016/j.jcis.2025.137683.
[72] L. Li, M. Wu, Binary compound bilayer and multilayer with vertical polarizations: two-dimensional ferroelectrics, multiferroics, and nanogenerators, *ACS Nano*, 2017, **11**, 6382-6388, doi: 10.1021/acsnano.7b02756.
[73] M. Vizner Stern, Y. Waschitz, W. Cao, I. Nevo, K. Watanabe, T. Taniguchi, E. Sela, M. Urbakh, O. Hod, M. Ben Shalom, Interfacial ferroelectricity by van der waals sliding, *Science*, 2021, **372**, 1462-1466, doi: 10.1126/science.abe8177.
[74] K. Yasuda, X. Wang, K. Watanabe, T. Taniguchi, P. Jarillo-Herrero, Stacking-engineered ferroelectricity in bilayer boron nitride, *Science*, 2021, **372**, 1458-1462, doi: 10.1126/science.abd3230.
[75] L. You, F. Liu, H. Li, Y. Hu, S. Zhou, L. Chang, Y. Zhou, Q. Fu, G. Yuan, S. Dong, H. J. Fan, A. Gruverman, Z. Liu, J. Wang, In-plane ferroelectricity in thin flakes of van der waals hybrid perovskite, *Advanced Materials*, 2018, **30**, 1803249, doi: 10.1002/adma.201803249.
[76] M. Küpers, P. M. Konze, A. Meledin, J. Mayer, U. Englert, M. Wuttig, R. Dronskowski, Controlled crystal growth of indium selenide, In_2Se_3, and the crystal structures of α-In_2Se_3, *Inorganic Chemistry*, 2018, **57**, 11775-11781, doi: 10.1021/acs.inorgchem.8b01950.
[77] R. Piner, R. S. Ruoff, Cross talk between friction and height signals in atomic force microscopy, *Review of Scientific Instruments*, 2002, **73**, 3392-3394, doi: 10.1063/1.1499539.
[78] Hoffmann, T. Jungk, E. Soergel, Cross-talk correction in atomic force microscopy, *Review of Scientific Instruments*, 2007,

78, 016101, doi: 10.1063/1.2424448.
[79] R. C. Miller, G. Weinreich, Mechanism for the sidewise motion of 180° domain walls in barium titanate, *Physical Review*, 1960, **117**, 1460-1466, doi: 10.1103/physrev.117.1460.
[80] M. Hayashi, Kinetics of domain wall motion in ferroelectric switching. I. general formulation, *Journal of the Physical Society of Japan*, 1972, **33**, 616-628, doi: 10.1143/jpsj.33.616.
[81] Z.-X. Wang, X.-G. Chen, X.-J. Song, Y.-L. Zeng, P.-F. Li, Y.-Y. Tang, W.-Q. Liao, R.-G. Xiong, Domain memory effect in the organic ferroics, *Nature Communications*, 2022, **13**, 2379, doi: 10.1038/s41467-022-30085-1.
[82] Z. Fei, W. Zhao, T. A. Palomaki, B. Sun, M. K. Miller, Z. Zhao, J. Yan, X. Xu, D. H. Cobden, Ferroelectric switching of a two-dimensional metal, *Nature*, 2018, **560**, 336-339, doi: 10.1038/s41586-018-0336-3.
[83] W.-J. Wang, W.-Z. Liu, S.-H. Xu, D.-Y. Zhou, Z.-Y. Peng, Z.-Q. Feng, L. Feng, L.-S. Liao, Secondary grain growth of perovskite films induced by a phosphonate derivative for high-performance near-infrared light–emitting diodes, *Advanced Functional Materials*, 2025, **35**, 2504744, doi: 10.1002/adfm.202504744.
[84] T. H. Yang, B.-W. Liang, H.-C. Hu, F.-X. Chen, S.-Z. Ho, W.-H. Chang, L. Yang, H.-C. Lo, T.-H. Kuo, J.-H. Chen, P.-Y. Lin, K. B. Simbulan, Z.-F. Luo, A. C. Chang, Y.-H. Kuo, Y.-S. Ku, Y.-C. Chen, Y.-J. Huang, Y.-C. Chang, Y.-F. Chiang, T.-H. Lu, M.-H. Lee, K.-S. Li, M. Wu, Y.-C. Chen, C.-L. Lin, Y.-W. Lan, Ferroelectric transistors based on shear-transformation-mediated rhombohedral-stacked molybdenum disulfide, *Nature Electronics*, 2024, **7**, 29-38, doi: 10.1038/s41928-023-01073-0.
[85] T. N. Ng, B. Russo, B. Krusor, R. Kist, A. C. Arias, Organic inkjet-patterned memory array based on ferroelectric field-effect transistors, *Organic Electronics*, 2011, **12**, 2012-2018, doi: 10.1016/j.orgel.2011.08.019.
[86] V. Misra, S. Khan, M. Yadav, A. Singh, V. Singh, Recent advances in dielectric materials for energy storage devices, *Energy Harvesting and Storage Devices*, CRC Press, New York, 2023, 211-243, doi: 10.1201/9781003340539-9.
[87] G. A. Samara, T. Sakudo, K. Yoshimitsu, Important generalization concerning the role of competing forces in displacive phase transitions, *Physical Review Letters*, 1975, **35**, 1767-1769, doi: 10.1103/physrevlett.35.1767.
[88] J. Guo, N. University, L. Zhang, M. Zhang, N. University, S. Ji, N. University, Z. Xiao, N. University, C. Gao, N. University, F. Liu, N. University, Z. Hu, N. University, Y. Zhou, N. University, X. Fu, N. University, N. University, Femtosecond laser manipulation of multistage phase switching in two-dimensional In_2Se_3 visualized *via* an *in situ* transmission electron microscope, *ACS Nano*, 2025, **19**, 13264-13272, doi: 10.1021/acsnano.5c00538.
[89] M. Peršin, A. Peršin, B. Čelustka, B. Etlinger, Properties of flash evaporated thin films of In_2Se_3, *Thin Solid Films*, 1972, **11**, 153-160, doi: 10.1016/0040-6090(72)90354-9.
[90] Q. He, Z. Tang, M. Dai, H. Shan, H. Yang, Y. Zhang, X. Luo, Epitaxial growth of large area two-dimensional ferroelectric α-In_2Se_3, *Nano Letters*, 2023, **23**, 3098-3105, doi: 10.1021/acs.nanolett.2c04289.
[91] J. Muller, T. S. Boscke, U. Schroder, R. Hoffmann, T. Mikolajick, L. Frey, Nanosecond polarization switching and long retention in a novel MFIS-FET based on ferroelectric hbox{HfO}$_2$, *IEEE Electron Device Letters*, 2012, **33**, 185-187, doi: 10.1109/LED.2011.2177435.
[92] W. Chung, M. Si, P. R. Shrestha, J. P. Campbell, K. P. Cheung, P. D. Ye, First direct experimental studies of $Hf_{0.5}Zr_{0.5}O_2$ ferroelectric polarization switching down to 100-picosecond in sub-60mV/dec germanium ferroelectric nanowire FETs, *IEEE Symposium on VLSI Technology*, Honolulu, USA, June 18-22, 2018, 89-90, doi: 10.1109/VLSIT.2018.8510652.
[93] Dünkel, S., *et al*. A FeFET based super-low-power ultra-fast embedded NVM technology for 22nm FDSOI and beyond, *IEEE International Electron Devices Meeting (IEDM)*, San Francisco, USA, 2017, 19.7.1-19.7.4, doi: 10.1109/IEDM.2017.8268425.
[94] Lyu, X., Polarization and Switching Dynamics Study of Ferroelectric Hafnium Zirconium Oxide for Feram and Fefet Applications, 2023, Thesis, Purdue University, doi: 10.25394/PGS.23514816.
[95] P. K. Larsen, G. L. M. Kampschöer, M. J. E. Ulenaers, G. A. C. M. Spierings, R. Cuppens, Nanosecond switching of thin ferroelectric films, *Applied Physics Letters*, 1991, **59**, 611-613, doi: 10.1063/1.105402.
[96] S. L. Miller, P. J. McWhorter, Physics of the ferroelectric nonvolatile memory field effect transistor, *Journal of Applied Physics*, 1992, **72**, 5999-6010, doi: 10.1063/1.351910.
[97] R. Ramesh, B. Dutta, T. S. Ravi, J. Lee, T. Sands, V. G. Keramidas, Scaling of ferroelectric properties in La-Sr-co-O/Pb-La-Zr-Ti-O/La-Sr-co-O capacitors, *Applied Physics Letters*, 1994, **64**, 1588-1590, doi: 10.1063/1.111848.
[98] S. Mathews, R. Ramesh, T. Venkatesan, J. Benedetto, Ferroelectric field effect transistor based on epitaxial perovskite heterostructures, *Science*, 1997, **276**, 238-240, doi: 10.1126/science.276.5310.238.
[99] X. Chai, J. Jiang, Q. Zhang, X. Hou, F. Meng, J. Wang, L. Gu, D. W. Zhang, A. Q. Jiang, Nonvolatile ferroelectric field-effect transistors, *Nature Communications*, 2020, **11**, 2811, doi: 10.1038/s41467-020-16623-9.
[100] Y. Zheng, G.-X. Ni, C.-T. Toh, M.-G. Zeng, S.-T. Chen, K. Yao, B. Özyilmaz, Gate-controlled nonvolatile graphene-ferroelectric memory, *Applied Physics Letters*, 2009, **94**, 163505, doi: 10.1063/1.3119215.
[101] R. C. G. Naber, C. Tanase, P. W. M. Blom, G. H. Gelinck, A. W. Marsman, F. J. Touwslager, S. Setayesh, D. M. de Leeuw, High-performance solution-processed polymer ferroelectric field-effect transistors, *Nature Materials*, 2005, **4**, 243-248, doi: 10.1038/nmat1329.
[102] P. M. Heyman, G. H. Heilmeier, A ferroelectric field effect device, *Proceedings of the IEEE*, 1966, **54**, 842-848, doi: 10.1109/PROC.1966.4889.
[103] Shu, y., a new ferroelectric memory device, metal-ferroelectrisemiconductor transitor, In *IEEE Transactions on Electron Devices*, 1974, **21**, 499-504, doi: 10.1109/T-ED.1974.17955.

[104] K.-H. Kim, J.-P. Han, S.-W. Jung, T.-P. Ma, Ferroelectric DRAM (FEDRAM) FET with metal/$SrBi_2Ta_2O_9$/ SiN/Si gate structure, *IEEE Electron Device Letters*, 2002, **23**, 82-84, doi: 10.1109/55.981313.
[105] C. Hou, S. Zhang, R. Liu, T. Gemming, A. Bachmatiuk, H. Zhao, H. Jia, S. Huang, W. Zhou, J.-B. Xu, J. Pang, M. H. Rümmeli, J. Bi, H. Liu, G. Cuniberti, Boosting flexible electronics with integration of two-dimensional materials, *InfoMat*, 2024, **6**, e12555, doi: 10.1002/inf2.12555.
[106] D. Loke, T. H. Lee, W. J. Wang, L. P. Shi, R. Zhao, Y. C. Yeo, T. C. Chong, S. R. Elliott, Breaking the speed limits of phase-change memory, *Science*, 2012, **336**, 1566-1569, doi: 10.1126/science.1221561.
[107] R. Waser, M. Aono, Nanoionics-based resistive switching memories, *Nature Materials*, 2007, **6**, 833-840, doi: 10.1038/nmat2023.
[108] J. Yang, Y. Liu, E.-Y. Wang, J. Pang, S. Huang, T. Gemming, J. Bi, A. Bachmatiuk, H. Jia, S.-X. Hu, C. Jiang, H. Liu, G. Cuniberti, W. Zhou, M. H. Rümmeli, Modulating p-type doping of two dimensional material palladium diselenide, *Nano Research*, 2024, **17**, 3232-3244, doi: 10.1007/s12274-023-6196-7.
[109] Z. Wang, S. Joshi, S. E. Savel'ev, H. Jiang, R. Midya, P. Lin, M. Hu, N. Ge, J. P. Strachan, Z. Li, Q. Wu, M. Barnell, G.-L. Li, H. L. Xin, R. S. Williams, Q. Xia, J. J. Yang, Memristors with diffusive dynamics as synaptic emulators for neuromorphic computing, *Nature Materials*, 2017, **16**, 101-108, doi: 10.1038/nmat4756.
[110] Q. Xia, J. J. Yang, Memristive crossbar arrays for brain-inspired computing, *Nature Materials*, 2019, **18**, 309-323, doi: 10.1038/s41563-019-0291-x.
[111] F. Xue, X. He, Z. Wang, J. R. D. Retamal, Z. Chai, L. Jing, C. Zhang, H. Fang, Y. Chai, T. Jiang, W. Zhang, H. N. Alshareef, Z. Ji, L.-J. Li, J.-H. He, X. Zhang, Ferroelectric switching: giant ferroelectric resistance switching controlled by a modulatory terminal for low-power neuromorphic in-memory computing, *Advanced Materials*, 2021, **33**, 2170167, doi: 10.1002/adma.202170167.
[112] M. Faizan, S. University, Z. Qian, S. University, H. Zhu, S. University, S. Fan, S. University, N. Abas, S. Rauf, G. A. Khan, S. University, H. U. Huzaibi, S. University, Emerging ferroelectric materials for high-performance next-generation memory devices, *ACS Applied Electronic Materials*, 2025, **7**, 7473-7502, doi: 10.1021/acsaelm.5c01058.
[113] M. Faizan, K. Han, X. Wang, M. Z. Yousaf, Mathematical model-based analysis and mitigation of GaN switching oscillations, *IEEE Access*, 2024, **12**, 55551-55567.
[114] V. Garcia, M. Bibes, Ferroelectric tunnel junctions for information storage and processing, *Nature Communications*, 2014, **5**, 4289, doi: 10.1038/ncomms5289.
[115] S. Pi, C. Li, H. Jiang, W. Xia, H. Xin, J. J. Yang, Q. Xia, Memristor crossbar arrays with 6-nm half-pitch and 2-nm critical dimension, *Nature Nanotechnology*, 2019, **14**, 35-39, doi: 10.1038/s41565-018-0302-0.
[116] A. Chanthbouala, V. Garcia, R. O. Cherifi, K. Bouzehouane, S. Fusil, X. Moya, S. Xavier, H. Yamada, C. Deranlot, N. D. Mathur, M. Bibes, A. Barthélémy, J. Grollier, A ferroelectric memristor, *Nature Materials*, 2012, **11**, 860-864, doi: 10.1038/nmat3415.
[117] D. J. Kim, H. Lu, S. Ryu, C.-W. Bark, C.-B. Eom, E. Y. Tsymbal, A. Gruverman, Ferroelectric tunnel memristor, *Nano Letters*, 2012, **12**, 5697-5702, doi: 10.1021/nl302912t.
[118] Q. Zhao, H. Wang, Z. Ni, J. Liu, Y. Zhen, X. Zhang, L. Jiang, R. Li, H. Dong, W. Hu, Random access memory: organic ferroelectric-based 1T1T random access memory cell employing a common dielectric layer overcoming the half-selection problem (adv. mater. 34/2017), *Advanced Materials*, 2017, **29**, adma.201770246, doi: 10.1002/adma.201770246.
[119] P. Singh, S. Baek, H. H. Yoo, J. Niu, J.-H. Park, S. Lee, Two-dimensional CIPS-InSe van der Waal heterostructure ferroelectric field effect transistor for nonvolatile memory applications, *ACS Nano*, 2022, **16**, 5418-5426, doi: 10.1021/acsnano.1c09136.
[120] J. Wei, G. Ji, C. Zhang, L. Yan, Q. Luo, C. Wang, Q. Chen, J. Yang, L. Chen, C.-Q. Ma, Silane-capped ZnO nanoparticles for use as the electron transport layer in inverted organic solar cells, *ACS Nano*, 2018, **12**, 5518-5529, doi: 10.1021/acsnano.8b01178.
[121] X. Wang, C. Zhu, Y. Deng, R. Duan, J. Chen, Q. Zeng, J. Zhou, Q. Fu, L. You, S. Liu, J. H. Edgar, P. Yu, Z. Liu, Van der Waals engineering of ferroelectric heterostructures for long-retention memory, *Nature Communications*, 2021, **12**, 1109, doi: 10.1038/s41467-021-21320-2.
[122] M. Faizan, Z. Qian, H. Zhu, S. Fan, M. Z. Yousaf, M. Bajaj, Z. Chen, A. Aziz, GaN HEMTs-based compact power factor corrected 96.1% peak efficiency LED driver with gate assisted circuit, *Scientific Reports*, 2025, **15**, 14115, doi: 10.1038/s41598-025-92341-w.
[123] W. Huang, F. Wang, L. Yin, R. Cheng, Z. Wang, M. G. Sendeku, J. Wang, N. Li, Y. Yao, J. He, Gate-coupling-enabled robust hysteresis for nonvolatile memory and programmable rectifier in van der waals ferroelectric heterojunctions, *Advanced Materials*, 2020, **32**, 1908040, doi: 10.1002/adma.201908040.
[124] P. J. Jeon, S.-W. Min, J. S. Kim, S. R. Ali Raza, K. Choi, H. S. Lee, Y. T. Lee, D. K. Hwang, H. J. Choi, S. Im, Enhanced device performances of WSe_2–MoS_2 van der Waals junction p–n diode by fluoropolymer encapsulation, *Journal of Materials Chemistry C*, 2015, **3**, 2751-2758, doi: 10.1039/c4tc02961e.
[125] M. Faizan, X. Wang, M. Z. Yousaf, Design and comparative analysis of an ultra-highly efficient, compact half-bridge LLC resonant GaN converter for low-power applications, *Electronics*, 2023, **12**, 2850, doi: 10.3390/electronics12132850.
[126] K. Um, C. Jung, H. Nam, H. Lee, S. Yeom, J. H. Moon, Janus architecture host electrode for mitigating lithium-ion polarization in high-energy-density Li–S full cells, *Energy & Environmental Science*, 2024, **17**, 9112-9121, doi: 10.1039/d4ee02297a.
[127] S. Han, J. S. Kim, E. Park, Y. Meng, Z. Xu, A. C. Foucher, G. Y. Jung, I. Roh, S. Lee, S. O. Kim, J.-Y. Moon, S.-I. Kim, S. Bae, X. Zhang, B.-I. Park, S. Seo, Y. Li, H. Shin, K. Reidy, A. T. Hoang, S. Sundaram, P. Vuong, C. Kim, J. Zhao, J. Hwang, C.

Wang, H. Choi, D.-H. Kim, J. Kwon, J.-H. Park, A. Ougazzaden, J.-H. Lee, J.-H. Ahn, J. Kim, R. Mishra, H.-S. Kim, F. M. Ross, S.-H. Bae, High energy density in artificial heterostructures through relaxation time modulation, *Science*, 2024, **384**, 312-317, doi: 10.1126/science.adl2835.

[128] S. Seo, B.-S. Kang, J.-J. Lee, H.-J. Ryu, S. Kim, H. Kim, S. Oh, J. Shim, K. Heo, S. Oh, J.-H. Park, Artificial van der Waals hybrid synapse and its application to acoustic pattern recognition, *Nature Communications*, 2020, **11**, 3936, doi: 10.1038/s41467-020-17849-3.

[129] S. Baek, H. H. Yoo, J. H. Ju, P. Sriboriboon, P. Singh, J. Niu, J.-H. Park, C. Shin, Y. Kim, S. Lee, Ferroelectric field-effect-transistor integrated with ferroelectrics heterostructure, *Advanced Science*, 2022, **9**, 2270132, doi: 10.1002/advs.202270132.

[130] Wulf, W.A. and S.A. McKee, Hitting the memory wall: Implications of the obvious, *Computer architecture news*, 1995, **23**, 20-24, doi: 10.1145/216585.216588

[131] F. Lalchhandama, K. Datta, S. Chakraborty, R. Drechsler, I. Sengupta, CoMIC: complementary memristor based in-memory computing in 3D architecture, *Journal of Systems Architecture*, 2022, **126**, 102480, doi: 10.1016/j.sysarc.2022.102480.

[132] K. Fan, Q. Chen, J. Zhao, Y. Liu, Preparation of MnO_2-carbon materials and their applications in photocatalytic water treatment, *Nanomaterials*, 2023, **13**, 541, doi: 10.3390/nano13030541.

[133] Y. H. Zhao, M. Y. Zong, J. H. Dong, Z. Zhang, J. J. Liu, J. Liu, L. B. Su, Mid-infrared lightly Er^{3+}-doped CaF_2 laser under acousto–optical modulation, *Chinese Physics B*, 2023, **32**, 283-287.

[134] J. Chen, J. Li, Q. Zhang, S. Xiong, High-performance ferroelectric field-effect transistors based on ultrathin indium oxide for neuromorphic computing, *ACS Nano*, 2025, **19**, 19706-19714, doi: 10.1021/acsnano.5c01607.

[135] A. I. Khan, A. Keshavarzi, S. Datta, The future of ferroelectric field-effect transistor technology, *Nature Electronics*, 2020, **3**, 588-597, doi: 10.1038/s41928-020-00492-7.

[136] M. Faizan, J. Bi, M. Liu, L. Wang, V. Stempitsky, M. Z. Yousaf, Long life power factor corrected LED driver with capacitive energy mechanism for street light applications, *Sustainability*, 2023, **15**, 3991, doi: 10.3390/su15053991.

[137] Cho, Y., *et al*., Opto-electronic properties of alpha-In2Se3: single-layer to bulk, *arXiv preprint arXiv:1911.01784*, 2019.

[138] S. Fang, C. Yang, Q. Li, B. Wu, L. Xu, S. Liu, J. Yang, J. Ma, J. Dong, Y. Li, J. Yang, J. Lu, Ferroelectric-tunable photoresponse in α- In_2Se_3 photovoltaic photodetectors: an ab InitioQuantum transport study, *Physical Review Applied*, 2023, **19**, 024024, doi: 10.1103/physrevapplied.19.024024.

[139] W. Shockley, H. Queisser, Detailed balance limit of efficiency of p–n junction solar cells, *Renewable Energy*, London, Routledge, 2018, 35-54, doi: 10.4324/9781315793245-44.

[140] J. E. Spanier, V. M. Fridkin, A. M. Rappe, A. R. Akbashev, A. Polemi, Y. Qi, Z. Gu, S. M. Young, C. J. Hawley, D. Imbrenda, G. Xiao, A. L. Bennett-Jackson, C. L. Johnson, Power conversion efficiency exceeding the Shockley–Queisser limit in a ferroelectric insulator, *Nature Photonics*, 2016, **10**, 611-616, doi: 10.1038/nphoton.2016.143.

[141] W. T. H. Koch, R. Munser, W. Ruppel, P. Würfel, Bulk photovoltaic effect in $BaTiO_3$, *Solid State Communications*, 1975, **17**, 847-850, doi: 10.1016/0038-1098(75)90735-8.

[142] T. Choi, S. Lee, Y. J. Choi, V. Kiryukhin, S.-W. Cheong, Switchable ferroelectric diode and photovoltaic effect in $BiFeO_3$, *Science*, 2009, **324**, 63-66, doi: 10.1126/science.1168636.

[143] C. Ma, S. Yuan, P. Cheung, K. Watanabe, T. Taniguchi, F. Zhang, F. Xia, Intelligent infrared sensing enabled by tunable moiré quantum geometry, *Nature*, 2022, **604**, 266-272, doi: 10.1038/s41586-022-04548-w.

[144] S. Wu, Y. Chen, X. Wang, H. Jiao, Q. Zhao, X. Huang, X. Tai, Y. Zhou, H. Chen, X. Wang, S. Huang, H. Yan, T. Lin, H. Shen, W. Hu, X. Meng, J. Chu, J. Wang, Ultra-sensitive polarization-resolved black phosphorus homojunction photodetector defined by ferroelectric domains, *Nature Communications*, 2022, **13**, 3198, doi: 10.1038/s41467-022-30951-y.

[145] Y. J. Zhang, T. Ideue, M. Onga, F. Qin, R. Suzuki, A. Zak, R. Tenne, J. H. Smet, Y. Iwasa, Enhanced intrinsic photovoltaic effect in tungsten disulfide nanotubes, *Nature*, 2019, **570**, 349-353, doi: 10.1038/s41586-019-1303-3.

[146] D. Yang, J. Wu, B. T. Zhou, J. Liang, T. Ideue, T. Siu, K. M. Awan, K. Watanabe, T. Taniguchi, Y. Iwasa, M. Franz, Z. Ye, Spontaneous-polarization-induced photovoltaic effect in rhombohedrally stacked MoS_2, *Nature Photonics*, 2022, **16**, 469-474, doi: 10.1038/s41566-022-01008-9.

[147] Y. Li, J. Fu, X. Mao, C. Chen, H. Liu, M. Gong, H. Zeng, Enhanced bulk photovoltaic effect in two-dimensional ferroelectric CuInP2S6, *Nature Communications*, 2021, **12**, 5896, doi: 10.1038/s41467-021-26200-3.

[148] F. Lyu, Y. Sun, Q. Yang, B. Tang, M. Li, Z. Li, M. Sun, P. Gao, L.-H. Ye, Q. Chen, Thickness-dependent band gap of α-In_2Se_3: from electron energy loss spectroscopy to density functional theory calculations, *Nanotechnology*, 2020, **31**, 315711, doi: 10.1088/1361-6528/ab8998.

[149] W. Ji, K. Yao, Y. C. Liang, Bulk photovoltaic effect at visible wavelength in epitaxial ferroelectric $BiFeO_3$ thin films, *Advanced Materials*, 2010, **22**, 1763-1766, doi: 10.1002/adma.200902985.

[150] H. Yuan, X. Wang, B. Lian, H. Zhang, X. Fang, B. Shen, G. Xu, Y. Xu, S.-C. Zhang, H. Y. Hwang, Y. Cui, Generation and electric control of spin–valley-coupled circular photogalvanic current in WSe_2, *Nature Nanotechnology*, 2014, **9**, 851-857, doi: 10.1038/nnano.2014.183.

[151] M. Nakamura, S. Horiuchi, F. Kagawa, N. Ogawa, T. Kurumaji, Y. Tokura, M. Kawasaki, Shift current photovoltaic effect in a ferroelectric charge-transfer complex, *Nature Communications*, 2017, **8**, 281, doi: 10.1038/s41467-017-00250-y.

[152] N. Ogawa, M. Sotome, Y. Kaneko, M. Ogino, Y. Tokura, Shift Current in the ferroelectric semiconductor SbSI, *Physical Review B*, 2017, **96**, 241203, doi: 10.1103/physrevb.96.241203.

[153] P.-J. Huang, K. Taniguchi, H. Miyasaka, Bulk photovoltaic effect in a pair of chiral–polar layered perovskite-type lead

iodides altered by chirality of organic cations, *Journal of the American Chemical Society*, 2019, **141**, 14520-14523, doi: 10.1021/jacs.9b06815.
[154] Y. Zhang, R. Taniguchi, S. Masubuchi, R. Moriya, K. Watanabe, T. Taniguchi, T. Sasagawa, T. Machida, Switchable out-of-plane shift current in ferroelectric two-dimensional material $CuInP_2S_6$, *Applied Physics Letters*, 2022, **120**, 013103, doi: 10.1063/5.0074371.
[155] W. Tang, X. Zhang, H. Yu, L. Gao, Q. Zhang, X. Wei, M. Hong, L. Gu, Q. Liao, Z. Kang, Z. Zhang, Y. Zhang, A van der waals ferroelectric tunnel junction for ultrahigh-temperature operation memory, *Small Methods*, 2022, **6**, 2101583, doi: 10.1002/smtd.202101583.
[156] Akamatsu, T., *et al*., A van der Waals interface that creates in-plane polarization and a spontaneous photovoltaic effect, *Science*, 2021, **372**, 68-72, doi: 10.1126/science.aaz9146.
[157] T. Morimoto, N. Nagaosa, Topological nature of nonlinear optical effects in solids, *Science Advances*, 2016, **2**, e1501524, doi: 10.1126/sciadv.1501524.
[158] F. Lyu, X. Li, J. Tian, Z. Li, B. Liu, Q. Chen, Temperature-driven α-β phase transformation and enhanced electronic property of 2H α-In_2Se_3, *ACS Applied Materials & Interfaces*, 2022, **14**, 23637-23644, doi: 10.1021/acsami.2c03270.
[159] H. Jiao, X. Wang, Y. Chen, S. Guo, S. Wu, C. Song, S. Huang, X. Huang, X. Tai, T. Lin, H. Shen, H. Yan, W. Hu, X. Meng, J. Chu, Y. Zhang, J. Wang, HgCdTe/black phosphorus van der Waals heterojunction for high-performance polarization-sensitive midwave infrared photodetector, *Science Advances*, 2022, **8**, eabn1811, doi: 10.1126/sciadv.abn1811.
[160] Z. I. Chowdhury, M. H. Imtiaz, M. M. Azam, M. Rumana Aktar Sumi, N. S. Nur, Design and implementation of Pyroelectric Infrared sensor based security system using microcontroller, *IEEE Technology Students' Symposium*, Kharagpur, India, January 14-16, 2011, 1-5, doi: 10.1109/TECHSYM.2011.5783853.
[161] A. Thakre, A. Kumar, H.-C. Song, D.-Y. Jeong, J. Ryu, Pyroelectric energy conversion and its applications: flexible energy harvesters and sensors, *Sensors*, 2019, **19**, 2170, doi: 10.3390/s19092170.
[162] R. W. Whatmore, S. J. Ward, Pyroelectric infrared detectors and materials: a critical perspective, *Journal of Applied Physics*, 2023, **133**, 080902, doi: 10.1063/5.0141044.
[163] S. Bauer, S. B. Lang, Pyroelectric polymer electrets, *IEEE Transactions on Dielectrics and Electrical Insulation*, 1996, **3**, 647-676, doi: 10.1109/94.544186.
[164] Y. Jiang, Y. Song, Y. Zhang, L. Yu, S. Zhang, X. Li, X. Song, C. Xia, Ferroelectric-switchable single photodetector implementing complex optoelectronic logics, *Advanced Functional Materials*, 2025, **35**, 2418248, doi: 10.1002/adfm.202418248.
[165] T. Tan, X. Jiang, C. Wang, B. Yao, H. Zhang, 2D material optoelectronics for information functional device applications: status and challenges, *Advanced Science*, 2020, **7**, 2000058, doi: 10.1002/advs.202000058.
[166] H. Wang, S. Wu, Y. Chen, Q. Zhao, J. Zeng, R. Yin, Y. Zheng, C. Liu, S. Zhang, T. Lin, H. Shen, X. Meng, J. Ge, X. Wang, J. Chu, J. Wang, Bulk photovoltaic effect in two-dimensional ferroelectric α-In_2Se_3, *Science China Information Sciences*, 2024, **68**, 122401, doi: 10.1007/s11432-023-4070-8.
[167] F. Xue, X. He, Y. Ma, D. Zheng, C. Zhang, L.-J. Li, J.-H. He, B. Yu, X. Zhang, Unraveling the origin of ferroelectric resistance switching through the interfacial engineering of layered ferroelectric-metal junctions, *Nature Communications*, 2021, **12**, 7291, doi: 10.1038/s41467-021-27617-6.
[168] Y.-T. Huang, N.-K. Chen, Z.-Z. Li, X.-B. Li, X.-P. Wang, Q.-D. Chen, H.-B. Sun, S. Zhang, Mexican-hat potential energy surface in two-dimensional III2-VI_3 materials and the importance of entropy barrier in ultrafast reversible ferroelectric phase change, *Applied Physics Reviews*, 2021, **8**, 031413, doi: 10.1063/5.0056695.
[169] M. Gabel, Y. Gu, Understanding microscopic operating mechanisms of a van der waals planar ferroelectric memristor, *Advanced Functional Materials*, 2021, **31**, 2009999, doi: 10.1002/adfm.202009999.
[170] J. O. Island, S. I. Blanter, M. Buscema, H. S. J. van der Zant, A. Castellanos-Gomez, Gate controlled photocurrent generation mechanisms in high-gain In_2Se_3 phototransistors, *Nano Letters*, 2015, **15**, 7853-7858, doi: 10.1021/acs.nanolett.5b02523.
[171] J. Zhou, Q. Zeng, D. Lv, L. Sun, L. Niu, W. Fu, F. Liu, Z. Shen, C. Jin, Z. Liu, Controlled synthesis of high-quality monolayered α-In_2Se_3 *via* physical vapor deposition, *Nano Letters*, 2015, **15**, 6400-6405, doi: 10.1021/acs.nanolett.5b01590.
[172] R. B. Jacobs-Gedrim, M. Shanmugam, N. Jain, C. A. Durcan, M. T. Murphy, T. M. Murray, R. J. Matyi, R. L. Moore II, B. Yu, Extraordinary photoresponse in two-dimensional In_2Se_3 nanosheets, *ACS Nano*, 2014, **8**, 514-521, doi: 10.1021/nn405037s.
[173] M. Lin, D. Wu, Y. Zhou, W. Huang, W. Jiang, W. Zheng, S. Zhao, C. Jin, Y. Guo, H. Peng, Z. Liu, Controlled growth of atomically thin In_2Se_3 flakes by van der waals epitaxy, *Journal of the American Chemical Society*, 2013, **135**, 13274-13277, doi: 10.1021/ja406351u.

Publisher's Note: Engineered Science Publisher remains neutral with regard to jurisdictional claims in published maps and institutional affiliations.

Open Access
This article is licensed under a Creative Commons Attribution-NonCommercial-NoDerivatives 4.0 International, which permits the use, sharing, adaptation, distribution and reproduction in any medium or format, as long as appropriate credit to the original author(s) and the source is given by providing a link to the Creative Commons license. This usage for commercial purposes is not allowed. If modifications, adaptations or any other transformation were made, it is not allowed for distribution. The images or other third-party material in this article are included in the article's Creative Commons license, unless indicated otherwise in a credit line to the material. If material is not included in the article's

Creative Commons license and your intended use is not permitted by statutory regulation or exceeds the permitted use, you will need to obtain permission directly from the copyright holder. To view a copy of this license, visit https://creativecommons.org/licenses/by-nc-nd/4.0/.

©The Author(s) 2025.